Bolted Flanged Connections Made of Fiber Reinforced Plastic Materials

LIGUO SUN

A THESIS
IN
THE DEPARTMENT
OF
MECHANICAL ENGINEERING

PRESENTED IN PARTIAL FULFILLMENT OF THE REQUIREMENTS
FOR THE DEGREE OF DOCTOR OF PHILOSOPHY
CONCORDIA UNIVERSITY
MONTRÉAL, QUÉBEC, CANADA

SEPTEMBER 1995

ISBN 0-612-05076-9

Canada

Name Ligua SUN

Dissertation Abstracts International is arranged by broad, general subject categories. Please select the one subject which most nearly describes the content of your dissertation. Enter the corresponding four-digit code in the spaces provided.

Mechanical Engineering
SUBJECT TERM

0548
SUBJECT CODE

U·M·I

Subject Categories

THE HUMANITIES AND SOCIAL SCIENCES

COMMUNICATIONS AND THE ARTS
Architecture 0729
Art History 0377
Cinema 0900
Dance 0378
Fine Arts 0357
Information Science 0723
Journalism 0391
Library Science 0399
Mass Communications 0708
Music 0413
Speech Communication 0459
Theater 0465

EDUCATION
General 0515
Administration 0514
Adult and Continuing 0516
Agricultural 0517
Art 0273
Bilingual and Multicultural 0282
Business 0688
Community College 0275
Curriculum and Instruction 0727
Early Childhood 0518
Elementary 0524
Finance 0277
Guidance and Counseling 0519
Health 0680
Higher 0745
History of 0520
Home Economics 0278
Industrial 0521
Language and Literature 0279
Mathematics 0280
Music 0522
Philosophy of 0998
Physical 0523
Psychology 0525
Reading 0535
Religious 0527
Sciences 0714
Secondary 0533
Social Sciences 0534
Sociology of 0340
Special 0529
Teacher Training 0530
Technology 0710
Tests and Measurements 0288
Vocational 0747

LANGUAGE, LITERATURE AND LINGUISTICS
Language
- General 0679
- Ancient 0289
- Linguistics 0290
- Modern 0291

Literature
- General 0401
- Classical 0294
- Comparative 0295
- Medieval 0297
- Modern 0298
- African 0316
- American 0591
- Asian 0305
- Canadian (English) 0352
- Canadian (French) 0355
- English 0593
- Germanic 0311
- Latin American 0312
- Middle Eastern 0315
- Romance 0313
- Slavic and East European 0314

PHILOSOPHY, RELIGION AND THEOLOGY
Philosophy 0422
Religion
- General 0318
- Biblical Studies 0321
- Clergy 0319
- History of 0320
- Philosophy of 0322

Theology 0469

SOCIAL SCIENCES
American Studies 0323
Anthropology
- Archaeology 0324
- Cultural 0326
- Physical 0327

Business Administration
- General 0310
- Accounting 0272
- Banking 0770
- Management 0454
- Marketing 0338

Canadian Studies 0385
Economics
- General 0501
- Agricultural 0503
- Commerce-Business 0505
- Finance 0508
- History 0509
- Labor 0510
- Theory 0511

Folklore 0358
Geography 0366
Gerontology 0351
History
- General 0578
- Ancient 0579
- Medieval 0581
- Modern 0582
- Black 0328
- African 0331
- Asia, Australia and Oceania 0332
- Canadian 0334
- European 0335
- Latin American 0336
- Middle Eastern 0333
- United States 0337

History of Science 0585
Law 0398
Political Science
- General 0615
- International Law and Relations 0616
- Public Administration 0617

Recreation 0814
Social Work 0452
Sociology
- General 0626
- Criminology and Penology 0627
- Demography 0938
- Ethnic and Racial Studies 0631
- Individual and Family Studies 0628
- Industrial and Labor Relations 0629
- Public and Social Welfare 0630
- Social Structure and Development 0700
- Theory and Methods 0344

Transportation 0709
Urban and Regional Planning 0999
Women's Studies 0453

THE SCIENCES AND ENGINEERING

BIOLOGICAL SCIENCES
Agriculture
- General 0473
- Agronomy 0285
- Animal Culture and Nutrition 0475
- Animal Pathology 0476
- Food Science and Technology 0359
- Forestry and Wildlife 0478
- Plant Culture 0479
- Plant Pathology 0480
- Plant Physiology 0817
- Range Management 0777
- Wood Technology 0746

Biology
- General 0306
- Anatomy 0287
- Biostatistics 0308
- Botany 0309
- Cell 0379
- Ecology 0329
- Entomology 0353
- Genetics 0369
- Limnology 0793
- Microbiology 0410
- Molecular 0307
- Neuroscience 0317
- Oceanography 0416
- Physiology 0433
- Radiation 0821
- Veterinary Science 0778
- Zoology 0472

Biophysics
- General 0786
- Medical 0760

EARTH SCIENCES
Biogeochemistry 0425
Geochemistry 0996
Geodesy 0370
Geology 0372
Geophysics 0373
Hydrology 0388
Mineralogy 0411
Paleobotany 0345
Paleoecology 0426
Paleontology 0418
Paleozoology 0985
Palynology 0427
Physical Geography 0368
Physical Oceanography 0415

HEALTH AND ENVIRONMENTAL SCIENCES
Environmental Sciences 0768
Health Sciences
- General 0566
- Audiology 0300
- Chemotherapy 0992
- Dentistry 0567
- Education 0350
- Hospital Management 0769
- Human Development 0758
- Immunology 0982
- Medicine and Surgery 0564
- Mental Health 0347
- Nursing 0569
- Nutrition 0570
- Obstetrics and Gynecology 0380
- Occupational Health and Therapy 0354
- Ophthalmology 0381
- Pathology 0571
- Pharmacology 0419
- Pharmacy 0572
- Physical Therapy 0382
- Public Health 0573
- Radiology 0574
- Recreation 0575
- Speech Pathology 0460
- Toxicology 0383

Home Economics 0386

PHYSICAL SCIENCES
Pure Sciences
Chemistry
- General 0485
- Agricultural 0749
- Analytical 0486
- Biochemistry 0487
- Inorganic 0488
- Nuclear 0738
- Organic 0490
- Pharmaceutical 0491
- Physical 0494
- Polymer 0495
- Radiation 0754

Mathematics 0405
Physics
- General 0605
- Acoustics 0986
- Astronomy and Astrophysics 0606
- Atmospheric Science 0608
- Atomic 0748
- Electronics and Electricity 0607
- Elementary Particles and High Energy 0798
- Fluid and Plasma 0759
- Molecular 0609
- Nuclear 0610
- Optics 0752
- Radiation 0756
- Solid State 0611

Statistics 0463

Applied Sciences
Applied Mechanics 0346
Computer Science 0984
Engineering
- General 0537
- Aerospace 0538
- Agricultural 0539
- Automotive 0540
- Biomedical 0541
- Chemical 0542
- Civil 0543
- Electronics and Electrical 0544
- Heat and Thermodynamics 0348
- Hydraulic 0545
- Industrial 0546
- Marine 0547
- Materials Science 0794
- Mechanical 0548
- Metallurgy 0743
- Mining 0551
- Nuclear 0552
- Packaging 0549
- Petroleum 0765
- Sanitary and Municipal 0554
- System Science 0790

Geotechnology 0428
Operations Research 0796
Plastics Technology 0795
Textile Technology 0994

PSYCHOLOGY
General 0621
Behavioral 0384
Clinical 0622
Developmental 0620
Experimental 0623
Industrial 0624
Personality 0625
Physiological 0989
Psychobiology 0349
Psychometrics 0632
Social 0451

CONCORDIA UNIVERSITY

SCHOOL OF GRADUATE STUDIES

This is to certify that the thesis prepared

By: **LIGUO SUN**

Entitled: ***Bolted Flanged Connections Made of Fiber Reinforced Plastic Materials***

and submitted in partial fulfillment of the requirements for the degree of

DOCTOR OF PHILOSOPHY (Mechanical Engineering)

complies with the regulations of the University and meets the accepted standards with respect to originality and quality.

Signed by the final examining committee:

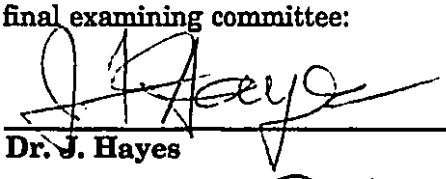

Dr. J. Hayes — Chair

Dr. G.E.O. Widera — External Examiner

Dr. M.M. El-Badry — External-to-Program

Dr. V.S. Hoa — Examiner

Dr. X. Xiao — Examiner

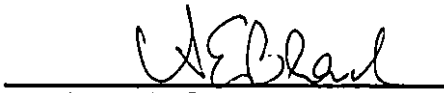

Dr. A.E. Blach — Thesis Supervisor

Approved by 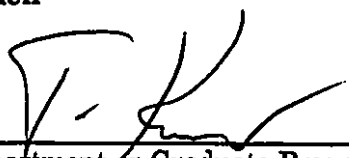

Chair of Department or Graduate Programme Director

October 18 1995

Dean of Faculty

Abstract

Bolted Flanged Connections Made of Fiber Reinforced Plastic Materials

Liguo Sun, Ph.D.
Concordia University, 1995

Fiber reinforced plastic (FRP) materials have been used in the chemical and process industries for several decades, chiefly because of the ability of many FRP materials to resist attack by various chemicals. FRP tanks, pressure vessels and piping have successfully been used to replace expensive equipment formerly made in stainless steel or nickel alloys. Although the laminate theory has been used to establish design formulas for cylindrical and spherical shells, little work has been done to investigate bolted flanged connections. The ASME Boiler and Pressure Vessel Code or the codes of other industrialized countries do not include specific rules for the design of FRP bolted flanged connections.

Up to now, the only work done on fiber reinforced plastic flanges has either been experimental investigations, or finite element analyses. No attempt has been made on a stress analysis of bolted flanged connections based on the laminate theory. Thus the current design practice is merely an extension of metallic flange design methods.

In this dissertation, two methods are proposed for a stress analysis of fiber reinforced plastic flanged connections with full face gaskets, using classical and shear deformation laminate theory, respectively. A sample calculation using the first proposed method is included. In order to verify the analytical results, a finite element analysis with 3-D anisotropic layered solid elements, using ANSYS is performed. Finally, an experimental investigation into the effects of outside to inside diameter ratios on the flange stress distribution and maximum stress values is conducted.

Acknoledgement

I wish to express my sincere appreciation to Dr. A.E. Blach for providing enthusiastic support and guidance leading to this dissertation.

Thanks are also due to the colleagues, faculty and staff at Concordia University, especially to Madame Li Lan and Mr. Paul Ouellette at the Center of Composites, who had sacrificed their precious time to help me on many occasions during the past years.

It is a pleasure to acknowledge, with many thanks, the cooperation of the technical staff, especially the late Mr. J.A. Kidd at CPF Dualam Ltd.

Finally, I would like to dedicate this work to the members of my family who always stood behind me with great patience and encouragement.

Contents

List of Tables

List of Figures

Chapter 1

INTRODUCTION

1.1 Objectives

Due to their strong resistance to chemical attack and their outstanding mechanical properties, fiber reinforced plastic (FRP) materials are increasingly being used in highly corrosive and stressed structures. Relatively long life expectancy and less environmental concerns, together with low installation and maintenance costs, also have made ways for fiber reinforced plastics in pressure vessel and piping applications.

Despite the fact that fiber reinforced plastics were introduced into pressure vessel and piping systems several decades ago, there was little research done on FRP flanged connections. There is a lack of standardization, from flange fabrication methods to design and dimensional considerations. This phenomenon results in many problems associated with FRP flanges.

After an exhausting literature search, the author has not found any contribution in analysis on FRP bolted flanged connection in a rigorous way. All design methods presently used are more or less modified versions of metallic flange design methods.

Since composite material flanges do, in general, not behave like metallic flanges, other method of analysis may be required.

The objectives of this study are:

- to develop analytical solutions for a stress analysis of fiber reinforced plastic flanged connections with full face gaskets, based on a classical and shear deformation laminate theory, respectively.

- to perform a finite element analysis with 3-D anisotropic layered solid elements, using ANSYS software, and to compare the result with the analytical solution.

- to obtain an experimental evaluation for the flange, and investigate the effect of outside to inside diameter ratios on stress distribution of FRP flanges, and also to compare the result with the analytical solution.

1.2 Background and Relevant Literature

1.2.1 Problem Definition

Sealing problems are encountered in the design of process equipment containing fluids, when convenient methods of connections are desired; for reason of fabrication, transportation, assembly, inspection, production, and so on. There are many types of such connections used in process equipment, the ones most widely used are bolted flanged connections. A detachable connection must satisfy the following requirements:

- To insure a reliable and tight joint, especially at severe operating conditions such as fluctuating pressure and temperature, or when containing corrosive fluids.

- Does not compromise the integrity of the vessel, and be able to withstand all forces induced upon it.

- Be capable of being repeatedly assembled and disassembled easily and quickly.

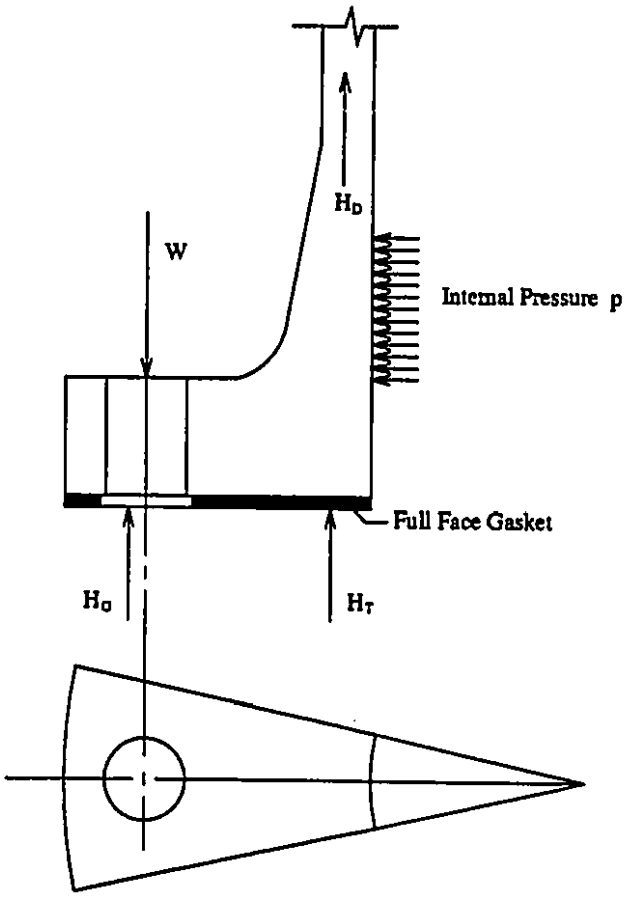

Figure 1: Flange Loads - Operating

- Be economical.

Flanged joints have good sealing characteristics and the required strength to meet the above expectations. Figure 1 shows a flange subjected to operating loads.

1.2.2 Metallic Flanged Connection

Present Design Codes

A bolted flanged connection is an interactive assembly of bolt, gasket and flange. It is often a critical component of a pressure vessel or pipe line.

Although a flange is simple in shape, there are many factors controlling the design of a flanged connection. The loading of the flange is very complicated. Many calculation methods for flange design exist; however, all use some kind of simplification. None has been recognized as a complete method which determines the exact state of stress in flange, bolts, and gasket. Different methods consider various factors in different ways and as such, use different levels of approximation. In general, most of the methods used in design standards of industrialized countries fall into two main types.

The first type is based on the theory of elasticity. It only permits allowable stresses within elastic limits using a generous factor of safety. This ensures a fairly rigid flanged connection and thus a tight joint.

The second type is based on elastic-plastic interaction with controlled deformation. The emphasis is on sealing of the joint instead of controlling stresses in flange or bolts. This approach was taken because a flanged joint rarely fails because of low strength, usually a failure occurs due to leakage. Maximum stresses in this method are controlled by plastic failure criteria.

The best known method of the first type due to Waters et al [86] [87] was successfully used for many years of service in industry. It forms the basis of the ASME Boiler and Pressure Vessel Code [1] which has been adopted as standard in many countries, including US, Canada, France, Japan, Britain and China.

As the flange is only a part of a flanged connection, the design of the flange has to relate to the choice of gasket and the bolt design. This design requires the choice of a suitable flange geometry, including gasket size, number and size of bolts, etc., and the verification of flange thickness. When the material and type have been decided, flange dimensions can often be chosen from tables of standard flanges. If needed, the dimensions are then modified to agree with results of stress calculations.

However, for most flanged connections, more important than stress calculations is the problem of sealing. This depends on the fluid being sealed: liquid is easily sealed, for vapors and gases this is not so. Sealing is related to the rotation of the flange, hence to its rigidity.

The presently used gasket design factors, known as "m" for operating and "y" for gasket seating, introduced by Rossheim and Markl [69], have drawn broad inquiries about their validity. These factors do not seem to be based on test results, and thus their concept is rather empirical.

Recently, research into gasket performance and leakage has become a major activity throughout the world. Leakage of dangerous fluids, a problem formerly neglected, must now be addressed in the context of environmental protection.

Over the decades, numerous efforts have been made on metallic flanged connections research around the world. Blach [18] has made a comprehensive survey and study on relevant literature ever published in English, German, Russian and French up to early eighties. All the publications included were commented on systematically,

thus providing readers with a description of the contents. Since then, in the following ten years, the research interest on flanged connection has been focused on several main topics explained below.

Pressure Vessel Research Council(PVRC) Sponsored Room and Elevated Temperature Gasket Test Program

The main purpose of a flanged connection is to provide a leak-free connecting device in pressure vessels or pipelines. To fulfill this task, the sealing mechanism must be properly understood. More meaningful gasket design factors must be developed other than those still used in present codes. In order to adopt these later design factors, standard test procedures and design procedures must be established. References [41] and [42] have summarized the large scale research activities directed by the PVRC Committee on Bolted Flanged Connections over a decade, on gasket performance under ambient and elevated temperature conditions. From the ambient temperature test program, it was found that leak rate is related to fluid pressure which in turn results in the new concept of Tightness Parameter T_P [8] [9]. This parameter is defined as follows:

$$T_P = \frac{p}{p^*} \left[\frac{L_T^*}{L_T}\right]^{0.5} \tag{1}$$

where

T_p	=	nondimensional tightness parameter
p^*	=	reference atmospheric pressure (1 bar=100 kPa=14.7 psi)
p	=	design pressure (kPa, psi)
L_T^*	=	reference mass leak rate (1 mg/sec)
L_T	=	mass leak rate for a 150 mm OD gasket (mg/sec)

A single T_P can be used to define the leakage level of a gasketed joint: A tight joint has a high value.

The effects of high temperature on gaskets in flanged joints were investigated in a series of tests over several years [10]. A multitude of useful test results were generated by these experiments. It is expected that, in the near future, the presently used gasket factors of the flange design rules in the ASME code will be replaced.

Bolted Flanges Analytical and Experimental Methods

The ASME Code contains rules for two classes of bolted flanged connections: flanges with ring gaskets lying entirely inside the bolt circle, and flanges with metal-to-metal contact outside the bolt circle. For a third type of flanges with gaskets across the full width of the flange, no Code rules exist at present. However, two design methods are available. The first was published by the Taylor-Forge and Pipe Works [6]. It is based on the method of analysis by Waters et al [87], assuming two gaskets to simulate one full face gasket: one inside the bolt circle, one outside. The gasket force is then proportionally assigned to both gaskets according to their cross sections. This assumption violates the fact that during rotation of the flanges, the outer part of the gasket is more highly loaded than the inner part, regardless of their cross sections. Moreover, the method does not fully take into account the resistance of the gasket against flange rotation, and thus yields results very much on the safe side.

The second design method is developed by Blach et al [19]. It is based on the assumption of a linearized triangular gasket force distribution which is zero at the inner diameter and maximum at the outer flange diameter for operating condition. The procedure follows the ASME BPV Code ring flange nomenclature except that the modulus of elasticity of the gasket is required. This method yields stresses closer to the experimental values, but still on the safe side.

An important part of any bolted flanged connection are the bolts which hold the flanges together. Modern bolting techniques, in keeping pace with demands of various industries, were described by Bickford [12]. Numerous studies have shown the correlation between bolt load, leakage and gasket stress. To properly control gasket

stress, a precise bolt preload is required. This can easily be achieved in the laboratory but is very difficult in actual field conditions [13] [14].

The design bolt load for a flanged connection may be calculated based on a defined leakage level for gasket seating and operating, as suggested by Payne [62]. Bouzid and Chaaban [26] discussed the failure phenomenon due to loss of tightness on otherwise structurally sound bolted joints. They present a simple analytical model based on an extension of the Taylor Forge method, taking into account flange rotation, flexibility of both the gasket and the bolts, and, when applicable, the stiffness of the end closure. Quite similarly a few years earlier, Cascales et al [31] introduced an approximate formula which ascertained the flange ring rotation, in an attempt to evaluate the joint sealing capacity by knowing the gasket non-linear behavior and the bolt loading. The same effort can be found in Zheng et al [90].

Sawa et al [71] used a three-dimensional theory of elasticity to analyze the distribution of contact stresses of the gasket which governed the sealing performance. Elastic stress analysis of circular or ribbed flange can also be found in Cao and Bell [30] and Rao et al [64]. Efremov et al [35] studied the heat exchange bolted flange connecting body and closure subjected to cyclic loading.

Substitution of adhesives for traditional gaskets in bolted flange connections was also explored in Sawa et al [75].

The bending flexibility of flanges made of soft materials such as aluminum was studied by Kohmura et al [45], and Modestova et al [56].

In many references [23][24][36][37][44][50][57][68][73][74][85], the bending effect on flanges has been studied. Flanges in piping systems and also pressure vessel flanges on tall columns are often subjected to longitudinal bending moments of considerable magnitude, be it from thermal expansion stresses in piping systems or from wind or

seismic loadings on tall vertical pressure vessels. Except for the ASME Code, Section III, Subsections NB, NC, and ND, other pressure vessel and piping codes do not contain design rules for such bending moments. In Subsections NB, NC, and ND of the ASME Nuclear Power Plant Code (Section III), an empirical formula is given, expressing a longitudinal bending moment in bolted flanged connections in terms of an equivalent internal pressure to be added to the design pressure of the flange. However, it was shown that the empirical formula of Section III does not hold equally well for different flange geometries. In particular for standard pipe flanges per ANSI B16.5, there are great differences which seem to rule out a single empirical expression.

References [17], [28] and [63] have dealt with non-circular flanged connections. The ASME Boiler and Pressure Vessel Code contains rules for non-circular pressure vessels of unreinforced and reinforced construction. These rules are given in Section VIII, Division 1, Appendix 13, and cover the sides, reinforcing ribs, and end plates of such vessels. For bolted flanged connections of such non-circular pressure vessels, which are used extensively in industry (cyclone inlets, chutes and feeders, etc.), no design rules are available at present.

Finite Element Analysis and Other Computer Aided Method

A few references including [70], [79], [89] have addressed the analysis of bolted flanged connections using the finite element method. [58], [88] presented a flange design modeling technique taking into account non-linear gasket load-compression curves, gasket hysteresis, and thermal effects. [33] discusses a software package using an integration method including optimization, modeling and finite element analysis for the design of thin bolted flanged connections.

Flanged connections frequently leak or fail in high-temperature service. Although it is recommended by the various Codes to avoid such operating condition, severe thermal shock may be encountered in nuclear power plant flanges during start-up and shut-down conditions. In such applications, conformance with standard design

practices may not ensure a leak-tight flanged joint. Both the finite element method and the finite difference method were used to analyze this heat conduction problem [11], [15], [60], [72].

Above referenced analyses and design methods were for flanges made of metallic materials having isotropic characteristics. For non-metallic flanges having anisotropic composite materials characteristics, a brief review is given below:

1.2.3 Non-metallic Flanged Connection

Up to the present time, few publications on stress analysis of fiber reinforced plastic flanged connections have appeared in print. The ones published have used mainly an experimental evaluation or the finite element method [39] [52]. No attempt has been made to use an analysis based on the laminate theory.

Matthews, Foulkes,Godwin and Kilty [38] [54] have used the FINEL finite element software to perform stress analyses for a number of flange geometries together with supporting experimental results. The flange was made from continuously chopped strand mat(CSM)/polyester resin pipe conforming to British Standards specifications. The pipe was folded out to form the front face of the flange. A resin-rich layer was placed on the outer surface of the pipe, and, on top of this layer, additional chopped strand mat layers were bonded to the outside of the pipe and folded round to form the back face and outer edges of the flange. The body of the flange was made from resin containing short fibers.

McLarty [55] detailed the design of an integral flange for a very large composite fiber shell and concluded that flanges of that size can be filament wound as an integral part of a cylindrical structure and that interspersing layers of short fibers will be beneficial.

Campbell [29] has recommended the adoption of the fabrication technique of a

one-piece integral flange which has been used on many projects over the years. When built to the proposed dimensions, it will eliminate the common problems associated with fiberglass flanged joints. However, it indicated that great accuracy is required in all phases of design, fabrication and installation of the contact molded FRP flange, in order to achieve the desired results. This accuracy is even more crucial when dealing with large diameter flanges, or with flanges for high pressure ratings. Campbell also pointed out that proper bolt torquing to seat the gasket is crucial. A washer should be placed under both the bolt head and nut to avoid excessive bearing stresses during bolt-up which could easily lead to crushing of the composite. The proposed dimensional standards by Campbell are largely based on metal flanges per ASME/ANSI B16.5.

Leon [49] has addressed some of the metallic flange design methods presently utilized for FRP bolted flanged connections, including reinforced thermoset and unreinforced thermoplastic flanges. The design methods were evaluated and compared with finite element analysis results.

A preliminary design method for FRP flanges with full face gaskets was given in Blach and Hoa [20]. The stresses due to flange "pull-back", caused during the resin curing process, have been evaluated.

Sun and Blach [77] [78] have proposed a new design method for FRP flanges based on the laminate theory. In [22], the effects of outside to inside diameter ratios on stress levels were investigated through a series of tests. It was found that the bolt circle of FRP flanges should be closer to the mean diameter of the flange and not, as it is the case with standard steel flange dimensions, close to the outside diameter of the flange.

A useful book by Hoa [40] explains the application of the laminate theory in the design of fiber reinforced pressure vessels and piping, as used in the chemical process industry and provides practical knowledge in the aspects of design, testing and fabrication techniques. An interesting work on resin problems during flange

fabrication can be found in Blach [25].

1.3 Thesis Overview

The text is organized in ten chapters. Up to this page, the background and relevant literature on metallic and FRP flanged connections have been surveyed.

In Chapter 2, some useful basic equations of linear elasticity are reviewed.

In Chapter 3, general features about FRP flanges such as material systems, fabrication techniques and end uses are described. Flange geometry, gasket compression and flange loading assumption which form the basis for analytical analysis are detailed in Chapter 4.

Classical laminate theory gives a simpler solution while shear deformation theory yields a more accurate solution. In Chapter 5, a design method is proposed, based on the classical laminate theory, and an analytical formulation based on the shear deformation theory is developed in Chapter 6. An illustrative example for the proposed design method is given in Chapter 7.

In Chapter 8, a finite element analysis on FRP flanges is presented. Comparisons of results of the analytical method and the FEM method are conducted within the same chapter.

Chapter 9 deals with the experimental investigation of effects of diameter ratio on the strength of dissimilar pairs of FRP flanges. Comparisons of results of the analytical method and the experiment are also given.

Chapter 10 concludes the study by final remarks along with the recommendations for future work.

Chapter 2

BASIC EQUATIONS OF LINEAR ELASTICITY

2.1 Introduction

A bolted flanged connection can be structurally analyzed as a circular plate connected to a cylindrical shell. Cylindrical coordinates are most suitable for this problem. Some basic equations of linear elasticity in cylindrical coordinates, which will be utilized through the content of this dissertation, are introduced in advance.

2.2 Linear Strain Tensor

The definition of a linear strain tensor is

$$\varepsilon_{ij} = \frac{1}{2}(u_{i,j} + u_{j,i}) \tag{2}$$

The strain-displacement relation in cylindrical coordinates is

$$\begin{aligned}
\varepsilon_r &= \frac{\partial u}{\partial r} \\
\varepsilon_\theta &= \frac{1}{r}\frac{\partial v}{\partial \theta} + \frac{u}{r} \\
\varepsilon_z &= \frac{\partial w}{\partial z} \\
\varepsilon_{rz} &= \frac{1}{2}(\frac{\partial u}{\partial z} + \frac{\partial w}{\partial r}) \\
\varepsilon_{\theta z} &= \frac{1}{2}(\frac{\partial v}{\partial z} + \frac{1}{r}\frac{\partial w}{\partial \theta}) \\
\varepsilon_{r\theta} &= \frac{1}{2}(\frac{1}{r}\frac{\partial u}{\partial \theta} + \frac{\partial v}{\partial r} - \frac{v}{r})
\end{aligned} \tag{3}$$

In the full 3-dimensional case, there are no more than 6 independent components of the strain to be found. Furthermore, whereas deformations have the units of length, strain measures are unitless.

2.3 Hooke's Law

Figure 2 shows a three dimentional elastic body. The Hooke's law for an orthotropic body with cylindrical anisotropy is [48]

$$\begin{aligned}
\varepsilon_r &= \frac{1}{E_r}\sigma_r - \frac{\nu_{\theta r}}{E_\theta}\sigma_\theta - \frac{\nu_{zr}}{E_z}\sigma_z \\
\varepsilon_\theta &= -\frac{\nu_{r\theta}}{E_r}\sigma_r + \frac{1}{E_\theta}\sigma_\theta - \frac{\nu_{z\theta}}{E_z}\sigma_z \\
\varepsilon_z &= -\frac{\nu_{rz}}{E_r}\sigma_r - \frac{\nu_{\theta z}}{E_\theta}\sigma_\theta + \frac{1}{E_z}\sigma_z \\
\varepsilon_{\theta z} &= \frac{1}{2G_{\theta z}}\sigma_{\theta z} \\
\varepsilon_{rz} &= \frac{1}{2G_{rz}}\sigma_{rz} \\
\varepsilon_{r\theta} &= \frac{1}{2G_{r\theta}}\sigma_{r\theta}
\end{aligned} \tag{4}$$

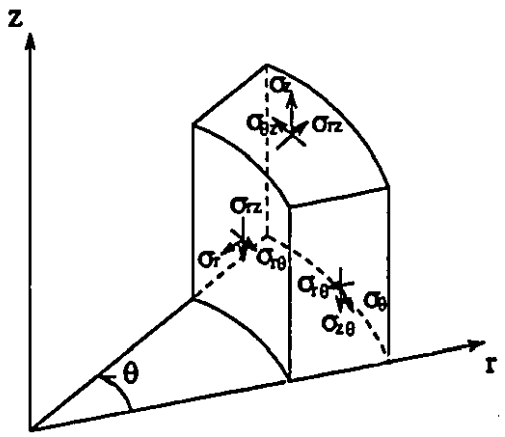

Figure 2: Three Dimensional Elastic Body

where: E_r,E_θ,E_z are the Young's moduli for tension (compression) in directions r,θ,z, the radial, tangential and axial directions (which are at the same time the principal directions of elasticity); $\nu_{r\theta}$ is the Poisson's ratio which characterizes the compression in the θ-direction when tension is applied in the r-direction, etc; and $G_{\theta z}$,G_{rz},$G_{r\theta}$ are the shear moduli which characterize the change of angles between directions θ and z, r and z, r and θ.

By neglecting σ_z, the three Hooke's law equations for an axisymmetric plate possessing cylindrical anisotropy, as shown in Figure 3, are in the form

$$\begin{aligned} \varepsilon_r &= \frac{1}{E_r}(\sigma_r - \nu_r\sigma_\theta) \\ \varepsilon_\theta &= \frac{1}{E_\theta}(\sigma_\theta - \nu_\theta\sigma_r) \\ \varepsilon_{rz} &= \frac{1}{2G_{rz}}\sigma_{rz} \end{aligned} \tag{5}$$

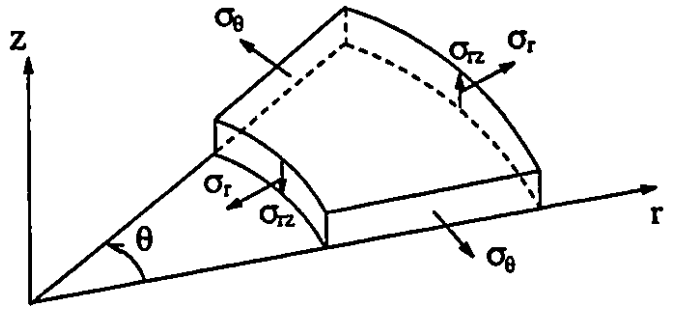

Figure 3: Axisymmetric Circular Plate

Here, E_r, E_θ are the Young's moduli for tension (compression) in the radial r and tangential θ directions; ν_r, ν_θ are the principal Poisson's ratio ($E_r\nu_\theta = E_\theta\nu_r$). G_{rz} is the shear modulus for r and z directions (principal).

The inverse of Equation 5 is often required. Rewriting it, then:

$$\begin{aligned} \sigma_r &= Q_{rr}\varepsilon_r + Q_{r\theta}\varepsilon_\theta \\ \sigma_\theta &= Q_{r\theta}\varepsilon_r + Q_{\theta\theta}\varepsilon_\theta \\ \sigma_{rz} &= Q_{rz}\varepsilon_{rz} \end{aligned} \tag{6}$$

where the elastic constants are:

$$\begin{aligned} Q_{rr} &= \frac{E_r}{1-\nu_r\nu_\theta} \\ Q_{r\theta} &= \frac{E_r\nu_\theta}{1-\nu_r\nu_\theta} \\ Q_{\theta\theta} &= \frac{E_\theta}{1-\nu_r\nu_\theta} \\ Q_{rz} &= 2G_{rz} \end{aligned} \tag{7}$$

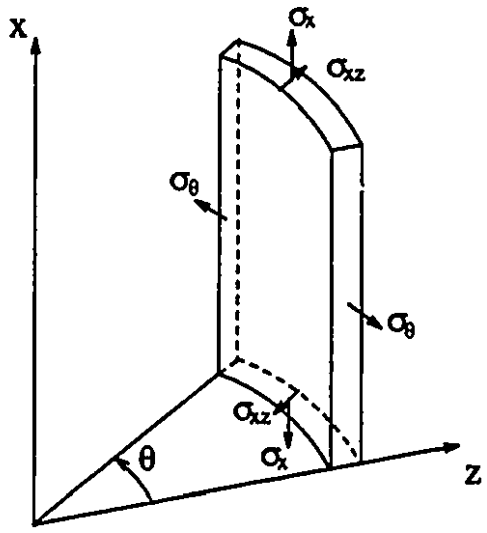

Figure 4: Axisymmetric Cylindrical Shell

In the case of an axisymmetric cylindrical shell, as shown in Figure 4, by neglecting σ_z, the reverse form of Hooke's law is quite similarly:

$$\begin{aligned} \sigma_x &= Q_{xx}\varepsilon_x + Q_{x\theta}\varepsilon_\theta \\ \sigma_\theta &= Q_{x\theta}\varepsilon_x + Q_{\theta\theta}\varepsilon_\theta \\ \sigma_{xz} &= Q_{xz}\varepsilon_{xz} \end{aligned} \tag{8}$$

where

$$\begin{aligned} Q_{xx} &= \frac{E_x}{1-\nu_{\theta x}\nu_{x\theta}} \\ Q_{x\theta} &= \frac{E_x\nu_{x\theta}}{1-\nu_{\theta x}\nu_{x\theta}} \\ Q_{\theta\theta} &= \frac{E_\theta}{1-\nu_{\theta x}\nu_{x\theta}} \\ Q_{xz} &= 2G_{xz} \end{aligned} \tag{9}$$

Here, E_x, E_θ are the young's moduli for tension (compression) in the longitudinal x and tangential θ directions; $\nu_{x\theta}, \nu_{\theta,x}$ are the principal Poisson's ratio . G_{xz} is the shear modulus for x and z directions (principal).

The two inverse equations of Hooke's law, (6) and (8) will be used later in analytical formulations.

2.4 Principal of Minimum Total Potential Energy

For any generalized elastic body, as shown in Figure 5, the potential energy of that body can be written as follows [84]:

$$\Pi = \int_R U_0 dR - \int_{S_T} t_i u_i dS - \int_R f_i u_i dR \tag{10}$$

where

U_0	=	strain energy density function, defined later
R	=	volume of the elastic body
t_i	=	i^{th} component of the surface traction
u_i	=	t^{th} component of the deformation
S_T	=	portion of the body surface over which tractions are prescribed
f_i	=	i^{th} component of a body force

It is seen that the first term on the right hand side of Equation 10 is the strain energy of the elastic body, which is to be labeled 'U'. The second and third terms are the work done by the surface tractions and the body forces, which are to be labeled together 'V'.

The Principal of Minimum Total Potential Energy can be stated as:
"Of all of the displacements satisfying compatibility and the prescribed boundary conditions, those which satisfy the equilibrium equations make the potential energy

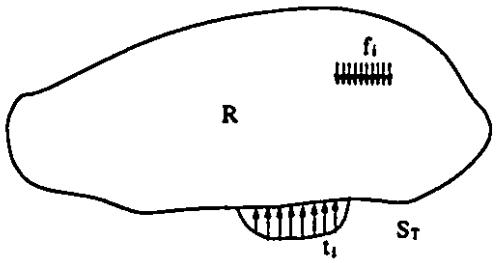

Figure 5: Generalized Elastic Body

a minimum."

Mathematically, the operation is simply

$$\delta\Pi \equiv \delta(U + V) = 0 \tag{11}$$

The lower case delta is a mathematical operation known as a variation. Operationally, it is analogous to partial differentiation. To employ variational operations in structural mechanics in this study only the following operations are needed:

$$\delta(\frac{du}{dr}) = \frac{d}{dr}(\delta u) \tag{12}$$

$$\delta(\frac{d^2u}{dr^2}) = \frac{d^2}{dr^2}(\delta u) \tag{13}$$

$$\delta(r^2) = 2r\delta r \tag{14}$$

$$\delta(\int u dr) = \int \delta u dr \tag{15}$$

And also

$$\delta[f(r) + g(r)] = \delta f(r) + \delta g(r) \tag{16}$$

or in a more general form

$$\delta F = \frac{\partial F}{\partial u}\delta u + \frac{\partial F}{\partial u'}\delta u' \tag{17}$$

for

$$F = F(r, u, u'), u = u(r), u' = u'(r) \tag{18}$$

In Equation 10, the strain energy density function of a linear elastic body, U_0, is defined as follows:

$$U_0 = \frac{1}{2}\sigma_{ij}\epsilon_{ij} \tag{19}$$

Sum on repeated subscripts is implied. The variational operation of strain energy takes the form

$$\delta U = \int_R \delta(\frac{1}{2}\sigma_{ij}\epsilon_{ij})dR = \int_R \sigma_{ij}\delta\epsilon_{ij}dR \tag{20}$$

2.5 Summary

To utilize the Principal of Minimum Total Potential Energy, the stress strain relations for the elastic body are employed to change the stress in Equation 20 to strains, and the strain displacement relations are employed to change all strains to displacements.

More on energy method for stress analysis of plates and shells can be found in references [47] [67] [76].

Chapter 3

FIBER REINFORCED PLASTIC FLANGES

3.1 Material Systems

3.1.1 Resins

Fiber reinforced plastics are composites made by reinforcing a resin with fibers. There are generally two groups of resins known as thermoplastic and thermoset used in FRP pressure vessels and piping systems.

Thermoplastic Resins

A thermoplastic is capable of being repeatedly softened by increase of temperature and hardened by decrease in temperature. The change in those materials upon heating is mainly physical rather than chemical.

Thermoplastic resins are not extensively used with FRP combinations because most of them have lower creep resistance and thermal stability than that of thermoset polymers. Incorporation of continuous fibers into thermoplastic matrices is difficult due to their high melt or solution viscosities. However, their importance is

expected to increase because of their distinct advantages over thermoset resins such as high impact strength and fracture resistance, which in turn impart an excellent damage tolerance characteristic to the composite material. In general, thermoplastic polymers have higher strains to failure than thermoset polymers, which may provide a better resistance to matrix microcracking in the composite laminate. Most of the non metallic liners in vessels are made of them. Popular types of plastic piping and fitting materials include:

- Polyvinyl Chloride (PVC)
- Chlorinated Polyvinyl Chloride (CPVC)
- Polybutylene (PB)
- Polyethylene (PE)
- Acrylonitrile Butadiene Styrene (ABS)
- Polyvinylidene Chloride (PVDC)
- Polytetra Flouroethylene (PTFE)
- Polyvinylidene Flouride (PVDF)
- Fluoroethylene Propylene (FEP)

Thermoset Resins

Thermoset plastic, on the other hand, when cured by application of heat, or by chemical means, changes into a practically infusible and insoluble material . The polymer does not further flow under the application of heat and pressure.

Thermoset resins are more commonly used with FRP products because of their ease of incorporating fibers into a matrix without the aid of high temperature or pressure. Thermoset resins exhibit less creep and stress relaxation than thermoplastic polymers, they also show superior thermal stability.

In the ASME BPV Code, Section X [2], thermoset resins include polyesters, epoxies, vinyl esters, phenolics and furan.

Polyesters are low in cost and cure fast at moderate to low temperatures. Polyester resins are water and chemical resistant and have good weatherability characteristics. They can claim to be among the first of the many synthetic resins which now form the basis of the plastics industry. However, comparing to other resins, polyester resins possess the highest cure shrinkage. This is undesirable in the fabrication of flanges because it is the main factor causing "pull-back", a convex distortion of flange faces during curing [21].

Epoxy resins provide plastics with good mechanical and fatigue strength and corrosion resistance. The shrinkage after cure is usually the lowest among this group of resins. They are among the best matrix materials for many fiber reinforced composites. Epoxies have lower water absorption characteristics, and better resistant to chemical attack than most other resins; they are, however, less extensively used because of their high cost. Epoxies also cause greater curing problems, such as long curing time and poor mold release characteristics, but their superior performance is often worth the higher initial cost.

Vinyl ester resins are largely used in chemical resistant FRP equipment. They possess good characteristic of epoxy resins, such as excellent chemical resistance and tensile strength, and of unsaturated polyester resins, such as low viscosity and fast curing. Upon cure, the volumetric shrinkage of vinyl ester resins is generally lower than that of unsaturated polyester resins but higher than that of epoxy resins.

Phenolic resins are used to provide high mechanical strength, good thermal stability, and good water and chemical resistance to many acids, except attack by alkalis. They are generally less expensive than polyesters. Higher curing pressures, longer curing times and shorter shelf life than polyesters are their disadvantages. One of the physical properties is their extreme brittleness, which may be overcome by the use of plasticizers; however, this usually results in a degradation of their properties.

Furan resins have better heat resistance, better chemical resistance, particularly to alkalis, greater hardness and better water resistance than polyesters, phenolic and even often epoxy resins. Unlike the epoxy resins, they have a poor adhesion to wood and metal, this being somewhat improved by incorporating plasticizers at the price of reduction in chemical resistance.

3.1.2 Fibers

In ASME Code, Section X, reinforcements embedded in a resin matrix shall be one or a combination of fibers such as glass, carbon or graphite and aramid.

Glass Fibers

Glass fibers are used in about 70 per cent of todays FRP production. There are several basic types of glass fiber which are commonly used. These fibers are manufactured from different combinations of component materials to meet various application needs.

'E' glass fiber is made from a calcium-alumina boro-silicate glass with an alkali content of less than 1 per cent. It is capable of being drawn into fine filaments and has high strength and a high Young's modulus, and also good resistance to weathering.

Soda lime glass with an alkali content varying from 10 to 15 per cent, known as 'A' glass has superior resistance to attack by acids than E glass. It is inexpensive to produce, but is inferior in physical strength to E glass. It is more vulnerable to attack by moisture than E glass.

'S' glass consisting of silica, alumina and magnesia in proportional combination, is mechanically stronger and higher temperature resistant than E glass. However, it is more expensive to produce than E glass and is mainly used in the military and

aerospace applications.

Besides the different types of glass fibers mentioned above, Type E-CR and Type C glass are also included in ASME Code, Section X. E-CR glass is developed from E glass as a corrosion resistant fiber. Compared to E-glass, E-CR glass shows much less strength reduction in corrosive environments. C-glass is also a high strength fiber used in special chemical environments instead of E-glass. In addition to thermoplastics, C-glass is also used as corrosion resistant liner in thermoset plastics.

E glass, because of its versatility and its unique all-round properties, such as good textile processing and suitability as a fiber reinforcement in both fabric and strand form, has been the major type of glass fiber used in reinforced plastic pressure vessels and piping systems.

Aramid Fibers

Of the synthetic aramid fibers, the most commonly used are Kevlar 29 and Kevlar 49. The mechanical properties of aramid fibers are quite unique from other fibers. Tensile strength and modulus of elasticity are substantially higher than those of E glass, and fiber elongation is significantly lower. Aramid fibers are not brittle like the glass or graphite fibers. Kevlar 49 is particularly well suited for filament winding pressure vessels in tensile-critical applications. Its resistance to neutral chemicals is generally very high. But the fiber is susceptible to attack by acids and alkalis, especially by strong acids.

Kevlar composites usually have poor compressive properties, i.e. low compressive yield and ultimate strength. A hybrid composite, in which another fiber such as graphite or E-glass is added, can overcome the drawbacks of each fiber concerned. Such hybrids are now used in many applications in a diversity of combinations.

Carbon or Graphite Fibers

Carbon and graphite fibers are both made of relatively pure carbon. Carbon fibers are referred to as fibers processed at temperatures below 1700 °C with a tensile strength less than 345 GPa, whereas graphite fibers are fibers which are heat treated at a temperature above 1700 °C and have a tensile strength of more than 345 GPa and also a high degree of orientation. Carbon and graphite fibers, generally speaking, are predominantly used as high tensile strength and high modulus reinforcing agents in high performance resin matrix composites. It is primarily for this reason that carbon fiber composites are replacing metals in applications where weight saving is of prime importance.

Further information on the subject of FRP material system can be found in [27] [32] [53] [61].

3.2 End Uses

Besides the various glass fibers used chiefly with phenolic resins, there are also more advanced fibers such as aramid, carbon, graphite, and others. These fibers impregnated in a thermoset resin matrix such as epoxy are usually considered advanced composites. Because of the increased cost of such materials and the higher level of technical expertise required for their effective use, their usage is limited to military and aerospace applications.

The end uses of fiber/resin systems in pressure vessels are detailed in Table 1 (from reference [51]):

Service Pressure MPa (psi)	Industrial Market	Military Market	Aerospace/Aeronautical Market	Remaining Challenges
Low 0-3.5 (0-500)	E glass/polyester		S glass, Kevlar, Carbon/epoxy	manufacturing economics
	-compressor tanks -chemical storage/ processing -filtration tanks		-rocket fuel/oxidizer storage	
Moderate 3.5-14 (500-2000)	E glass, S glass/epoxy		S glass, Kevlar, Carbon/epoxy	manufacturing economics
	-chemical storage/ processing -salt water desalination		-rocket fuel/oxidizer storage -nitrogen storage for space-	
High 14-70 (2000-10000)	S glass, Kevlar/epoxy	S glass,Kevlar, Carbon/epoxy	Kevlar/epoxy	-liner buckling -liner weight -manufacturing variability
	-compressed natural gas -compressed air back pack	-rocket launching tubes	-compressed air(Boeing 747) -compressed helium(shuttle) -air tanks/space suits -hydrogen storage(Venus probe)	
Ultra-High 70+ (10000+)	Metals	S glass/Kevlar/ Carbon hybrids	S glass, Kevlar, Carbon hybrids	-composite material properties -liner problems
	-high pressure processing -material research -detonation tanks	-compressed helium/missile systems	-compressed helium/spacecraft	

Table 1: Composite Pressure Vessel End Uses [51]

3.3 Fiber Reinforced Plastic Flanges

3.3.1 General Fabrication Techniques

There are a variety of manufacturing processes for fiber reinforced plastics. For flange production, several methods are used including contact molding or hand lay-up, injection molding, filament winding, compression molding, resin transfer molding and centrifugal casting. These techniques are briefly explained as follows:

Contact molding is the least expensive of all the molding processes. Layers are applied to the mold by hand. Resin is sprayed or brushed on after each layer is positioned. The mats or cloths are applied until a desired thickness is achieved. The resin is allowed to dry in air. The lay-up usually cures at room temperature; however, heat may be applied to accelerate curing. Contact molding is the principal method used in the manufacture of low cost, large or special size and special application flanges.

In the injection molding technique, the molding compound is injected into the mold cavity by pressure. The material solidifies in the cavity and is removed after curing. Injection molding can be done manually, or automatically on specially designed machines. Material quantities to be injected into the mold are measured on a volume or a weight basis. Because of size limits of injection molding machines, this method is usually used to produce small-size flanges. The initial costs of tooling are also higher than those of the contact molding method.

Filament winding is done with continuous lengths of fiber rovings either preimpregnated or impregnated during winding onto a mandrel. Specially designed winding machines wind the fiber at desired distance about mandrels of various cylindrical shapes and diameters until a desired thickness is achieved. Additional resin is applied thereafter. By changing the distance and angle of fiber winding, a variety of physical strengths can be obtained. Filament winding is usually employed in the fabrication of high strength flanges.

The compression molding method employs two molds to pressure and shape the liquid molding compound as the resin cures.

Resin transfer molding is done in compression presses with integral-type molds. The molding material is placed into the the mold cavity before it cures. A transfer plunger is used to force the compound into the mold.

In centrifugal casting the mixture of chopped fibers with resin is placed into a rotating cylindrical mold. The mold rotates as the resin cures. An isotropic oriented and cylindrically symmetrical flange is produced.

3.3.2 Contact Molded Flanges

Two-piece Construction

In the production of contact molded fiber reinforced plastic flanges, there are two general fabrication procedures used. The first method is the two-piece flange. In the two-piece construction of a contact molded flange, the flange is laid-up directly onto a piece of pipe or a cylindrical pressure vessel shell.

Figures 6 and 7 illustrate two examples of two-piece constructed flanges. Figure 6 shows a flange built onto a straight piece of pipe, while Figure 7 shows the use of a tapered pipe section in an effort to minimize the outside diameter in the hub region. In this case, no notches in the hub are required for the bolt heads as shown in Figure 6. There are two major problems with this method. Both types of the two-piece flange tend to crack at the bolt hole centerline in both the tangential and radial directions, and at the hub to flange intersection. While cracks that form in the flange of Figure 6 might not necessarily lead to leakage, the tapered pipe flange of Figure 7 would have leakage through the cracks and the flange would have to be replaced. Also, there is a built-in weakness along the bond between the flange ring and the pipe section. This bond is more susceptible to longitudinal stresses than that of the second type of the

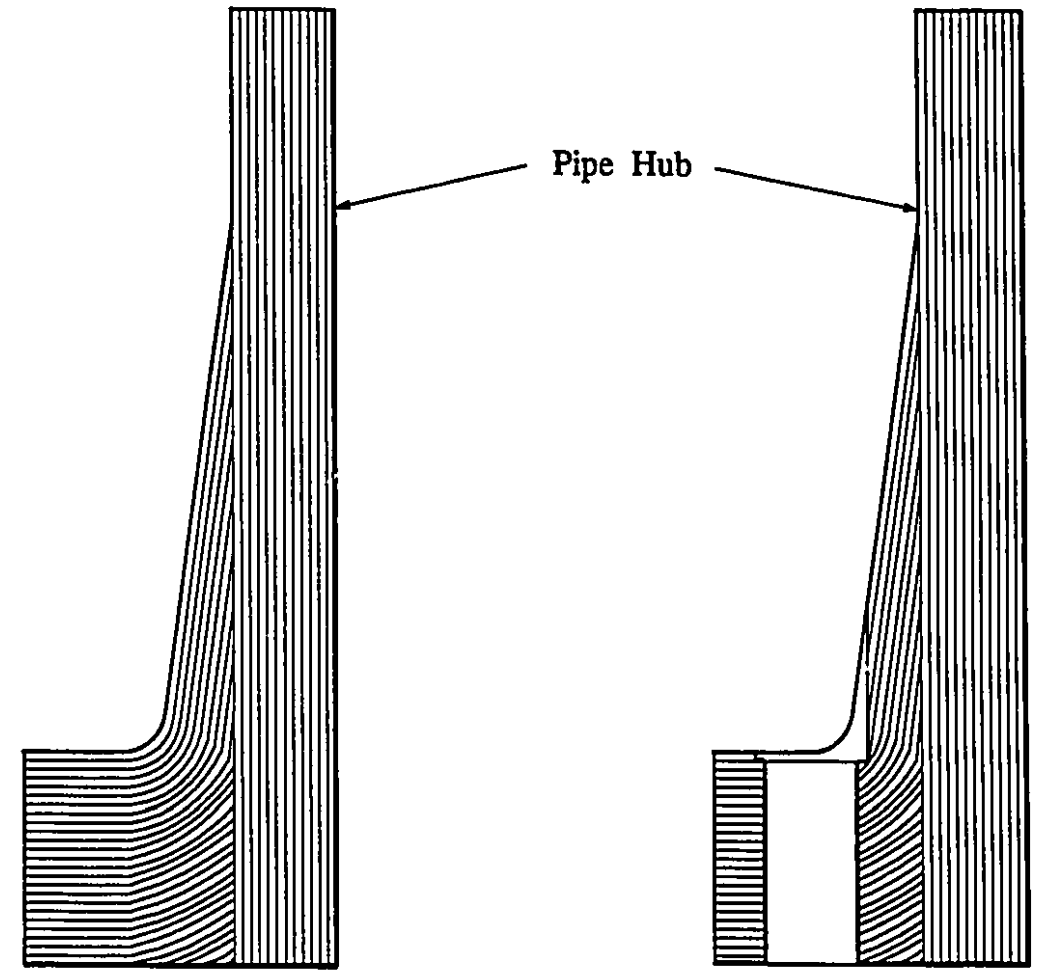

Figure 6: Flange Built on Straight Pipe Section

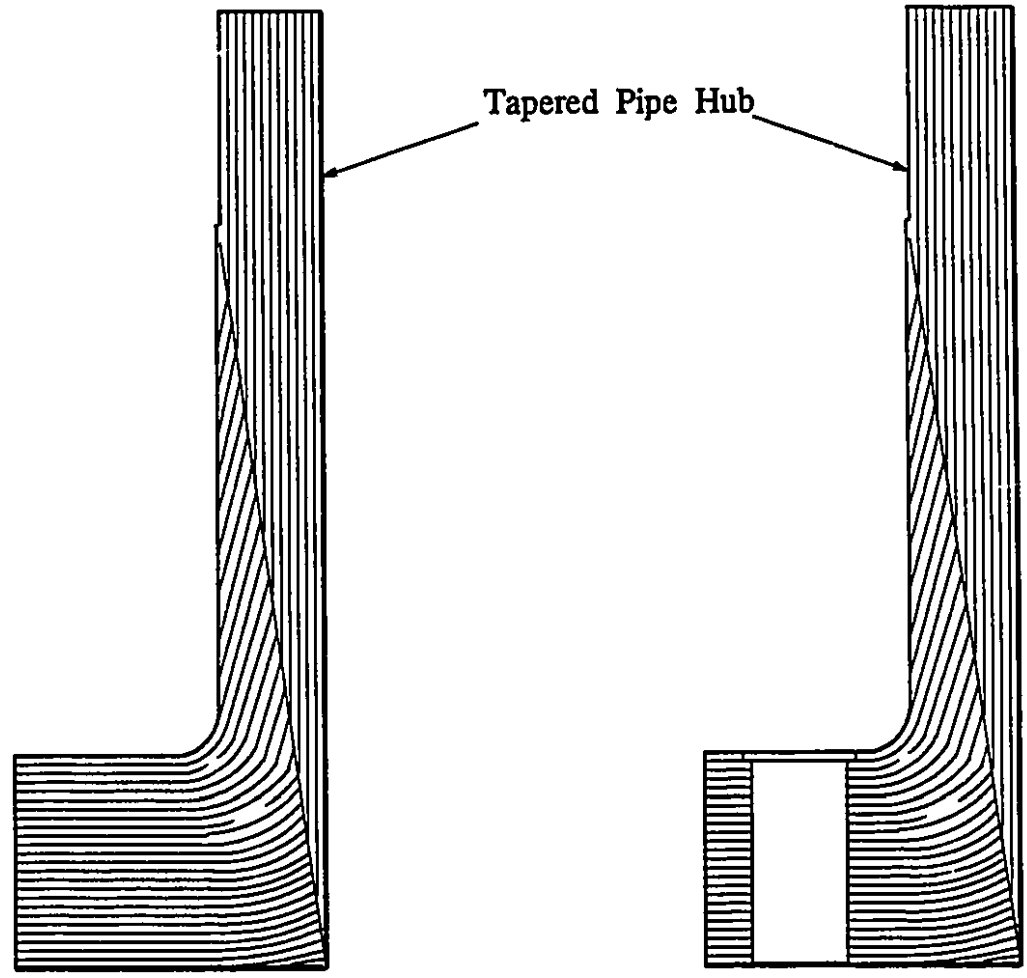

Figure 7: Flange Built on Tapered Pipe Section

contact moulded flange, the one-piece integral flange.

One-piece Construction

The second method, the one-piece flange, is fabricated integral with the connecting shell, shown in Figure 8. Woven roving, continuous axial glass filaments and mat are made continuous from the shell and hub into layers of the flange. The additional thickness of the flange is made up using donut shape sections of mat alternated between the layers of woven roving and mat. Any exposed glass at the edge of the flange is covered by a final resin layer of sufficient thickness. The final resin layer contains 3 to 5% of a 10% solution of paraffin in styrene.

The one-piece integral flange eliminates all the problems associated with the bond of the two-piece construction. It was recommended by Campbell and has successfully been used in industry application for almost two decades.

As shown in Figure 8, the one-piece flange possesses a straight hub. For this reason, all the following derivations of stresses are limited to flanges with straight hubs only, used in identical pairs.

In the field of lamination analysis, midplane symmetrically layered plates and shells require much less mathematical work than un-symmetrically layered ones. Since circular flanges and cylindrical shells can easily be layered symmetrically, all solutions provided in this thesis are limited to this midplane symmetry.

Further, the exact solution is given only for materials possessing equivalent elastic properties in the radial and tangential direction.

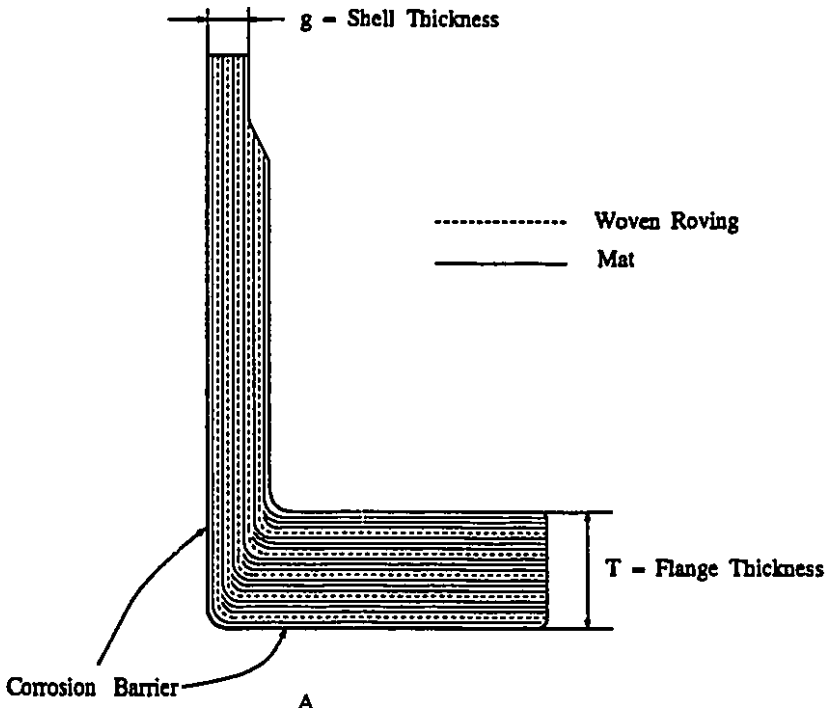

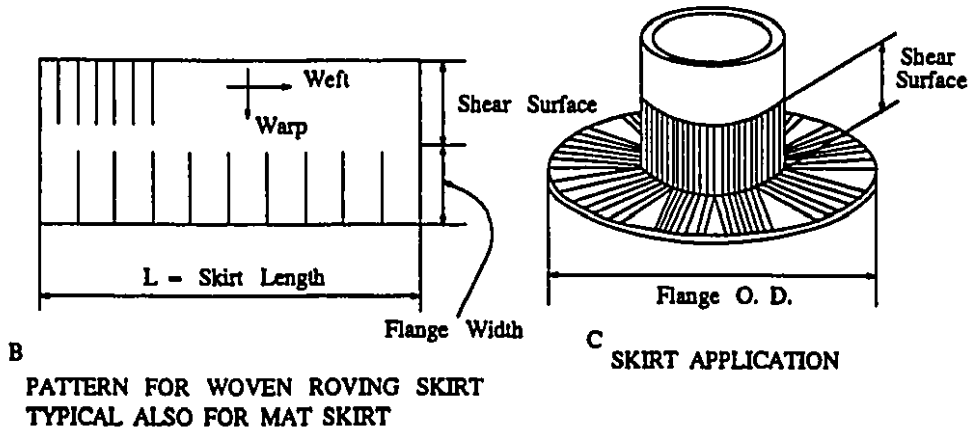

Figure 8: Integral Stub Flange

Chapter 4

FULL FACE GASKETED FLANGED CONNECTIONS

4.1 Introduction

In order to achieve a tight flanged joint, the choice of suitable sealing surface is important. In practice, existing types of gasketed flanges in terms of flange facing are raised face flange, male and female flange, tongue and groove flange, ring joint flange, o-ring gasket flange and flat face flange, shown in Figure 9.

The raised face flange is simple in shape and easy to produce. However, during bolt-up, soft gaskets tend to be pushed or squeezed out of the sealing surfaces. Metal gaskets or gaskets with metal rings avoid this problem. Nevertheless, the raised face flange is mainly used in low and medium pressure applications. Another disadvantage of this type of flange is the high stress level near the hub region due to a large rotation of the flange about the gasket as pivot.

The male and female flange has a recessed gasket contact face. The gasket is protected against extrusion by internal pressure. It is easy to assemble this type of flange in any position, the gasket is always centered. Sealing is better than in a raised face flange because of its narrower gasket contact surface. Thus, the service pressure

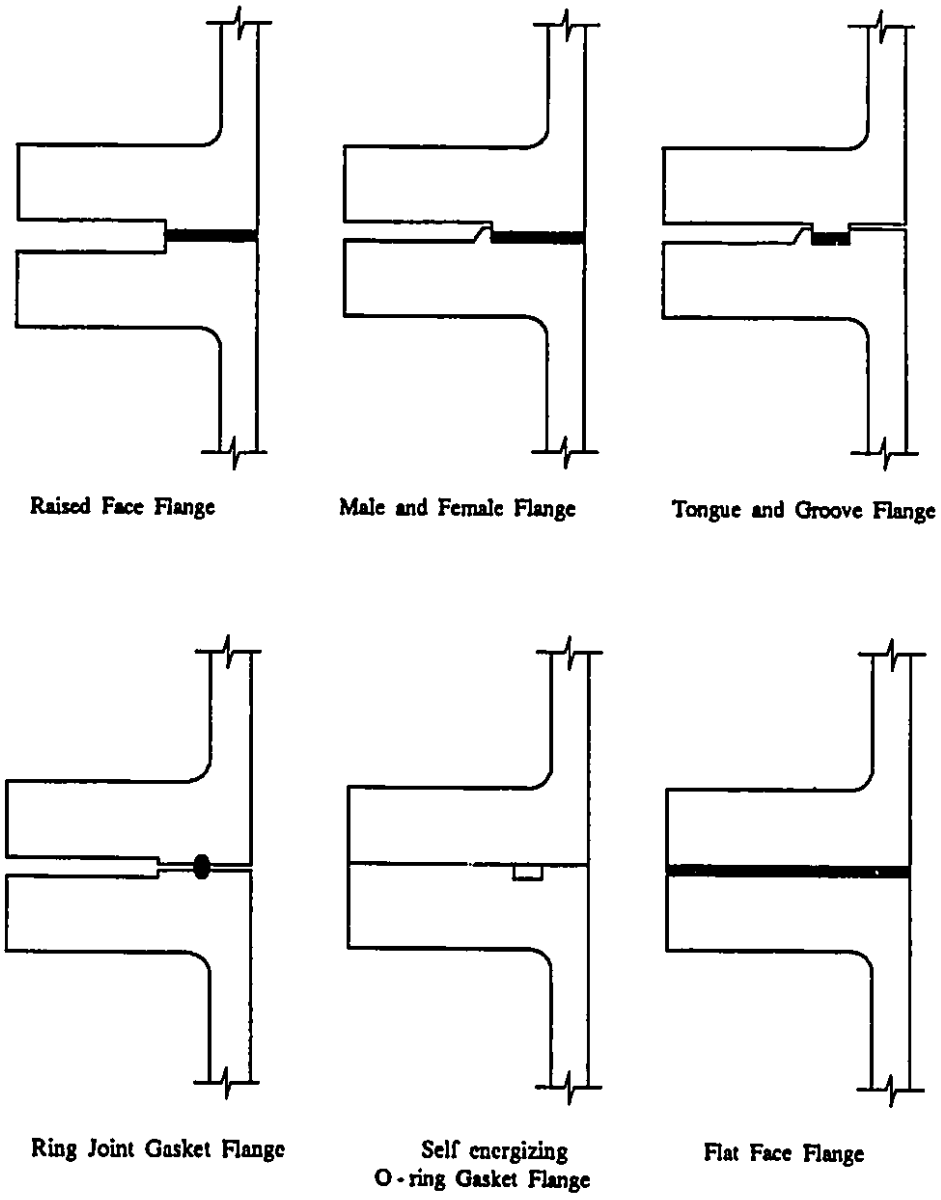

Figure 9: Basic Flange Types

is higher than that of a raised face flange but lower than a tongue and groove flange.

The tongue and groove flange has a recessed grove gasket face and a rib on the mating flange. The gasket is placed into the groove. Being fully supported in the groove, the gasket cannot be pushed out during assembly or in service. The assembly is relatively easy and reliable, the gasket being evenly compressed. However, the disadvantage of this type of flange facing is that the replacement of the gasket is sometimes quite difficult. This type of flange is preferred for use for flammable, explosive and toxic fluids.

A very popular flange facing is the ring joint, using a soft metal ring of oval or octogonal cross section in two identical grooves in the flange faces. This joint seals by deforming the metal gasket into the grooves on the flanges. This type of gasket is popular for rugged environment such as oil fields and refineries. It is also the preferred method for high pressure flanges.

The o-ring (or V ring) gasket flange employs a soft gasket made of materials capable of self-energizing, and metal-to-metal contact outside the bolt circle. The flange rotation is thus greatly limited. This type of flange is rarely used in FRP connections, because of the fabrication accuracy required for the gasket groove in order to provide a tight joint. The grooving of the flange surface if a corrosion resistant liner is used may be a source of concern. Nevertheless, for FRP pressure vessel and piping applications for high pressure, o-ring gasketed flanges can be considered an alternative to the flat face gasketed flange.

The flat face flange provides the benefit of limiting the flange bending due to bolt-up as the o-ring gasket flange does. It is common practice to use full face gaskets for FRP flanged connections, similar to cast iron and other brittle materials. Because of the large area of contact surface for a full face gasket, high bolt seating force is required. Thus this flange facing is preferred for low pressure application with soft gaskets.

The full face gasket acts as an elastic foundation underneath the circular plate subjected to bolt force and pressure loads. Two methods of analysis exist, one by Taylor Forge [6], the other by Blach [19]. The stress analysis within the plate is too complicated to permit an exact solution without any simplification.

4.2 Gasket Compression

The full face gasket is compressed unevenly under the flange. In order to avoid leakage, the gasket section inside the bolt circle must be in compression all the time, and be tight enough to resist the fluid pressure from inside.

During flange bolt-up, the gasket is fully compressed. When the flange connection is gradually pressurized, the flanges rotate and the inside region of the compressed gasket will unload. When the pressure further increases, more of the gasket will lose contact pressure and leakage will start when the bolt holes are reached.

The following Figure 10 shows the three phases of assumed gasket compression starting from bolt-up to operating(pressurized) to leakage.

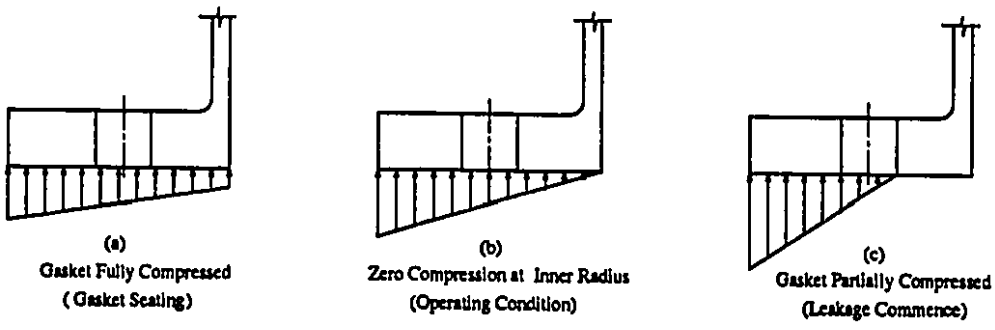

Figure 10: Assumed Gasket Compression

The first two phases (a) and (b) will be considered as bases for flange analysis. Phase (c) is to be ruled out for safety reason. When leakage commences, the flange connection is generally considered a failure.

When a flange is relatively thick and stiff when compared to the gasket, which is usually the case with FRP flanges, the assumption of linear deflection of the flange is justifiable.

The linearized triangular gasket force distribution allows a static solution of the complex problem.

To experimentally verify this assumption, an electrical sensor measuring system manufactured by Force Image Technologies, U.S. is on the market [34]. It is claimed that this sensor is able to measure and record stress distribution during the gasket's loading and unloading cycle. The stress measurement is obtained with a change of the electrical conduct resistance in a thin flexible film placed between gasket and flanges. The sensor is available in many sizes with enough electrical pressure responsive contact points to be capable of monitoring various stresses in three dimensions. The unloading of a gasket due to hydrostatic forces, thermal motions, and external loads can thus be observed and measured.

4.3 Flange Geometry

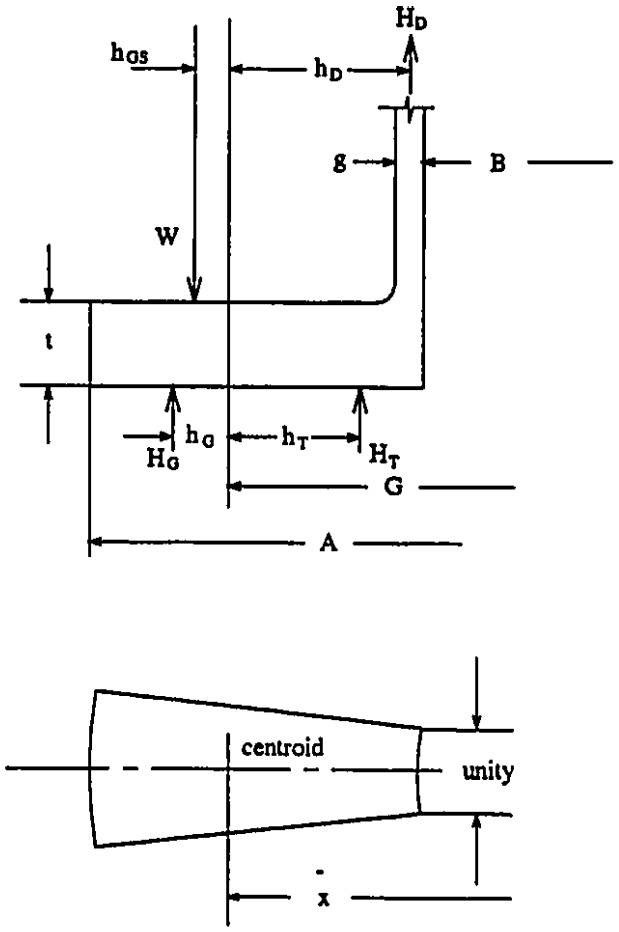

Figure 11: Flange Geometry

Flange geometry is shown in Figure 11. For a flange with a full face gasket, the centroid of a circular sector of unit width is taken as the equilibrium pivot. The location of this centroid is given below.

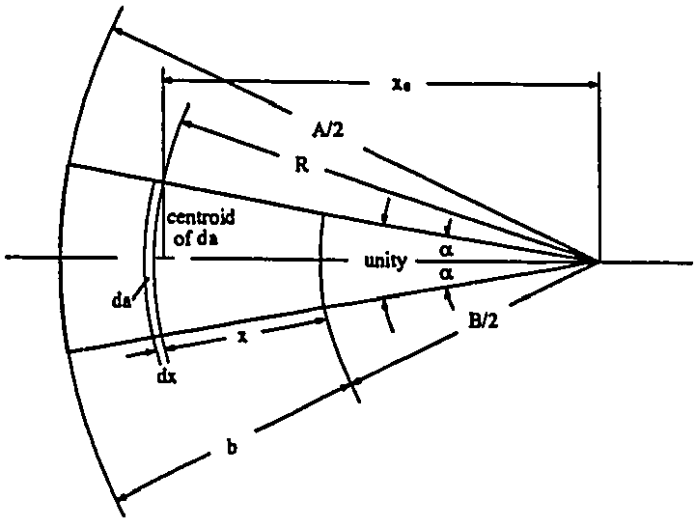

Figure 12: Centroid of Unit Sector

For an area of da as shown in Figure 12, the centroid is

$$x_0 = R\frac{\sin\alpha}{\alpha} = \frac{\sin\alpha}{\alpha}(\frac{B}{2} + x) \tag{21}$$

$$\alpha = \frac{1}{B} \tag{22}$$

$$b = \frac{1}{2}(A - B) \tag{23}$$

The area of the sector of unit width is

$$da = 2R\alpha dx = 2\alpha(\frac{B}{2} + x)dx \tag{24}$$

$$\begin{aligned} a &= 2\alpha\int_0^b(\frac{B}{2} + x)dx = 2\alpha[\frac{Bb}{2} + \frac{b^2}{2}] \\ &= \alpha b(B + b) \end{aligned} \tag{25}$$

The centroid of the total area then is

$$\begin{aligned}\bar{x} &= \frac{1}{a}\int da x_0 = \frac{1}{a}\int_0^b 2\sin\alpha(\frac{B}{2}+x)^2 dx \\ &= \frac{2\sin\alpha}{\alpha b(B+b)}[\frac{B^2 b}{4}+\frac{Bb^2}{2}+\frac{b^3}{3}] \\ &= B\frac{\sin\alpha}{3\alpha}(1+\frac{K^2}{K+1}) \end{aligned} \tag{26}$$

where

$$K = \frac{A}{B} \tag{27}$$

The effective diameter G is

$$\begin{aligned} G &= 2\bar{x} \\ &= B\frac{2\sin\alpha}{3\alpha}(1+\frac{K^2}{K+1}) \\ &= \frac{2B^2}{3}\sin(\frac{1}{B})(1+\frac{K^2}{K+1}) \end{aligned} \tag{28}$$

4.4 Flange Moments

4.4.1 Operating Condition

Hydrostatic Force Under Gasket

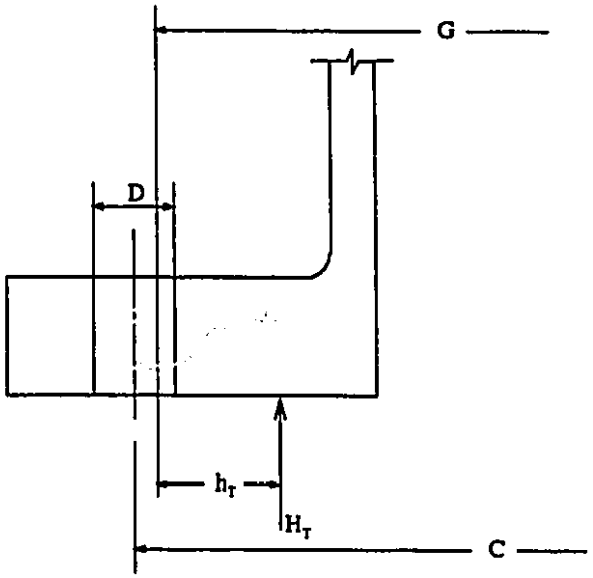

Figure 13: Hydrostatic Force Under Gasket

For full face gaskets, the hydrostatic force is represented by an additional load, presumed to be acting in the area between the inside diameter of the flange and bolt holes, about one half this gasket contact area. Interested reader may see discussion in Blach [16].

Figure 13 shows the hydrostatic force applied under the gasket. The maximum hydrostatic force under the gasket before leakage commences and the moment arm are

$$H_T = \frac{\pi}{4}[(C-D)^2 - B^2]p \tag{29}$$

$$h_T = \frac{1}{4}(2G - B - C + D) \tag{30}$$

The moment due to the hydrostatic force under the gasket is

$$M_T = H_T h_T \tag{31}$$

Hydrostatic End Force

The hydrostatic end force acting on the vessel of inside diameter B is

$$H_D = \frac{\pi}{4} B^2 p \tag{32}$$

From Figure 11 , the moment arm is

$$h_D = \frac{1}{2}(G - B - g) \tag{33}$$

The moment due to the hydrostatic end force is therefore

$$M_D = H_D h_D \tag{34}$$

Centroid of Gasket Force

Figure 14 shows the nomenclature used in calculating the centroid of the gasket force of a sectorial wedge.

As displayed in this figure:

$$x_0 = \frac{\sin\alpha}{\alpha}(\frac{B}{2} + x) \tag{35}$$

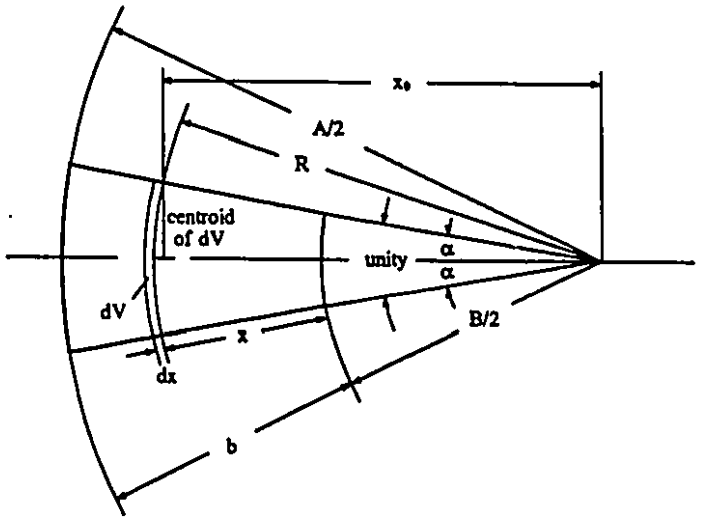

Figure 14: Centroid of Gasket Force

$$dV = 2R\alpha(\frac{2x\sigma_G}{b})dx = \frac{2\alpha\sigma_G}{b}(Bx + 2x^2)dx \tag{36}$$

$$\begin{aligned} V &= \frac{2\alpha\sigma_G}{b}\int_o^b (Bx + 2x^2)dx = \frac{2\alpha\sigma_G}{b}[\frac{Bb^2}{2} + \frac{2b^3}{3}] \\ &= \frac{\sigma_G b}{3}(1 + 2K) \end{aligned} \tag{37}$$

where V is the "volume" of the gasket compression force sectorial wedge shown above, and σ_G the gasket compression stress.

The centroid is found as follows

$$\begin{aligned} \bar{x} &= \frac{1}{V}\int dV x_0 = \frac{1}{V}\int_0^b \frac{4\alpha\sigma_G}{b}\frac{\sin\alpha}{\alpha}(\frac{B}{2} + x)^2 x dx \\ &= \frac{3}{\alpha\sigma_G b(3B + 4b)}\frac{4\alpha\sigma_G \sin\alpha}{\alpha b}\int_0^b (\frac{B^2 x}{4} + Bx^2 + x^3)dx \end{aligned}$$

$$
\begin{aligned}
&= \frac{12\sin\alpha}{\alpha b^2(3B+4b)}[\frac{B^2b^2}{8}+\frac{Bb^3}{3}+\frac{b^4}{4}] \\
&= \frac{\sin\alpha}{2\alpha(3B+4b)}[3B^2+8Bb+6b^2] \\
&= \frac{B^2}{4}\sin(\frac{1}{B})(1+\frac{3K^2}{1+2K}) \qquad (38)
\end{aligned}
$$

where K is the ratio of flange diameters defined in Equation 27.

The moment arm is

$$
\begin{aligned}
h_G &= \bar{x}-\frac{G}{2} \\
&= \frac{B^2}{4}\sin(\frac{1}{B})(1+\frac{3K^2}{1+2K})-\frac{G}{2} \qquad (39)
\end{aligned}
$$

and

$$h_{GS}=\frac{1}{2}(C-G) \qquad (40)$$

For the operating condition, the bolt load on the flange is

$$W = H_D + H_T + H_G \qquad (41)$$

The total flange moment about the bolt circle is

$$
\begin{aligned}
M_0 &= H_D h_D + H_T h_T + W h_{GS} - H_G h_G \\
&= M_D + M_T + (H_D + H_T + H_G)h_{GS} - M_G \\
&= M_D + M_T + (H_D + H_T)h_{GS} - (1-\frac{h_{GS}}{h_G})M_G \qquad (42)
\end{aligned}
$$

or

$$M_0 = M_D + M_T + M_B - \eta M_G \tag{43}$$

where

$$M_B = (H_D + H_T)h_{GS} \tag{44}$$

$$\eta = 1 - \frac{h_{GS}}{h_G} \tag{45}$$

Only H_G, M_G are unknown and will be determined later.

4.4.2 Gasket Seating Condition

For the gasket seating (bolt-up) condition, as shown in Figure 15, the bolting force is taken as the total bolt area times the maximum allowable stress of the bolt material.

$$H_{GS} = A_b S_a \tag{46}$$

The moment arm is

$$h_{GS} = \frac{1}{2}(C - G) \tag{47}$$

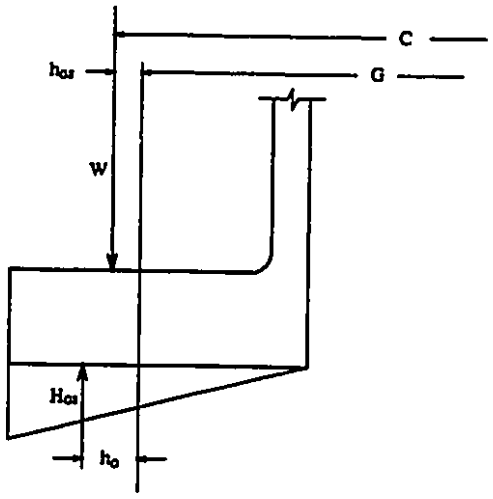

Figure 15: Gasket Load, Bolt-up

The total external moment due to bolting force then is

$$M_{GS} = H_{GS} h_{GS} \tag{48}$$

and the total flange moment

$$M_0^* = M_{GS} - M_G^* \tag{49}$$

where the gasket compression moment M_G^* is unknown and will be determined later in the flange-shell continuity equation.

4.5 Flange Rotation - Gasket Compression

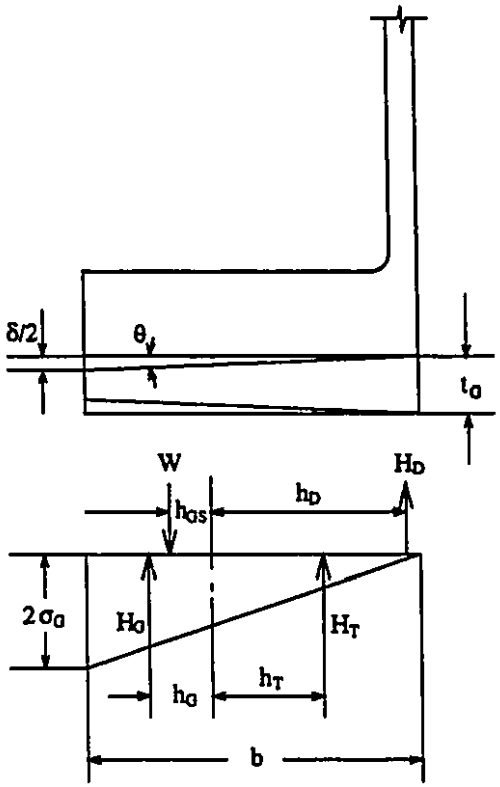

Figure 16: Flange Rotation - Gasket Compression (operating)

When the flange is treated as rigid body, as shown in Figure 16, its rotation can be expressed by gasket compression moments as following:

The relation of H_G, the gasket load and σ_G, the gasket compression can be found using Figure 16 and Equation 37, assuming rotation of the flange about its centroid [16]:

$$\frac{H_G}{G\pi} = \frac{\sigma_G b}{3}(1 + 2K) \tag{50}$$

or

$$\sigma_G = \frac{3}{1+2K}\frac{H_G}{G\pi b} \tag{51}$$

σ_G is also related to gasket deflection δ as:

$$\sigma_G = \frac{\delta E_G}{t_G} \tag{52}$$

where E_G is the modulus of the gasket and t_G the gasket thickness. The flange rotation θ is

$$\theta = \frac{\delta}{b} \tag{53}$$

Substituting Equations 52 and 53 into 51, we have

$$\theta = \frac{\sigma_G t_G}{E_G b} = \frac{t_G}{E_G b}\frac{3}{1+2K}\frac{H_G}{G\pi b} \tag{54}$$

or

$$\theta = \frac{3}{1+2K}\frac{M_G t_G}{G\pi E_G b^2 h_G} \tag{55}$$

For the bolt-up condition, M_G in Equation 55 is replaced by M_G^*.

4.6 Summary

Due to the complexity of the problem, certain simplifying assumptions in this chapter were made to arrive at manageable equations. The effects of these assumptions on the accuracy of the method are believed to be within tolerable limits.

The assumption of gasket compression in this chapter is one of the key aspects in dealing with full face gasketed flange. A rather safe FRP flange design based on this assumption can be expected.

Chapter 5

LAMINATION ANALYSIS

5.1 Introduction

The theory of laminated plates and shells includes the theories of ordinary shells, flat plates and curved beams as special cases. A number of theories were developed originally for thin plates and shells, and are based on the Kirchhoff-Love hypothesis that straight lines normal to the middle surface remain straight after deformation and undergo no thickness stretching. In the Kirchhoff-Love hypothesis, the transverse shear deformation is neglected. However, since the side-to-thickness ratio of the plate or shell is usually large for low to medium pressure flange application, the classical theory is expected to yield preliminary results for laminated flanged connections presently used.

Although there exist many references on laminated plate and shell theory, no existing formulae can be found for the special case of FRP flanged connections. It is necessary to derive such equations from basic principles in order to solve the problem of FRP flange analysis.

Basic knowledge on laminate theory and mechanics of composite material can be found in [7] [43] [81] [82].

5.2 Flange Equations

The laminated flange is modeled as a circular plate subjected to circular line loads vertical to the plate plane on its free inner edge, while the plate is balanced by simple support with its outer edge, as shown in Figure 17.

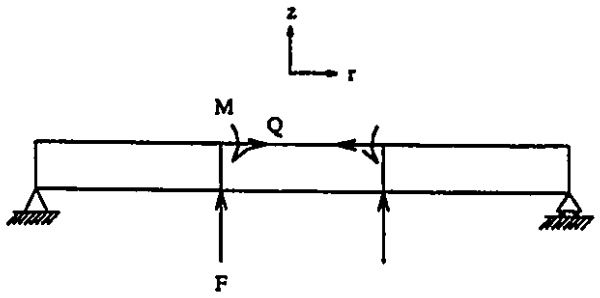

Figure 17: Flange Plate

The displacement field in the classical theory of axisymmetric bending of circular plates is

$$\begin{aligned} u^f(r,z) &= u_0^f(r) + z \times \psi(r) \\ v^f(r,z) &= 0 \\ w^f(r,z) &= w_0^f(r) \end{aligned} \tag{56}$$

where u^f, v^f and w^f represent the flange displacements in the r, θ and z direction respectively; the midplane displacements are symbolized by a subscript o; and the displacement function $\psi(r)$ will be determined later.

According to the strain-displacement relation, Equation 3, the strains for this displacement field are

$$\begin{aligned}
\varepsilon_r &= \frac{du_0^f}{dr} + z\frac{d\psi}{dr} \\
\varepsilon_\theta &= \frac{u_0^f}{r} + z\frac{\psi}{r} \\
\varepsilon_{rz} &= \frac{1}{2}(\psi + \frac{dw_0^f}{dr}) \\
\varepsilon_z &= 0 \\
\varepsilon_{\theta z} &= 0 \\
\varepsilon_{r\theta} &= 0
\end{aligned} \tag{57}$$

Above expressions for the displacement field and the strains in terms of displacements, can also be used for a shear deformable (first order) plate theory in which the transverse shear strain is retained. Retaining the transverse shear strain in the derivation of certain equations in this chapter, enable us to make correct use of the energy method.

The variations in strains are

$$\begin{aligned}
\delta\varepsilon_r &= \frac{d}{dr}(\delta u_0^f) + z\frac{d}{dr}(\delta\psi) \\
\delta\varepsilon_\theta &= \frac{\delta u_0^f}{r} + \frac{z}{r}\delta\psi \\
\delta\varepsilon_{rz} &= \frac{1}{2}[\delta\psi + \frac{d}{dr}(\delta w_0^f)] \\
\delta\varepsilon_z &= 0 \\
\delta\varepsilon_{\theta z} &= 0 \\
\delta\varepsilon_{r\theta} &= 0
\end{aligned} \tag{58}$$

To derive the governing equilibrium equations of the classic laminate plate theory, the principal of minimum total potential energy is used. For the circular plate of linear elastic behavior, the strain energy within the plate is:

$$U = \frac{1}{2}\int_0^{2\pi}\int_{\frac{B}{2}}^{\frac{A}{2}}\int_{-\frac{t}{2}}^{\frac{t}{2}}(\sigma_r\varepsilon_r + \sigma_\theta\varepsilon_\theta + 2\sigma_{r\theta}\varepsilon_{r\theta} + 2\sigma_{rz}\varepsilon_{rz} + 2\sigma_{\theta z}\varepsilon_{\theta z})dzrdrd\theta \tag{59}$$

where A and B are outside and inside diameters of the flange, respectively. After retaining only nonzero terms and integrating with respect to θ, the following is obtained:

$$U = \pi\int_{\frac{B}{2}}^{\frac{A}{2}}\int_{-\frac{t}{2}}^{\frac{t}{2}}(\sigma_r\varepsilon_r + \sigma_\theta\varepsilon_\theta + 2\sigma_{rz}\varepsilon_{rz})dzrdr \tag{60}$$

From Equation 20 , the variation of strain energy takes the form

$$\delta U = 2\pi\int_{\frac{B}{2}}^{\frac{A}{2}}\int_{-\frac{t}{2}}^{\frac{t}{2}}(\sigma_r\delta\varepsilon_r + \sigma_\theta\delta\varepsilon_\theta + 2\sigma_{rz}\delta\varepsilon_{rz})dzrdr \tag{61}$$

Now replacing the strains with the strain variations, Equation 58, the following is obtained:

$$\delta U = 2\pi\int_{\frac{B}{2}}^{\frac{A}{2}}\int_{-\frac{t}{2}}^{\frac{t}{2}}[\sigma_r\frac{d}{dr}\delta u_0^f + \sigma_r z\frac{d}{dr}\delta\psi + \sigma_\theta\frac{1}{r}\delta u_0^f + \sigma_\theta z\frac{1}{r}\delta\psi + \sigma_{rz}\delta\psi + \sigma_{rz}\frac{d}{dr}\delta w_0^f]dzrdr \tag{62}$$

Now the inplane stress resultants are introduced:

$$N_r = \int_{-\frac{t}{2}}^{\frac{t}{2}}\sigma_r dz \tag{63}$$

$$N_\theta = \int_{-\frac{t}{2}}^{\frac{t}{2}}\sigma_\theta dz \tag{64}$$

and the bending moment resultants

$$M_r = \int_{-\frac{t}{2}}^{\frac{t}{2}}\sigma_r z dz \tag{65}$$

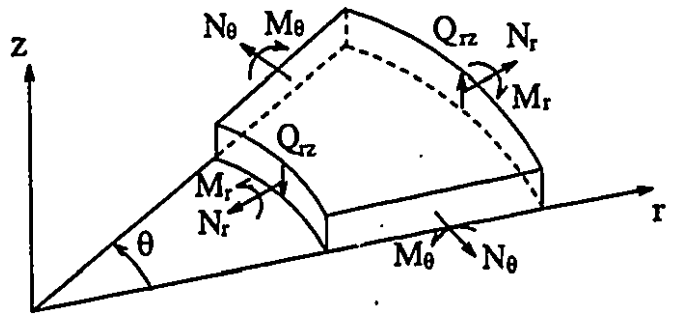

Figure 18: Flange Stress Resultants

$$M_\theta = \int_{-\frac{t}{2}}^{\frac{t}{2}} \sigma_\theta z dz \tag{66}$$

also the shear force resultants

$$Q_{rz} = \int_{-\frac{t}{2}}^{\frac{t}{2}} \sigma_{rz} dz \tag{67}$$

Integrating with respect to z in Equation 62 while noting that u_0^f, ψ, w_0^f are not functions of z and using the above nomenclature, the following is obtained:

$$\delta U = 2\pi \int_{\frac{B}{2}}^{\frac{A}{2}} [N_r \frac{d}{dr}\delta u_0^f + M_r \frac{d}{dr}\delta\psi + N_\theta \frac{1}{r}\delta u_0^f + M_\theta \frac{1}{r}\delta\psi + Q_{rz}\delta\psi + Q_{rz}\frac{d}{dr}\delta w_0^f] r dr \tag{68}$$

Note next that the variation of work done by flange external forces is:

$$\delta V = 2\pi \frac{B}{2}(-pt + Q)\delta u_0^f(\frac{B}{2}) + 2\pi \frac{B}{2}(M + \frac{Qt}{2})\delta\psi(\frac{B}{2}) - 2\pi(\frac{BF}{2})\delta w_0^f(\frac{B}{2}) \tag{69}$$

where p is internal pressure, Q discontinuity force, M discontinuity moment and F

flange rotation force.

For the variation of total potential energy, the following is obtained:

$$\delta(U+V) =$$
$$2\pi\int_{\frac{B}{2}}^{\frac{A}{2}}[N_r\frac{d}{dr}\delta u_0^f + M_r\frac{d}{dr}\delta\psi + N_\theta\frac{1}{r}\delta u_0^f + M_\theta\frac{1}{r}\delta\psi Q_{rz}\delta\psi + Q_{rz}\frac{d}{dr}\delta w_0^f]rdr$$
$$+2\pi\frac{B}{2}(-pt+Q)\delta u_0^f(\frac{B}{2}) + 2\pi\frac{B}{2}(M+\frac{Qt}{2})\delta\psi(\frac{B}{2}) - 2\pi(\frac{BF}{2})\delta w_0^f(\frac{B}{2}) = 0 \tag{70}$$

This may be written as

$$\int_{\frac{B}{2}}^{\frac{A}{2}}[rN_r\frac{d}{dr}\delta u_0^f + rM_r\frac{d}{dr}\delta\psi + N_\theta\delta u_0^f + M_\theta\delta\psi + rQ_{rz}\delta\psi + rQ_{rz}\frac{d}{dr}\delta w_0^f]dr$$
$$+\frac{B}{2}(-pt+Q)\delta u_0^f(\frac{B}{2}) + \frac{B}{2}(M+\frac{Qt}{2})\delta\psi(\frac{B}{2}) - (\frac{BF}{2})\delta w_0^f(\frac{B}{2}) = 0 \tag{71}$$

Integration by parts, and collecting coefficients of δu_0, $\delta\psi$ and δw_0, the following is obtained:

$$\int_{\frac{B}{2}}^{\frac{A}{2}}[N_\theta - \frac{d}{dr}(rN_r)]\delta u_0^f dr + \int_{\frac{B}{2}}^{\frac{A}{2}}[M_\theta + rQ_{rz} - \frac{d}{dr}(rM_r)]\delta\psi dr$$
$$-\int_{\frac{B}{2}}^{\frac{A}{2}}[rQ_{rz}]\delta w_0^f dr + rN_r\delta u_0^f|_{\frac{B}{2}}^{\frac{A}{2}} + rM_r\delta\psi|_{\frac{B}{2}}^{\frac{A}{2}} + rQ_{rz}\delta w_0^f|_{\frac{B}{2}}^{\frac{A}{2}}$$
$$+\frac{B}{2}(-pt+Q)\delta u_0^f(\frac{B}{2}) + \frac{B}{2}(M+\frac{Qt}{2})\delta\psi(\frac{B}{2}) - (\frac{BF}{2})\delta w_0^f(\frac{B}{2}) = 0 \tag{72}$$

The equations of equilibrium are then obtained

$$\delta u_0^f \;:\; N_\theta - \frac{d(rN_r)}{dr} = 0 \tag{73}$$

$$\delta\psi \;:\; M_\theta + rQ_{rz} - \frac{d}{dr}(rM_r) = 0 \tag{74}$$

$$\delta w_0^f \;:\; \frac{d}{dr}(rQ_{rz}) = 0 \tag{75}$$

Also the edge boundary condition.

At $r = \frac{B}{2}$,

$$rN_r = \frac{B}{2}(-pt + Q) \tag{76}$$

$$rM_r = \frac{B}{2}(M + \frac{Qt}{2}) \tag{77}$$

$$rQ_{rz} = -\frac{BF}{2} \tag{78}$$

At $r = \frac{A}{2}$,

$$N_r = 0 \tag{79}$$

$$M_r = 0 \tag{80}$$

$$w_0^f = 0 \tag{81}$$

In order to express the plate equations in terms of displacements, note from Hooke's law Equation 6 and the strain expressions, Equation 57, that

$$\begin{aligned} N_r &= \int_{-\frac{t}{2}}^{\frac{t}{2}} \sigma_r dz = \int_{-\frac{t}{2}}^{\frac{t}{2}} (Q_{rr}\varepsilon_r + Q_{r\theta}\varepsilon_\theta) dz \\ &= \int_{-\frac{t}{2}}^{\frac{t}{2}} [Q_{rr}(\frac{du_0^f}{dr} + z\frac{d\psi}{dr}) + Q_{r\theta}(\frac{u_0^f}{r} + \frac{z}{r}\psi)] dz \\ &= \frac{du_0^f}{dr}A_{rr} + \frac{d\psi}{dr}B_{rr} + \frac{u_0^f}{r}A_{r\theta} + \frac{\psi}{r}B_{r\theta} \end{aligned} \tag{82}$$

Similarly

$$N_\theta = \frac{u_0^f}{r}A_{\theta v} + \frac{\psi}{r}B_{\theta\theta} + \frac{du_0^f}{dr}A_{r\theta} + \frac{d\psi}{dr}B_{r\theta} \quad (83)$$

$$M_r = \frac{du_0^f}{dr}B_{rr} + \frac{d\psi}{dr}D_{rr} + \frac{u_0^f}{r}B_{r\theta} + \frac{\psi}{r}D_{r\theta} \quad (84)$$

$$M_\theta = \frac{u_0^f}{r}B_{\theta\theta} + \frac{\psi}{r}D_{\theta\theta} + \frac{du_0^f}{dr}B_{r\theta} + \frac{d\psi}{dr}D_{r\theta} \quad (85)$$

$$Q_{rz} = \frac{1}{2}(\psi + \frac{dw_0^f}{dr})A_{rz} \quad (86)$$

where the plate stiffnesses are

$$(A_{rr}, A_{r\theta}, A_{\theta\theta}) = \int_{-\frac{t}{2}}^{\frac{t}{2}}((Q_{rr}, Q_{r\theta}, Q_{\theta\theta}))dz \quad (87)$$

$$(B_{rr}, B_{r\theta}, B_{\theta\theta}) = \int_{-\frac{t}{2}}^{\frac{t}{2}}((Q_{rr}, Q_{r\theta}, Q_{\theta\theta}))zdz \quad (88)$$

$$(D_{rr}, D_{r\theta}, D_{\theta\theta}) = \int_{-\frac{t}{2}}^{\frac{t}{2}}((Q_{rr}, Q_{r\theta}, Q_{\theta\theta}))z^2dz \quad (89)$$

$$A_{rz} = \int_{-\frac{t}{2}}^{\frac{t}{2}} Q_{rz}dz \quad (90)$$

When the material properties are symmetrical about plate midplane, the stiffnesses

$$B_{rr} = B_{r\theta} = B_{\theta\theta} = 0 \quad (91)$$

Then the stress resultants in Equations 82 to 86 can be simplified to

$$N_r = \frac{du_0^f}{dr}A_{rr} + \frac{u_0^f}{r}A_{r\theta} \quad (92)$$

$$N_\theta = \frac{u_0^f}{r}A_{\theta\theta} + \frac{du_0^f}{dr}A_{r\theta} \quad (93)$$

$$M_r = \frac{d\psi}{dr}D_{rr} + \frac{\psi}{r}D_{r\theta} \quad (94)$$

$$M_\theta = \frac{\psi}{r}D_{\theta\theta} + \frac{d\psi}{dr}D_{r\theta} \quad (95)$$

$$Q_{rz} = \frac{1}{2}(\psi + \frac{dw_0^f}{dr})A_{rz} \quad (96)$$

The plate stretching and bending effects are thus uncoupled due to midplane symmetry. The Equilibrium Equations 73 , 74 and 75 can now be explained as follows, using the preceding results for $N_r, N_\theta, M_r, M_\theta$ and Q_{rz}:

For Equation 73, there is

$$\delta u_0^f : r^2\frac{d^2u_0^f}{dr^2} + r\frac{du_0^f}{dr} - \frac{A_{\theta\theta}}{A_{rr}}u_0^f = 0 \quad (97)$$

Noting the boundary condition at $r = \frac{B}{2}$

$$rQ_{rz} = -\frac{BF}{2} \quad (98)$$

This holds for Equation 75. Equation 74 can be written as

$$r\frac{d^2\psi}{dr^2} + \frac{d\psi}{dr} - \frac{D_{\theta\theta}}{D_{rr}}\frac{\psi}{r} = -\frac{BF}{2D_{rr}} \quad (99)$$

The solution of Equation 97, upon imposing boundary condition, is given as

$$u_0^f = \frac{(pt-Q)(\frac{A}{2})^{m_2-1}}{4(A_{r\theta}+\sqrt{A_{rr}A_{\theta\theta}})\Delta}r^{m_1} + \frac{(-pt+Q)(\frac{A}{2})^{m_1-1}}{4(A_{r\theta}-\sqrt{A_{rr}A_{\theta\theta}})\Delta}r^{m_2} \quad (100)$$

where

$$\begin{aligned} m_1 &= \sqrt{\frac{A_{\theta\theta}}{A_{rr}}} \\ m_2 &= -m_1 \\ \Delta &= A^{m_1-1}B^{m_2-1} - A^{m_2-1}B^{m_1-1} \end{aligned} \tag{101}$$

If the plate possesses equivalent elastic properties in the radial and tangential directions, i.e. $A_{\theta\theta} = A_{rr}$, the solution is reduced to

$$\begin{aligned} m_1 &= -m_2 = 1 \\ \Delta &= B^{-2} - A^{-2} = \frac{A^2 - B^2}{A^2B^2} \\ u_0^f &= \frac{(pt-Q)B^2}{(A_{r\theta}+A_{rr})(A^2-B^2)}r + \frac{(-pt+Q)A^2B^2}{4(A_{r\theta}-A_{rr})(A^2-B^2)}\frac{1}{r} \end{aligned} \tag{102}$$

Identically, if $D_{\theta\theta} = D_{rr}$, the solution of Equation 99 is then

$$\psi = -\frac{BF}{8D_{rr}}(2rlnr - r) - \frac{c_1}{2}r - \frac{c_2}{r} \tag{103}$$

and its derivative is

$$\frac{d\psi}{dr} = -\frac{BF}{8D_{rr}}(2lnr + 1) - \frac{c_1}{2} + \frac{c_2}{r^2} \tag{104}$$

where the integral constants c_1,c_2 will be determined from the boundary conditions, Equations 77 and 80. They are

$$M_r|_{r=\frac{B}{2}} = (\frac{d\psi}{dr}D_{rr} + \frac{\psi}{r}D_{r\theta})|_{r=\frac{B}{2}} = M + \frac{Qt}{2} \tag{105}$$

$$M_r|_{r=\frac{A}{2}} = (\frac{d\psi}{dr}D_{rr} + \frac{\psi}{r}D_{r\theta})|_{r=\frac{A}{2}} = 0 \tag{106}$$

This can be expanded as

$$-c_1(\frac{D_{rr}}{2}+\frac{D_{r\theta}}{2}) + c_2(\frac{4D_{rr}}{B^2}-\frac{4D_{r\theta}}{B^2}) - \frac{BF}{8}(2\ln\frac{B}{2}+2\frac{D_{r\theta}}{D_{rr}}\ln\frac{B}{2}+1-\frac{D_{r\theta}}{D_{rr}}) = M+\frac{Qt}{2} \tag{107}$$

$$-c_1(\frac{D_{rr}}{2}+\frac{D_{r\theta}}{2}) + c_2(\frac{4D_{rr}}{A^2}-\frac{4D_{r\theta}}{A^2}) - \frac{BF}{8}(2\ln\frac{A}{2}+2\frac{D_{r\theta}}{D_{rr}}\ln\frac{A}{2}+1-\frac{D_{r\theta}}{D_{rr}}) = 0 \tag{108}$$

from which, the following is obtained:

$$\begin{aligned} c_1 = \quad & \frac{-A^2B^2}{2(B^2-A^2)(D_{rr}+D_{r\theta})} \times \\ & \{F[\frac{B}{2A^2}(2\ln\frac{B}{2}+2\frac{D_{r\theta}}{D_{rr}}\ln\frac{B}{2}+1-\frac{D_{r\theta}}{D_{rr}}) \\ & -\frac{1}{2B}(2\ln\frac{A}{2}+2\frac{D_{r\theta}}{D_{rr}}\ln\frac{A}{2}+1-\frac{D_{r\theta}}{D_{rr}})] + M\frac{4}{A^2}+\frac{Qt}{2}\frac{4}{A^2}\} \end{aligned} \tag{109}$$

$$\begin{aligned} c_2 = \quad & \frac{A^2B^2}{4(B^2-A^2)(D_{rr}-D_{r\theta})} \times \\ & [\frac{BF}{8}(2\ln\frac{A}{2}-2\ln\frac{B}{2}+2\frac{D_{r\theta}}{D_{rr}}\ln\frac{A}{2}-2\frac{D_{r\theta}}{D_{rr}}\ln\frac{B}{2})-M-\frac{Qt}{2}] \end{aligned} \tag{110}$$

The flange rotation from Equation 103 then transforms into

$$\begin{aligned} \psi = \quad & -\frac{BF}{8D_{rr}}(2rlnr-r) \\ & +\frac{A^2B^2r}{4(B^2-A^2)(D_{rr}+D_{r\theta})} \times \\ & \{F[\frac{B}{2A^2}(2\ln\frac{B}{2}+2\frac{D_{r\theta}}{D_{rr}}\ln\frac{B}{2}+1-\frac{D_{r\theta}}{D_{rr}}) \end{aligned}$$

$$
\begin{aligned}
&- \frac{1}{2B}(2\ln\frac{A}{2} + 2\frac{D_{r\theta}}{D_{rr}}\ln\frac{A}{2} + 1 - \frac{D_{r\theta}}{D_{rr}})] + M\frac{4}{A^2} + \frac{Qt}{2}\frac{4}{A^2}\} \\
&- \frac{A^2B^2}{4(B^2-A^2)(D_{rr}-D_{r\theta})r} \times \\
&\quad [\frac{BF}{8}(2\ln\frac{A}{2} - 2\ln\frac{B}{2} + 2\frac{D_{r\theta}}{D_{rr}}\ln\frac{A}{2} \\
&- 2\frac{D_{r\theta}}{D_{rr}}\ln\frac{B}{2}) - M - \frac{Qt}{2}]
\end{aligned} \tag{111}
$$

Load F may be substituted by:

$$F = \frac{2}{A-B}(\frac{M_0}{B\pi}) \tag{112}$$

where $(A-B)/2$ is the width of the flange and M_0 is the total flange bending moment causing the rotation of the flange ring. The formulae of the total bending moment can be found in Chapter 4, Section 4 for operating and gasket seating conditions.

In Timoshenko [80] and the ASME Code [1], for isotropic material flange design with ring gaskets and in Blach [19] with full face gaskets, the total bending moment is replaced by the twisting couple $F \times b$ in a way such that:

$$F \times b = \frac{M_0}{B\pi} - M - \frac{Qt}{2} \tag{113}$$

Apart from this treatment, the discontinuity loads M and Q are instead split into two boundary forces in the derivation of the flange plate equilibrium equations in this dissertation. The author believes, from the point of view of elasticity, that this adjustment encountered in an energy method is more close to the true nature of the problem concerned.

With this substitution, the following relation for ψ is obtained:

$$\begin{aligned}\psi = \quad & -\frac{M_0}{4(A-B)\pi D_{rr}}(2rlnr - r) \\ & +\frac{A^2B^2r}{4(B^2-A^2)(D_{rr}+D_{r\theta})}\{\frac{2M_0}{(A-B)B\pi}[\frac{B}{2A^2}(2\ln\frac{B}{2}+2\frac{D_{r\theta}}{D_{rr}}\ln\frac{B}{2}+1-\frac{D_{r\theta}}{D_{rr}}) \\ & -\frac{1}{2B}(2\ln\frac{A}{2}+2\frac{D_{r\theta}}{D_{rr}}\ln\frac{A}{2}+1-\frac{D_{r\theta}}{D_{rr}})] + M\frac{4}{A^2}+\frac{Qt}{2}\frac{4}{A^2}\} \\ & -\frac{A^2B^2}{4(B^2-A^2)(D_{rr}-D_{r\theta})r}[\frac{M_0}{4(A-B)\pi}(2\ln\frac{A}{2}-2\ln\frac{B}{2}+2\frac{D_{r\theta}}{D_{rr}}\ln\frac{A}{2} \\ & -2\frac{D_{r\theta}}{D_{rr}}\ln\frac{B}{2}) - M - \frac{Qt}{2}] \end{aligned} \tag{114}$$

Up to this point the classical plate theory simplifications have not been utilized in the derivations of above equations. This implies that the flange displacements and thereafter normal strains in radial and tangential directions obtained here, are the same as those from a shear deformable (first order) theory, since they share the same displacement field at the beginning of the chapter.

Shear deformable (first order) theory recognizes the shear deformation effect which is neglected in classical theory. In classical theory that is:

$$\varepsilon_{rz} = \frac{1}{2}(\psi + \frac{dw_0^f}{dr}) = 0 \tag{115}$$

by which the flange deflection w_0^f in z direction can thus be obtained from integration of function ψ.

5.3 Shell Equations

The laminated cylindrical shell is considered as a semi-infinite shell. It is pressurized from the inside. At the finite end, the shell deformation is constrained by the flange ring. Axial symmetry applies to the shell and its loading forces.

For axial symmetry the displacement field may be written:

$$\begin{aligned} u^s(x,z) &= u_0^s(x) + z\gamma(x) \\ v^s(x,z) &= 0 \\ w^s(x,z) &= w_0^s(x) \end{aligned} \tag{116}$$

Also the strain-displacement relations for the laminated shell, using Equation 3:

$$\begin{aligned} \varepsilon_x &= \frac{\partial u^s}{\partial x} \\ \varepsilon_\theta &= \frac{1}{z}\frac{\partial v^s}{\partial \theta} + \frac{w^s}{r} \\ \varepsilon_z &= \frac{\partial w^s}{\partial z} \\ \varepsilon_{\theta z} &= \frac{1}{2}\left(\frac{1}{z}\frac{\partial w^s}{\partial \theta} + \frac{\partial v^s}{\partial z} - \frac{v^s}{z}\right) \\ \varepsilon_{xz} &= \frac{1}{2}\left(\frac{\partial w^s}{\partial x} + \frac{\partial u^s}{\partial z}\right) \\ \varepsilon_{\theta x} &= \frac{1}{2}\left(\frac{\partial v^s}{\partial x} + \frac{1}{z}\frac{\partial u^s}{\partial \theta}\right) \end{aligned} \tag{117}$$

For a thin laminated shell, the radius r in Equation 117 is taken to be $\frac{B}{2}$ in the following expressions. Because of axial symmetry

$$\frac{\partial}{\partial \theta} = 0 \tag{118}$$

Substituting 116 and 118 into 117 results in corresponding strains

$$\begin{aligned}
\varepsilon_x &= \frac{du_0^s}{dx} + z\frac{d\gamma}{dx} \\
\varepsilon_\theta &= \frac{2w_0^s}{B} \\
\varepsilon_{xz} &= \frac{1}{2}(\gamma + \frac{dw_0^s}{dx}) \\
\varepsilon_z &= 0 \\
\varepsilon_{\theta z} &= 0 \\
\varepsilon_{\theta x} &= 0
\end{aligned} \tag{119}$$

for which the first variations in strains are

$$\begin{aligned}
\delta\varepsilon_x &= \frac{d}{dx}(\delta u_0^s) + z\frac{d}{dx}(\delta\gamma) \\
\delta\varepsilon_\theta &= \frac{2}{B}(\delta w_0^s) \\
\delta\varepsilon_{xz} &= \frac{1}{2}[\delta\gamma + \frac{d}{dx}(\delta w_0^s)]
\end{aligned} \tag{120}$$

The shell in the flange connection is composed of mat layers and woven roving layers. On the inside of the shell, there is usually a layer of corrosion resistant barrier. This barrier is not given credit for load carrying, it is excluded from the upcoming analysis.

The integral equation of the principle of virtual work is:

$$\pi B \int_0^\infty (\sigma_x \delta\varepsilon_x + \sigma_\theta \delta\varepsilon_\theta + 2\sigma_{xz}\delta\varepsilon_{xz})dx - \pi B \int_0^\infty p\delta w_0^s dx = 0 \tag{121}$$

The first integral represents the strain energy contained in the deformed shell, the second integral is the work done by the surface pressure on the shell. The expression may be expanded as:

$$\int_0^\infty dx\{N_x\frac{d}{dx}(\delta u_0^s) + M_x\frac{d}{dx}(\delta\gamma) + N_\theta\frac{2}{B}\delta w_0^s + N_{xz}[\delta\gamma + \frac{d}{dx}(\delta w_0^s)]\} - \int_0^\infty p\delta w_0^s dx = 0 \tag{122}$$

from which the stress resultants are defined:

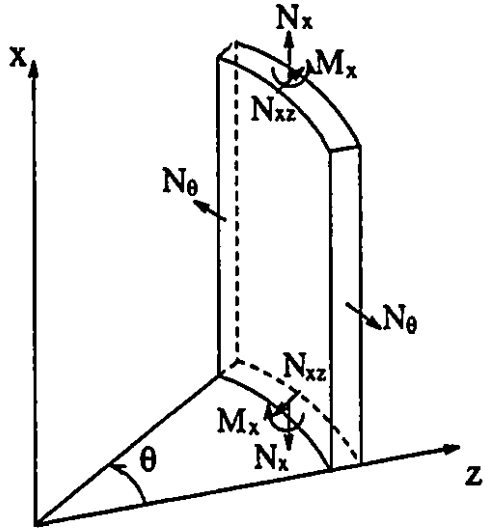

Figure 19: Shell Stress Resultants

$$N_x = \int \sigma_x dz \tag{123}$$

$$M_x = \int \sigma_x z dz \tag{124}$$

$$N_\theta = \int \sigma_\theta dz \tag{125}$$

$$N_{xz} = \int \sigma_{xz} dz \tag{126}$$

The stress resultants are further related to the shell displacements:

$$N_x = \frac{du_0^s}{dx} A_{xx} + \frac{d\gamma}{dx} B_{xx} + \frac{2w_0^s}{B} A_{x\theta} \tag{127}$$

$$N_\theta = \frac{du_0^s}{dx} A_{x\theta} + \frac{d\gamma}{dx} B_{x\theta} + \frac{2w_0^s}{B} A_{\theta\theta} \tag{128}$$

$$N_{xz} = \frac{1}{2}(\gamma + \frac{dw_0^s}{dx}) A_{xz} \tag{129}$$

$$M_x = \frac{du_0^s}{dx} B_{xx} + \frac{d\gamma}{dx} D_{xx} + \frac{2w_0^s}{B} B_{x\theta} \tag{130}$$

The shell stiffnesses are given by:

$$(A_{xx}, A_{x\theta}, A_{\theta\theta}) = \int (Q_{xx}, Q_{x\theta}, Q_{\theta\theta}) dz \tag{131}$$

$$(B_{xx}, B_{x\theta}) = \int (Q_{xx}, Q_{x\theta}) z dz \tag{132}$$

$$D_{xx} = \int Q_{xx} z^2 dz \tag{133}$$

$$A_{xz} = \int Q_{xz} dz \tag{134}$$

Integrating equation 122 by parts, and collecting coefficients of δu_0^s, δw_0^s and $\delta\gamma$, the following is obtained:

$$\begin{aligned} \int_0^\infty dx \quad & \{-\delta u_0^s \frac{dN_x}{dx} + \delta w_0^s (\frac{2N_\theta}{B} - \frac{dN_{xz}}{dx} - p) \\ & + \delta\gamma (N_{xz} - \frac{dM_x}{dx})\} \\ & + \{N_x \delta u_0^s + M_x \delta\gamma + N_{xz} \delta w_0^s\}|_0^\infty = 0 \end{aligned} \tag{135}$$

The equilibrium equations for the shell can be derived as:

$$\delta u_0^s \ : \ \frac{dN_x}{dx} = 0 \tag{136}$$

$$\delta w_0^s \ : \ \frac{2N_\theta}{B} - \frac{dN_{xx}}{dx} - p = 0 \tag{137}$$

$$\delta\gamma \ : \ N_{xx} - \frac{dM_x}{dx} = 0 \tag{138}$$

The boundary conditions for a loaded semi-infinite shell at the finite edge are

$$N_x(x=0) \ = \ H_D(for \delta u_0^s \neq 0) \tag{139}$$

$$M_x(x=0) \ = \ M(for \delta\gamma \neq 0) \tag{140}$$

$$N_{xx}(x=0) \ = \ -Q(for \delta w_0^s \neq 0) \tag{141}$$

For a symmetrically laminated shell

$$B_{xx} = B_{x\theta} = 0 \tag{142}$$

and the stress resultants become:

$$N_x \ = \ \frac{du_0^s}{dx} A_{xx} + \frac{2w_0^s}{B} A_{x\theta} \tag{143}$$

$$N_\theta \ = \ \frac{du_0^s}{dx} A_{x\theta} + \frac{2w_0^s}{B} A_{\theta\theta} \tag{144}$$

$$N_{xx} \ = \ \frac{1}{2}(\gamma + \frac{dw_0^s}{dx}) A_{xx} \tag{145}$$

$$M_x \ = \ \frac{d\gamma}{dx} D_{xx} \tag{146}$$

Considering stress resultant N_x, the first equilibrium equation in the direction of virtual displacement δu_0^s is

$$\frac{du_0^s}{dx}A_{xx} + \frac{2w_0^s}{B}A_{x\theta} = H_D \tag{147}$$

where the right side H_D is the constant axial load acting on the shell. This load is equal to the hydrostatic end force $\frac{\pi}{4}B^2p$ divided by πB, ie $\frac{Bp}{4}$.

From Equation 138, the following is obtained:

$$N_{xx} = \frac{dM_x}{dx} \tag{148}$$

Substituting Equation 146 into above equation,

$$N_{xx} = \frac{d^2\gamma}{dx^2}D_{xx} \tag{149}$$

By neglecting the shear deformation ε_{xx}, which in this case is equivalent to:

$$\gamma = -\frac{dw_0^s}{dx} \tag{150}$$

The formulation becomes equivalent to the classical plate and shell theory. Then

$$N_{xx} = -\frac{d^3w_0^s}{dx^3}D_{xx} \tag{151}$$

Substituting Equations 144 and 151 into 137, another equilibrium equation is obtained:

$$\frac{2A_{x\theta}}{B}\frac{du_0^s}{dx} + \frac{2A_{\theta\theta}}{B^2}w_0^s + D_{xx}\frac{d^4w_0^s}{dx^4} - p = 0 \tag{152}$$

By eliminating the u_0^s term from equilibrium equations 147 and 152, the following is obtained:

$$\frac{d^4 w_0^s}{dx^4} + w_0^s\left(\frac{A_{\theta\theta}A_{xx} - A_{x\theta}^2}{\frac{B^2}{4}D_{xx}A_{xx}}\right) = \frac{\frac{B}{2}pA_{xx} - H_D A_{x\theta}}{\frac{B}{2}D_{xx}A_{xx}} \tag{153}$$

Assuming that

$$4\varepsilon^4 = \frac{A_{\theta\theta}A_{xx} - A_{x\theta}^2}{\frac{B^2}{4}D_{xx}A_{xx}} \tag{154}$$

upon imposing boundary conditions, the displacement is

$$w_0^s(x) = \frac{Q - \varepsilon M}{2\varepsilon^3 D_{xx}} e^{-\varepsilon x}\cos\varepsilon x + \frac{M}{2\varepsilon^2 D_{xx}} e^{-\varepsilon x}\sin\varepsilon x + \frac{(A_{xx} - \frac{1}{2}A_{x\theta})p}{4\varepsilon^4 A_{xx}D_{xx}} \tag{155}$$

and the shell rotation

$$\gamma(x) = \frac{Q - 2\varepsilon M}{2\varepsilon^2 D_{xx}} e^{-\varepsilon x}\cos\varepsilon x + \frac{Q}{2\varepsilon^2 D_{xx}} e^{-\varepsilon x}\sin\varepsilon x \tag{156}$$

5.4 Continuity at the Junction

From the requirement of continuity, the adjacent displacements and rotations of flange and shell must be equal at the junction:

$$u_0^f\left(\frac{B}{2}\right) = w_0^s(0) \tag{157}$$

and

$$\psi\left(\frac{B}{2}\right) = \gamma(0) \tag{158}$$

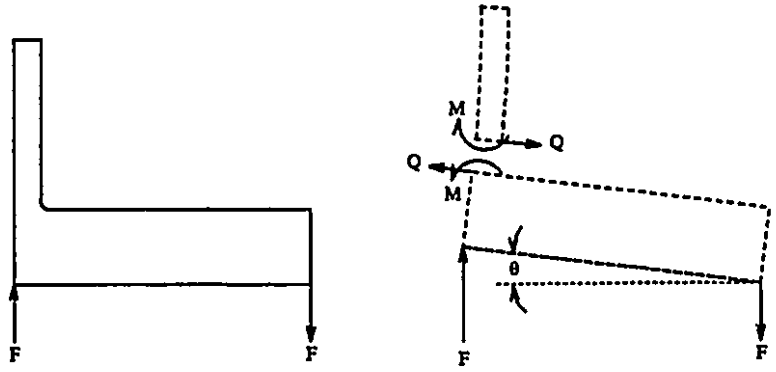

Figure 20: Flange Deformations - Discontinuity Loads

Substituting flange and shell displacements (100) and (155) into (157) and rotations (114) and (156) into (158), the following is obtained:

$$\frac{(pt-Q)B^3}{2(A_{r\theta}+A_{rr})(A^2-B^2)} + \frac{(-pt+Q)A^2B}{2(A_{r\theta}-A_{rr})(A^2-B^2)} = \frac{(Q-\epsilon M)}{2\epsilon^3 D_{xx}} + \frac{p}{4\epsilon^4 D_{xx}}(1-\frac{1}{2}\frac{A_{x\theta}}{A_{xx}}) \qquad (159)$$

and

$$\begin{aligned}
&-\frac{M_0}{4(A-B)\pi D_{rr}}(2\frac{B}{2}ln\frac{B}{2}-\frac{B}{2}) \\
&+\frac{A^2B^3}{8(B^2-A^2)(D_{rr}+D_{r\theta})}\{\frac{2M_0}{(A-B)B\pi}[\frac{B}{2A^2}(2\ln\frac{B}{2}+2\frac{D_{r\theta}}{D_{rr}}\ln\frac{B}{2}+1-\frac{D_{r\theta}}{D_{rr}}) \\
&-\frac{1}{2B}(2\ln\frac{A}{2}+2\frac{D_{r\theta}}{D_{rr}}\ln\frac{A}{2}+1-\frac{D_{r\theta}}{D_{rr}})]+M\frac{4}{A^2}+\frac{Qt}{2}\frac{4}{A^2}\} \\
&-\frac{A^2B}{2(B^2-A^2)(D_{r\cdot}-D_{r\theta})}[\frac{M_0}{4(A-B)\pi}(2\ln\frac{A}{2}-2\ln\frac{B}{2} \\
&+2\frac{D_{r\theta}}{D_{rr}}\ln\frac{A}{2}-2\frac{D_{r\theta}}{D_{rr}}\ln\frac{B}{2})-M-\frac{Qt}{2}] = \frac{-Q+2\epsilon M}{2\epsilon^2 D_{xx}}
\end{aligned} \qquad (160)$$

Equations 159 and 160 may be solved for the discontinuity force Q and the moment M_0.

To simplify this derivation, the following coefficients are defined:

$$l_1 = \frac{B^3}{2(A_{r\theta} + A_{rr})(A^2 - B^2)} \tag{161}$$

$$l_2 = \frac{A^2 B}{2(A_{r\theta} - A_{rr})(A^2 - B^2)} \tag{162}$$

$$l_3 = \frac{1}{2\varepsilon^3 D_{xx}} \tag{163}$$

$$l_4 = -\varepsilon l_3 \tag{164}$$

$$l_5 = \frac{l_3}{2\varepsilon}(1 - \frac{1}{2}\frac{A_{x\theta}}{A_{xx}}) \tag{165}$$

$$l_6 = B \ln \frac{B}{2} - \frac{B}{2} \tag{166}$$

$$l_7 = \frac{1}{4(A-B)\pi D_{rr}} l_6 \tag{167}$$

$$l_8 = \frac{B}{2A^2}(2 \ln \frac{B}{2} + 2\frac{D_{r\theta}}{D_{rr}} \ln \frac{B}{2} + 1 - \frac{D_{r\theta}}{D_{rr}}) \tag{168}$$

$$l_9 = \frac{1}{2B}(2 \ln \frac{A}{2} + 2\frac{D_{r\theta}}{D_{rr}} \ln \frac{A}{2} + 1 - \frac{D_{r\theta}}{D_{rr}}) \tag{169}$$

$$l_{10} = \frac{A^2 B^3}{8(B^2 - A^2)(D_{rr} + D_{r\theta})} \tag{170}$$

$$l_{11} = \frac{2}{(A-B)B\pi} \tag{171}$$

$$l_{12} = \frac{A^2 B}{2(B^2 - A^2)(D_{rr} - D_{r\theta})} \tag{172}$$

$$l_{13} = \frac{B}{8} l_{11} \tag{173}$$

$$l_{14} = 2 \ln \frac{A}{2} - 2 \ln \frac{B}{2} + 2\frac{D_{r\theta}}{D_{rr}} \ln \frac{A}{2} - 2\frac{D_{r\theta}}{D_{rr}} \ln \frac{B}{2} \tag{174}$$

$$l_{15} = -2\varepsilon l_4 \tag{175}$$

$$l_{16} = l_{10} l_{11} (l_8 - l_9) \tag{176}$$

$$l_{17} = \frac{4}{A^2} l_{10} \tag{177}$$

$$l_{18} = l_{12} l_{13} l_{14} \tag{178}$$

$$l_{19} = l_4 - \frac{t}{2} l_{12} - \frac{t}{2} l_{17} \tag{179}$$

$$l_{20} = -l_{12} + l_{15} - l_{17} \tag{180}$$

$$l_{21} = -l_7 + l_{16} - l_{18} \tag{181}$$

$$l_{22} = l_1 - l_2 + l_3 \tag{182}$$

$$l_{23} = t l_1 - t l_2 - l_5 \tag{183}$$

$$l_{24} = \frac{-l_{20} l_{23}}{l_4 l_{19} - l_{20} l_{22}} \tag{184}$$

$$l_{25} = \frac{l_4 l_{21}}{l_4 l_{19} - l_{20} l_{22}} \tag{185}$$

$$l_{26} = \frac{l_{19} l_{23}}{l_4 l_{19} - l_{20} l_{22}} \tag{186}$$

$$l_{27} = \frac{-l_{21} l_{22}}{l_4 l_{19} - l_{20} l_{22}} \tag{187}$$

Using l_1 to l_{27}, the discontinuity force and moment are obtained from Equation 159 and Equation 160:

$$Q = l_{24} p + l_{25} M_0 \tag{188}$$

$$M = l_{26} p + l_{27} M_0 \tag{189}$$

The rigid rotation of the flange plate has been established in Chapter 4 , Section 5. Rewriting Equation 55

$$\theta = \frac{3}{1 + 2K} \frac{M_G t_G}{G \pi E_G b^2 h_G} \tag{190}$$

From the left hand side of Equation 160, the rotation of the flange plate, using the coefficients above, then the following is obtained:

$$M_0 l_{21} + M(l_{12} + l_{17}) + \frac{Qt}{2}(l_{12} + l_{17}) = \frac{3}{1 + 2K} \frac{M_G t_G}{G\pi E_G b^2 h_G} \tag{191}$$

while from Equation 114, using previously defined coefficients,

$$M_0 = M_D + M_T + M_B - \eta M_G \tag{192}$$

By defining

$$l_{28} = \frac{3}{1 + 2K} \frac{t_G}{G\pi E_G b^2 h_G} \tag{193}$$

$$l_{29} = l_{21} + l_{27}(l_{12} + l_{17}) + \frac{t}{2} l_{25}(l_{12} + l_{17}) \tag{194}$$

$$l_{30} = l_{26}(l_{12} + l_{17}) + \frac{t}{2} l_{24}(l_{12} + l_{17}) \tag{195}$$

The gasket compression moment can be obtained directly:

$$M_G = \frac{l_{29}(M_D + M_T + M_B) + l_{30} p}{\eta l_{29} + l_{28}} \tag{196}$$

For the bolt-up condition, M_G is replaced by M_G^*

$$\frac{-Q^* B^3}{2(A_{r\theta} + A_{rr})(A^2 - B^2)} + \frac{Q^* A^2 B}{2(A_{r\theta} - A_{rr})(A^2 - B^2)} = \frac{(Q^* - \epsilon M^*)}{2\epsilon^3 D_{xx}} \tag{197}$$

Then

$$
\begin{aligned}
&-\frac{M_0^*}{4(A-B)\pi D_{rr}}(2\frac{B}{2}ln\frac{B}{2}-\frac{B}{2}) \\
&+\frac{A^2B^3}{8(B^2-A^2)(D_{rr}+D_{r\theta})}\{\frac{2M_0^*}{(A-B)B\pi}[\frac{B}{2A^2}(2\ln\frac{B}{2}+2\frac{D_{r\theta}}{D_{rr}}\ln\frac{B}{2}+1-\frac{D_{r\theta}}{D_{rr}}) \\
&-\frac{1}{2B}(2\ln\frac{A}{2}+2\frac{D_{r\theta}}{D_{rr}}\ln\frac{A}{2}+1-\frac{D_{r\theta}}{D_{rr}})]+M^*\frac{4}{A^2}+\frac{Q^*t}{2}\frac{4}{A^2}\} \\
&-\frac{A^2B}{2(B^2-A^2)(D_{rr}-D_{r\theta})}[\frac{M_0^*}{4(A-B)\pi}(2\ln\frac{A}{2}-2\ln\frac{B}{2} \\
&+2\frac{D_{r\theta}}{D_{rr}}\ln\frac{A}{2}-2\frac{D_{r\theta}}{D_{rr}}\ln\frac{B}{2})-M^*-\frac{Q^*t}{2}] \\
&\qquad\qquad =\frac{-Q^*+2\varepsilon M^*}{2\varepsilon^2 D_{xx}} \qquad (198)
\end{aligned}
$$

Using the coefficients defined previously, the following is obtained:

$$-Q^*l_1+Q^*l_2 = Q^*l_3+M^*l_4 \qquad (199)$$

$$M_0^*l_{21}+M^*(l_{12}+l_{17}) + \frac{Q^*t}{2}(l_{12}+l_{17}) = l_4Q^*+l_{15}M^* \qquad (200)$$

Defining two parameters

$$l_{31}=\frac{l_4l_{21}}{l_4l_{19}-l_{20}l_{22}} \qquad (201)$$

$$l_{32}=\frac{-l_{21}l_{22}}{l_4l_{19}-l_{20}l_{22}} \qquad (202)$$

then Q^* and M^* are obtained

$$Q^*=l_{31}M_0^* \qquad (203)$$

$$M^* = l_{32} M_0^* \tag{204}$$

Similarly to equation 191, for gasket seating the following is obtained:

$$M_0^* l_{21} + M^*(l_{12} + l_{17}) + \frac{Q^* t}{2}(l_{12} + l_{17}) = M_G^* l_{28} \tag{205}$$

which yields

$$M_0^* = M_{GS} - M_G^* \tag{206}$$

$$M_G^* = M_{GS} l_{34} \tag{207}$$

where

$$l_{33} = l_{21} + (l_{12} + l_{17}) l_{32} + \frac{t}{2}(l_{12} + l_{17}) l_{31} \tag{208}$$

$$l_{34} = \frac{l_{33}}{l_{28} + l_{33}} \tag{209}$$

5.5 Stress and Strain

From the Kirchhoff-Love assumptions, linear strain distributions are assumed across the laminate wall.

The general equation for the determination of strains in each ply of both, the flange and shell laminate, is represented by laminate midplane strain and its curvature as:

$$\varepsilon_i = \varepsilon_i^0 + z k_i \tag{210}$$

where z is the distance from the laminate midplane to the ply surface in question. For the flange i represents r, the radial direction (meridional), or θ, the tangential direction (circumferential); for the shell x, the longitudinal direction (meridional), or θ, the tangential direction (circumferential).

The stresses can then be calculated in a general form, as:

$$\begin{aligned} \sigma_i &= Q_{ii}\varepsilon_i + Q_{ij}\varepsilon_j \\ \sigma_j &= Q_{ij}\varepsilon_i + Q_{jj}\varepsilon_j \end{aligned} \tag{211}$$

where Q_{ii},Q_{ij},Q_{jj} are elastic constants.

5.5.1 Flange Laminate

For a midplane symmetrical flange laminate, deformations due to plate stretching are independent of deformations due to plate bending. The midplane strains are the results of only operating pressure (at operating condition) and discontinuity shear force. The flange total bending moment, including the twisting couple $F \times b$ and the boundary bending moment caused by discontinuity loads M and Q, contributes to the change of laminate curvature. M and Q are contained in the integration coefficients c_1 and c_2 appearing below.

$$\varepsilon_r^0 = \frac{du_0^f}{dr} = (pt - Q)\frac{2}{B}l_1 - (-pt + Q)\frac{B}{2}l_2\frac{1}{r^2} \tag{212}$$

$$\varepsilon_\theta^0 = \frac{u_0^f}{r} = (pt - Q)\frac{2}{B}l_1 + (-pt + Q)\frac{B}{2}l_2\frac{1}{r^2} \tag{213}$$

$$k_r = \frac{d\psi}{dr} = \frac{-BF}{8D_{rr}}(2lnr + 1) - \frac{1}{2}c_1 + c_2\frac{1}{r^2} \tag{214}$$

$$k_\theta = \frac{\psi}{r} = \frac{-BF}{8D_{rr}}(2lnr - 1) - \frac{1}{2}c_1 - c_2\frac{1}{r^2} \tag{215}$$

The stresses within mat layers may be expressed as

$$\sigma_{r(mat)} = Q_{rr(mat)}\varepsilon_r + Q_{r\theta(mat)}\varepsilon_\theta \tag{216}$$

$$\sigma_{\theta(mat)} = Q_{r\theta(mat)}\varepsilon_r + Q_{\theta\theta(mat)}\varepsilon_\theta \tag{217}$$

The stresses within the woven roving layers are

$$\sigma_{r(WR)} = Q_{rr(WR)}\varepsilon_r + Q_{r\theta(WR)}\varepsilon_\theta \tag{218}$$

$$\sigma_{\theta(WR)} = Q_{r\theta(WR)}\varepsilon_r + Q_{\theta\theta(WR)}\varepsilon_\theta \tag{219}$$

The maximum flange stresses, both radial and tangential, occur at the flange-shell junction.

5.5.2 Shell Laminate

The discontinuity shear force and bending moment cause a change in both midplane strains and curvatures. Internal pressure only contributes to the change of midplane strain.

$$\varepsilon_x^0 = \frac{du_0^s}{dx} = \frac{BP}{4A_{xx}} - \frac{2A_{x\theta}}{BA_{xx}}[(Q - \epsilon M)l_3 e^{-\epsilon x} cos\epsilon x - Ml_4 e^{-\epsilon x}\sin\epsilon x + pl_5] \tag{220}$$

and

$$k_x = \frac{d\gamma}{dx} = \epsilon e^{-\epsilon x}\cos\epsilon x(l_{15}M) + \epsilon e^{-\epsilon x}\sin\epsilon x(2l_4Q + l_{15}M) \tag{221}$$

$$\varepsilon_\theta^0 = \frac{2w_0^s}{B} = \frac{2}{B}((Q - \epsilon M)l_3 e^{-\epsilon x} cos\epsilon x - Ml_4 e^{-\epsilon x}\sin\epsilon x + pl_5) \tag{222}$$

$$k_\theta = 0 \tag{223}$$

The stresses within mat layers are

$$\sigma_{x(mat)} = Q_{xx(mat)}\varepsilon_x + Q_{x\theta(mat)}\varepsilon_\theta \tag{224}$$

$$\sigma_{\theta(mat)} = Q_{x\theta(mat)}\varepsilon_x + Q_{\theta\theta(mat)}\varepsilon_\theta \tag{225}$$

The stresses within the woven roving layers are

$$\sigma_{x(WR)} = Q_{xx(WR)}\varepsilon_x + Q_{x\theta(WR)}\varepsilon_\theta \tag{226}$$

$$\sigma_{\theta(WR)} = Q_{x\theta(WR)}\varepsilon_x + Q_{\theta\theta(WR)}\varepsilon_\theta \tag{227}$$

The maximum shell longitudinal stress σ_x occurs at the junction ($x = 0$ in.), while the maximum tangential stress σ_θ occurs at a very small distance from the junction.

5.6 Summary

An accurate analysis of FRP flanges needs to include transverse shear deformations because of the particular nature of composite materials. This will lead to tedious mathematical work, as it will be seen in the next chapter, not suitable for industrial design engineers. However, the analysis may be simplified by using the classical laminated plate and shell theory. This will reduce the complexity of the procedure considerably, which is vital in applying analytical analysis to industrial design methods.

Chapter 6

ANALYSIS VIA SHEAR DEFORMATION THEORY

6.1 Introduction

In the classical isotropic plate and shell theory, it is assumed that normals to the midplane before deformation remain straight and normal to the plane after deformation. This assumption results in the neglect of transverse shearing deformations. This is justifiable only if the isotropic plate or shell is relatively thin.

For FRP plates and shells, because of the unique properties of fibers and resin, neglecting the transverse shearing deformation will have a greater effect on strains and stresses than for isotropic materials, even for thin FRP plates and shells as discussed in Vinson and Chou [83]. To this end, more recently, some refined plate and shell theories have been proposed and classified into first and higher order shearing deformation theories. The distinction is drawn because the first order theory does not satisfy the shear stress free conditions on the top and bottom surfaces. The higher order theories attempt to correct this shortcoming by including thickness-related factors.

A flange plate laminate is relatively thicker than a shell laminate. Also, shell

formulations are more complicated and require more mathematical work than plate formulations. In order to achieve a proper balance between rigor and simplicity in this dissertation, a higher order shear deformable plate formulation will be used for the flange, while a classical theory formulation for the shell will be used, the same as in Chapter 5, Section 3.

6.2 Flange Equations

In this study the assumed higher order displacement field from Reddy's theory [65] [66] for axisymmetric bending of a circular plate flange is adopted:

$$\begin{aligned} u^f(r,z) &= u_0^f(r) + z \times \psi(r) + z^2 \times \xi(r) + z^3 \times \zeta(r) \\ v^f(r,z) &= 0 \\ w^f(r,z) &= w_0^f(r) \end{aligned} \tag{228}$$

The unknown functions ψ, ξ and ζ will be determined using the condition that the transverse shear stresses σ_{rz} and $\sigma_{\theta z}$ vanish on the flange top and bottom surfaces.

$$\sigma_{rz}(r,\theta,\pm\frac{t}{2}) = 0, \quad \sigma_{\theta z}(r,\theta,\pm\frac{t}{2}) = 0 \tag{229}$$

For flange isotropic or polarly orthotropic top and bottom layers, these conditions are equivalent to the requirement that the corresponding strains be zero on these surfaces. According to Equation 3, there is

$$\varepsilon_{rz} = \frac{1}{2}(\frac{\partial u^f}{\partial z} + \frac{\partial w^f}{\partial r}) = \frac{1}{2}(\psi(r) + 2z\xi(r) + 3z^2\zeta(r) + \frac{dw_0^f(r)}{dr}) \tag{230}$$

$$\varepsilon_{\theta z} = \frac{1}{2}(\frac{\partial v^f}{\partial z} + \frac{1}{r}\frac{\partial w^f}{\partial \theta}) = 0 \tag{231}$$

Setting $\varepsilon_{rz}(\pm\frac{t}{2})$ to zero, the following is obtained:

$$\xi(r) = 0 \tag{232}$$

$$\zeta(r) = \frac{-4}{3t^2}(\frac{dw_0^f(r)}{dr} + \psi(r)) \tag{233}$$

The corresponding displacement field then becomes

$$\begin{aligned} u^f(r,z) &= u_0^f(r) + z[\psi(r) - \frac{4}{3}(\frac{z}{t})^2(\psi(r) + \frac{dw_0^f(r)}{dr})] \\ v^f(r,z) &= 0 \\ w^f(r,z) &= w_0^f(r) \end{aligned} \tag{234}$$

The associated strains are

$$\begin{aligned} \varepsilon_r &= \frac{du_0^f}{dr} + z[\frac{d\psi}{dr} - \frac{4}{3}(\frac{z}{t})^2(\frac{d\psi}{dr} + \frac{d^2w_0^f}{dr^2})] \\ \varepsilon_\theta &= \frac{u_0^f}{r} + \frac{z}{r}[\psi - \frac{4}{3}(\frac{z}{t})^2(\psi + \frac{dw_0^f}{dr})] \\ \varepsilon_{rz} &= \frac{1}{2}[\psi - 4(\frac{z}{t})^2(\psi + \frac{dw_0^f}{dr}) + \frac{dw_0^f}{dr}] \\ \varepsilon_z &= 0 \\ \varepsilon_{\theta z} &= 0 \\ \varepsilon_{r\theta} &= 0 \end{aligned} \tag{235}$$

and the strain variations are

$$\delta\varepsilon_r = \frac{d}{dr}(\delta u_0^f) + z[\frac{d}{dr}(\delta\psi) - \frac{4}{3}(\frac{z}{t})^2(\frac{d}{dr}(\delta\psi) + \frac{d^2}{dr^2}(\delta w_0^f))]$$

$$
\begin{aligned}
\delta\varepsilon_\theta &= \frac{\delta u_0^f}{r} + \frac{z}{r}[\delta\psi - \frac{4}{3}(\frac{z}{t})^2(\delta\psi + \frac{d}{dr}(\delta w_0^f))] \\
\delta\varepsilon_{rz} &= \frac{1}{2}[\delta\psi - 4(\frac{z}{t})^2(\delta\psi + \frac{d}{dr}(\delta w_0^f)) + \frac{d}{dr}(\delta w_0^f)] \qquad (236) \\
\delta\varepsilon_z &= 0 \\
\delta\varepsilon_{\theta z} &= 0 \\
\delta\varepsilon_{r\theta} &= 0
\end{aligned}
$$

The principle of virtual displacements is used to derive the equilibrium equations. i.e.

$$0 = \delta V - \int_S (\sigma_r \delta\varepsilon_r + \sigma_\theta \delta\varepsilon_\theta + 2\sigma_{rz}\delta\varepsilon_{rz})dS \qquad (237)$$

where δV represents work done by surface loads, which is the same as Equation 69. The integral equation can be expanded as

$$
\begin{aligned}
0 = \delta V - 2\pi \int_{-t/2}^{t/2} r dr [&\frac{N_\theta}{r}\delta u_0 + N_r \frac{d}{dr}(\delta u_0) \\
&+ (\frac{M_\theta}{r} - \frac{4}{3t^2}\frac{P_\theta}{r} + Q_{rz} - \frac{4}{t^2}R_{rz})\delta\psi \\
&+ (M_r - \frac{4}{3t^2}P_r)\frac{d}{dr}(\delta\psi) + (Q_{rz} - \frac{4}{t^2}R_{rz} - \frac{4}{3t^2}\frac{P_\theta}{r})\frac{d}{dr}(\delta w_0) \\
&- \frac{4}{3t^2}P_r\frac{d^2}{dr^2}(\delta w_0)] \qquad (238)
\end{aligned}
$$

where the stress resultants are defined by

$$
\begin{aligned}
(N_i, M_i, P_i) &= \int \sigma_i(1, z, z^3)dz, \quad (i = r, \theta) \qquad (239) \\
(Q_{rz}, R_{rz}) &= \int \sigma_{rz}(1, z^2)dz \qquad (240)
\end{aligned}
$$

Integrating by parts, and collecting coefficients of δu_0, δw_0 and $\delta\psi$, the following equations of equilibrium are obtained:

$$\delta u_0 \ : \ N_\theta - \frac{d(rN_r)}{dr} = 0 \tag{241}$$

$$\delta w_0 \ : \ \frac{d}{dr}[r(Q_{rz} - \frac{4}{h^2}R_{rz} - \frac{4}{3h^2}\frac{P_\theta}{r})] + \frac{d^2}{dr^2}(\frac{4}{3h^2}rP_r) = 0 \tag{242}$$

$$\delta\psi \ : \ r(\frac{M_\theta}{r} - \frac{4}{3h^2}\frac{P_\theta}{r} + Q_{rz} - \frac{4}{h^2}R_{rz}) - \frac{d[r(M_r - \frac{4P_r}{3h^2})]}{dr} = 0 \tag{243}$$

The specific boundary conditions are

at $r = \frac{B}{2}$:

$$\begin{aligned} N_r &= -pt + Q \\ M_r &= M + \frac{Qt}{2} \\ P_r &= 0 \\ (Q_{rz} - \frac{4}{h^2}R_{rz} - \frac{4}{3h^2}\frac{P_\theta}{r}) &+ \frac{d}{dr}(\frac{4}{3h^2}rP_r) = -F \end{aligned} \tag{244}$$

at $r = \frac{A}{2}$:

$$\begin{aligned} N_r &= 0 \\ M_r &= 0 \\ P_r &= 0 \\ w_0 &= 0 \end{aligned} \tag{245}$$

The resultants defined in (239)(240) can be related to the displacements as follows:

$$N_r = \frac{du_0^f}{dr}A_{rr} + \frac{d\psi}{dr}B_{rr} - \frac{4}{3t^2}(\frac{d\psi}{dr} + \frac{d^2w_0^f}{dr^2})E_{rr}$$
$$+\frac{u_0^f}{r}A_{r\theta} + \frac{\psi}{r}B_{r\theta} - \frac{4}{3t^2r}(\psi + \frac{dw_0^f}{dr})E_{r\theta} \quad (246)$$

$$N_\theta = \frac{u_0^f}{r}A_{\theta\theta} + \frac{\psi}{r}B_{\theta\theta} - \frac{4}{3t^2r}(\psi + \frac{dw_0^f}{dr})E_{\theta\theta}$$
$$+\frac{du_0^f}{dr}A_{r\theta} + \frac{d\psi}{dr}B_{r\theta} - \frac{4}{3t^2}(\frac{d\psi}{dr} + \frac{d^2w_0^f}{dr^2})E_{r\theta} \quad (247)$$

$$M_r = \frac{du_0^f}{dr}B_{rr} + \frac{d\psi}{dr}D_{rr} - \frac{4}{3t^2}(\frac{d\psi}{dr} + \frac{d^2w_0^f}{dr^2})F_{rr}$$
$$+\frac{u_0^f}{r}B_{r\theta} + \frac{\psi}{r}D_{r\theta} - \frac{4}{3t^2r}(\psi + \frac{dw_0^f}{dr})F_{r\theta} \quad (248)$$

$$M_\theta = \frac{u_0^f}{r}B_{\theta\theta} + \frac{\psi}{r}D_{\theta\theta} - \frac{4}{3t^2r}(\psi + \frac{dw_0^f}{dr})F_{\theta\theta}$$
$$+\frac{du_0^f}{dr}B_{r\theta} + \frac{d\psi}{dr}D_{r\theta} - \frac{4}{3t^2}(\frac{d\psi}{dr} + \frac{d^2w_0^f}{dr^2})F_{r\theta} \quad (249)$$

$$P_r = \frac{du_0^f}{dr}E_{rr} + \frac{d\psi}{dr}F_{rr} - \frac{4}{3t^2}(\frac{d\psi}{dr} + \frac{d^2w_0^f}{dr^2})H_{rr}$$
$$+\frac{u_0^f}{r}E_{r\theta} + \frac{\psi}{r}F_{r\theta} - \frac{4}{3t^2r}(\psi + \frac{dw_0}{dr})H_{r\theta} \quad (250)$$

$$P_\theta = \frac{u_0}{r}E_{\theta\theta} + \frac{\psi}{r}F_{\theta\theta} - \frac{4}{3t^2r}(\psi + \frac{dw_0}{dr})H_{\theta\theta}$$
$$+\frac{du_0}{dr}E_{r\theta} + \frac{d\psi}{dr}F_{r\theta} - \frac{4}{3t^2}(\frac{d\psi}{dr} + \frac{d^2w_0}{dr^2})H_{r\theta} \quad (251)$$

$$Q_{rz} = \frac{1}{2}(\psi + \frac{dw_0^f}{dr})A_{rz} - \frac{2}{t^2}(\psi + \frac{dw_0^f}{dr})D_{rz} \tag{252}$$

$$R_{rz} = \frac{1}{2}(\psi + \frac{dw_0^f}{dr})D_{rz} - \frac{2}{t^2}(\psi + \frac{dw_0^f}{dr})F_{rz} \tag{253}$$

where the plate stiffnesses are formulated as

$$(A_{ij}, B_{ij}, D_{ij}, E_{ij}, F_{ij}, H_{ij}) = \int Q_{ij}(1, z, z^2, z^3, z^4, z^6)dz \quad (i,j = r,\theta) \tag{254}$$

$$(A_{ij}, D_{ij}, F_{ij}) = \int Q_{ij}(1, z^2, z^4)dz \quad (i,j = r,z) \tag{255}$$

If the laminate plate is midplane symmetrical, some of the stiffnesses become zero

$$B_{ij} = E_{ij} = 0 \quad (i,j = r,\theta) \tag{256}$$

Then, the resultants reduce to

$$N_r = \frac{du_0^f}{dr}A_{rr} + \frac{u_0^f}{r}A_{r\theta} \tag{257}$$

$$N_\theta = \frac{u_0^f}{r}A_{\theta\theta} + \frac{du_0^f}{dr}A_{r\theta} \tag{258}$$

$$M_r = \frac{d\psi}{dr}D_{rr} - \frac{4}{3t^2}(\frac{d\psi}{dr} + \frac{d^2w_0^f}{dr^2})F_{rr} + \frac{\psi}{r}D_{r\theta} - \frac{4}{3t^2 r}(\psi + \frac{dw_0^f}{dr})F_{r\theta} \tag{259}$$

$$M_\theta = \frac{\psi}{r} D_{\theta\theta} - \frac{4}{3t^2 r}(\psi + \frac{dw_0^f}{dr}) F_{\theta\theta} + \frac{d\psi}{dr} D_{r\theta} - \frac{4}{3t^2}(\frac{d\psi}{dr} + \frac{d^2 w_0^f}{dr^2}) F_{r\theta} \tag{260}$$

$$P_r = \frac{d\psi}{dr} F_{rr} - \frac{4}{3t^2}(\frac{d\psi}{dr} + \frac{d^2 w_0^f}{dr^2}) H_{rr} + \frac{\psi}{r} F_{r\theta} - \frac{4}{3t^2 r}(\psi + \frac{dw_0}{dr}) H_{r\theta} \tag{261}$$

$$P_\theta = \frac{\psi}{r} F_{\theta\theta} - \frac{4}{3t^2 r}(\psi + \frac{dw_0}{dr}) H_{\theta\theta} + \frac{d\psi}{dr} F_{r\theta} - \frac{4}{3t^2}(\frac{d\psi}{dr} + \frac{d^2 w_0}{dr^2}) H_{r\theta} \tag{262}$$

$$Q_{rz} = \frac{1}{2}(\psi + \frac{dw_0^f}{dr}) A_{rz} - \frac{2}{t^2}(\psi + \frac{dw_0^f}{dr}) D_{rz} \tag{263}$$

$$R_{rz} = \frac{1}{2}(\psi + \frac{dw_0^f}{dr}) D_{rz} - \frac{2}{t^2}(\psi + \frac{dw_0^f}{dr}) F_{rz} \tag{264}$$

Substituting above plate resultant formulations into the equilibrium equations, the following is obtained:

$$\delta u_0^f : r^2 \frac{d^2 u_0^f}{dr^2} + r\frac{du_0^f}{dr} - \frac{A_{\theta\theta}}{A_{rr}} u_0^f = 0 \tag{265}$$

$$\begin{aligned} \delta w_0^f : \quad & k_1(\frac{\psi}{r}) + k_2(r\psi) + k_3(\frac{d\psi}{dr}) + k_3(r\frac{d^2\psi}{dr^2}) + k_2(r\frac{dw_0^f}{dr}) \\ & + k_4(\frac{1}{r}\frac{dw_0^f}{dr}) + k_5(\frac{d^2 w_0^f}{dr^2}) + k_5(r\frac{d^3 w_0^f}{dr^3}) = -\frac{BF}{2} \end{aligned} \tag{266}$$

$$\begin{aligned} \delta\psi : \quad & k_6(\frac{\psi}{r}) + k_2(r\psi) + k_7(\frac{d\psi}{dr}) + k_7(r\frac{d^2\psi}{dr^2}) + k_1(\frac{1}{r}\frac{dw_0^f}{dr}) \\ & + k_2(r\frac{dw_0^f}{dr}) + k_3(\frac{d^2 w_0^f}{dr^2}) + k_3(r\frac{d^3 w_0^f}{dr^3}) = 0 \end{aligned} \tag{267}$$

where the structure coefficients are given by:

$$k_1 = -\frac{4}{3t^2}F_{\theta\theta} + \frac{16}{9t^4}H_{\theta\theta} \tag{268}$$

$$k_2 = \frac{1}{2}A_{rz} - \frac{4}{t^2}D_{rz} + \frac{8}{t^4}F_{rz} \tag{269}$$

$$k_3 = \frac{4}{3t^2}F_{rr} - \frac{16}{9t^4}H_{rr} \tag{270}$$

$$k_4 = \frac{16}{9t^4}H_{\theta\theta} \tag{271}$$

$$k_5 = -\frac{16}{9t^4}H_{rr} \tag{272}$$

$$k_6 = D_{\theta\theta} - \frac{8}{3h^2}F_{\theta\theta} + \frac{16}{9h^4}H_{\theta\theta} \tag{273}$$

$$k_7 = -D_{rr} + \frac{8}{3h^2}F_{rr} - \frac{16}{9h^4}H_{rr} \tag{274}$$

The solution of Equation 265, upon imposing boundary conditions, is given as

$$u_0 = \frac{(pt-Q)(\frac{A}{2})^{m_2-1}}{4(A_{r\theta}+\sqrt{A_{rr}A_{\theta\theta}})\Delta}r^{m_1} + \frac{(-pt+Q)(\frac{A}{2})^{m_1-1}}{4(A_{r\theta}-\sqrt{A_{rr}A_{\theta\theta}})\Delta}r^{m_2} \tag{275}$$

where

$$m_1 = \sqrt{\frac{A_{\theta\theta}}{A_{rr}}} \tag{276}$$

$$m_2 = -m_1 \tag{277}$$

$$\Delta = A^{m_1-1}B^{m_2-1} - A^{m_2-1}B^{m_1-1} \tag{278}$$

To solve the differential equation system consisting of Equation 266 and Equation 267, a function is assumed

$$f(r) = -r\frac{d}{dr}\frac{1}{r}\frac{d}{dr}(r\frac{dw_0}{dr}) \tag{279}$$

It can be observed that it is possible to obtain a one function ordinary differential

equation from the equation system.

$$\frac{d^2}{dr^2}f - \frac{1}{r}\frac{d}{dr}f + \frac{1}{a}f = -\frac{BF}{2aD_{\theta\theta}} \tag{280}$$

in which the material constant is

$$a = \frac{k_1^2 - k_4 k_6}{k_2 D_{\theta\theta}} \tag{281}$$

This equation has a singular point at $r = 0$, where the coefficient of $\frac{df}{dr}$ is not analytic.

The Frobenius method or extended power series method [46] is used. The indication equation is

$$\begin{aligned} & r^2 - 2r = 0 \\ & r = 0 \\ & r = 2 \end{aligned} \tag{282}$$

Its analytical solution can only be given in a power series

$$\begin{aligned} f(r) = \quad & c_1(r^2 - \frac{1}{a}\frac{1}{24}r^4 + \frac{1}{a^2}\frac{1}{24}\frac{1}{46}r^6 - \cdots) \\ & + c_2(r^2 - \frac{1}{a}\frac{1}{24}r^4 + \frac{1}{a^2}\frac{1}{24}\frac{1}{46}r^6 - \cdots)\ln r \\ & + c_2(-2a + \frac{1}{a}\frac{1}{24}(\frac{1}{2} + \frac{1}{4})r^4 - \frac{1}{a^2}\frac{1}{24}\frac{1}{46}(\frac{1}{2} + \frac{1}{4} + \frac{1}{4} + \frac{1}{6})r^6 + \cdots) \\ & - \frac{BF}{2D_{\theta\theta}} \end{aligned} \tag{283}$$

where c_1, c_2 are constants determined by the boundary conditions. Integrating the function $f(r)$, the deflection of the flange in the z direction is obtained:

$$w_0^f(r) = -\int [\frac{1}{r}\int (r\int \frac{f(r)}{r}dr)dr]dr \tag{284}$$

The expression for the flange rotation is

$$\frac{\partial u^f(r,z)}{\partial z} = \psi(r) - 4(\frac{z}{t})^2[\psi(r) + \frac{dw_0^f(r)}{dr}] \tag{285}$$

At the junction $r = \frac{B}{2}$, $z = \frac{t}{2}$, the rotation is

$$\frac{\partial u^f(\frac{B}{2},\frac{t}{2})}{\partial z} = -\frac{dw_0^f(\frac{B}{2})}{dr} \tag{286}$$

6.3 Shell Equations

From Chapter 5, the shell displacement, Equation 155, is

$$w_0^s(x) = \frac{Q-\epsilon M}{2\epsilon^3 D_{xx}}e^{-\epsilon x}\cos\epsilon x + \frac{M}{2\epsilon^2 D_{xx}}e^{-\epsilon x}\sin\epsilon x + \frac{(A_{xx}-\frac{1}{2}A_{x\theta})p}{4\epsilon^4 A_{xx}D_{xx}} \tag{287}$$

and the shell rotation, Equation 156,

$$\gamma(x) = \frac{Q-2\epsilon M}{2\epsilon^2 D_{xx}}e^{-\epsilon x}\cos\epsilon x + \frac{Q}{2\epsilon^2 D_{xx}}e^{-\epsilon x}\sin\epsilon x \tag{288}$$

6.4 Continuity at the Junction

The continuity at the flange and shell junction can be satisfied as:

$$u_0^f(\frac{B}{2}) = w_0^s(0) \tag{289}$$

and

$$-\frac{dw_0^f(\frac{B}{2})}{dr} = \gamma(0) \tag{290}$$

Equation 289 is exactly the same as Equation 157 in Chapter 5, using the classical laminate theory. This is because the flange laminate considered here is only midplane symmetrical layered. The assumed higher order displacement field in the beginning of this chapter has no effect on the midplane displacements. No coupling exists for flange plate stretching and bending. Thus the solution of Equation 289 is also the same as the one in the previous chapter.

The only difference between classical formulation and shear deformable formulation here is the left hand side of Equation 290, while the right hand side of the same equation is also the same as in the previous chapter. When $w_0^f(r)$ is obtained by solving above two discontinuity equations, it can be substituted into any one of the previous equilibrium equation system to obtain the unknown displacement function ψ. Then the flange plate displacements and strains can be solved accordingly using the displacement and strain relation. The shell displacements and strains can also be obtained in the same way as well.

6.5 Stress

In a general form, the stresses can be calculated by:

$$\begin{aligned} \sigma_i &= Q_{ii}\varepsilon_i + Q_{ij}\varepsilon_j \\ \sigma_j &= Q_{ij}\varepsilon_i + Q_{jj}\varepsilon_j \end{aligned} \tag{291}$$

where Q_{ii},Q_{ij} and Q_{jj} are elastic constants. For the flange i, j represent r and θ, for the shell they represent x and θ.

6.6 Summary

There is no doubt that the results given in this chapter are more accurate than those using the classical laminate theory. Not only the flange normal strains are given in a higher order form which guarantee their higher degree of accuracy, also the flange transverse shear strain is calculated.

However, applying higher order shear deformable theory in flange design here leads to the need of solving differential equation by power series method. Obviously, this may seem too complicated to some designer of process equipment.

Chapter 7

ILLUSTRATIVE EXAMPLE

7.1 Introduction

To illustrate the proposed design method based on classical laminate theory, a sample calculation is given in this chapter. The notations and nomenclatures used in the ongoing calculations follow ASME BPV Code, Section X closely. Calculated strain and stress results are given both in graphic and tabular form.

7.2 The Problem

A numerical example is given as shown in Figure 21, using a pair of flanges with 300 mm inside diameter, 480 mm outside diameter and 30 mm flange thickness. There are 12 bolt holes of 19 mm diameter on a 425 mm diameter bolt circle. The design pressure is 345 KPa at room temperature.

The full face gasket is of 3 mm thick synthetic rubber. Its modulus E_G is 55 MPa. The maximum allowable stress of the steel bolt M16 is 172 MPa.

Both flange and shell laminates are hand layered-up with midplane symmetry. The lamina elastic properties are given by Hoa [40] as in Table 2:

Table 2: Values of Elastic Constants of E glass/Vinyl Ester Laminae

Properties	Mat(1.5 oz)	Woven Roving
Directional	isotropic	square orthotropic
Fiber volume	20	35
E_L GPa(msi)	8.0(1.17)	18(2.63)
E_T GPa(msi)	8.0(1.17)	18(2.63)
E_S GPa(msi)	3.33(0.49)	3.6(0.53)
ν_L	0.20	0.13
ν_T	0.20	0.13

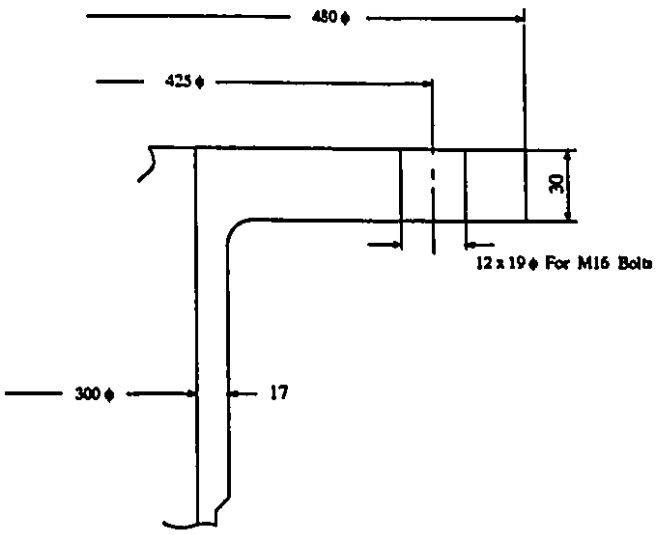

Figure 21: Flange Dimensions

The thickness of mat lamina is 1 mm, woven roving 0.9 mm.

7.3 Lamina Properties

The modulus components of the lamina are determined from the lamina elastic constants. For mat lamina, they are

$$Q_{LL} = E_L/(1-\nu_L\nu_T) = 8.33\ GPa \quad (292)$$

$$Q_{TT} = E_T/(1-\nu_L\nu_T) = 8.33\ GPa \quad (293)$$

$$Q_{LT} = \nu_T E_L/(1-\nu_L\nu_T) = 1.67\ GPa \quad (294)$$

$$Q_{TL} = Q_{LT} = 1.67\ GPa \quad (295)$$

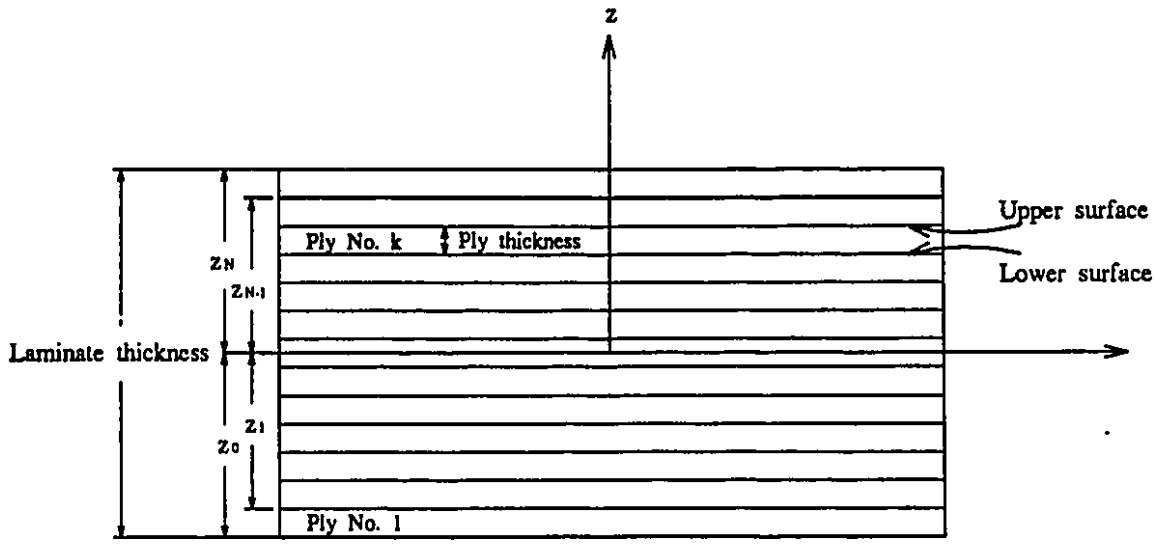

Figure 22: Laminate: Location and Numbering of Plies

For woven roving lamina, they are

$$Q_{LL} = 18.31\ GPa \quad (296)$$

$$Q_{TT} = 18.31\ GPa \quad (297)$$

$$Q_{LT} = 2.38\ GPa \quad (298)$$

$$Q_{TL} = 2.38\ GPa \quad (299)$$

Flange Laminate Moduli

The in-plane modulus components A_{ij} that couple stresses to strains are determined from an arithmetic summation of the modulus of each lamina as a function of the distance of each lamina from the laminate midplane.

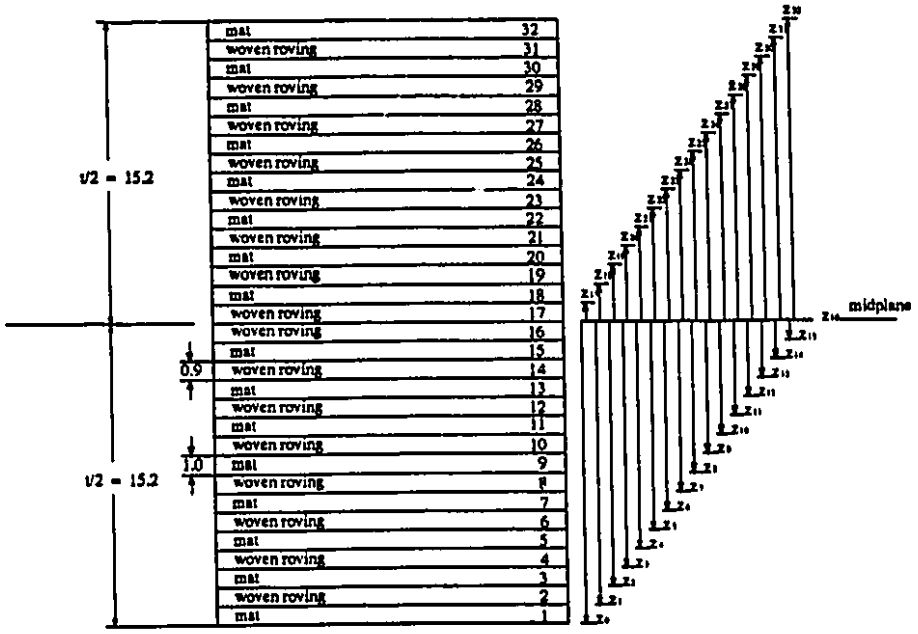

Figure 23: General Laminate for Flange

$$A_{rr} = \sum (Q_{rr} = Q_{LL})_k(Z_k - Z_{k-1}) = (Q_{rr})_1(Z_1 - Z_0) + (Q_{rr})_2(Z_2 - Z_1) + \cdots + (Q_{rr})_{32}(Z_{32} - Z_{31}) \quad (300)$$

$$A_{rr} = \sum (Q_{rr} = Q_{LL})_k(Z_k - Z_{k-1}) = 3.97 \times 10^8 \ N/m \quad (301)$$

$$A_{\theta\theta} = \sum (Q_{\theta\theta} = Q_{TT})_k(Z_k - Z_{k-1}) = 3.97 \times 10^8 \ N/m \quad (302)$$

$$A_{r\theta} = \sum (Q_{r\theta} = Q_{LT})_k(Z_k - Z_{k-1}) = 6.09 \times 10^7 \ N/m \quad (303)$$

The coupling modulus components B_{ij} that couple moment to strain and stress to curvature are determined from an arithmetic summation of the modulus of each lamina as a function of the square of the distance of each lamina from the laminate midplane.

$$B_{rr} = \frac{1}{2} \sum (Q_{rr} = Q_{LL})_k(Z_k^2 - Z_{k-1}^2) = \frac{1}{2}[(Q_{rr})_1(Z_1^2 - Z_0^2) + (Q_{rr})_2(Z_2^2 - Z_1^2) + \cdots + (Q_{rr})_{32}(Z_{32}^2 - Z_{31}^2)] \quad (304)$$

$$B_{rr} = \frac{1}{2} \sum (Q_{rr} = Q_{LL})_k(Z_k^2 - Z_{k-1}^2) = 0 \ N \quad (305)$$

$$B_{\theta\theta} = \frac{1}{2} \sum (Q_{\theta\theta} = Q_{TT})_k(Z_k^2 - Z_{k-1}^2) = 0 \ N \quad (306)$$

$$B_{r\theta} = \frac{1}{2} \sum (Q_{r\theta} = Q_{LT})_k(Z_k^2 - Z_{k-1}^2) = 0 \ N \quad (307)$$

The flexural modulus components D_{ij} that couple moments to curvature are determined from an arithmetic summation of the modulus of each lamina as a function

of the cube of the distance of each lamina from the laminate midplane.

$$D_{rr} = \frac{1}{3} \sum (Q_{rr} = Q_{LL})_k (Z_k^3 - Z_{k-1}^3) = \frac{1}{3}[(Q_{rr})_1 (Z_1^3 - Z_0^3) + (Q_{rr})_2 (Z_2^3 - Z_1^3) + \cdots + (Q_{rr})_{32} (Z_{32}^3 - Z_{31}^3)] \quad (308)$$

$$D_{rr} = \frac{1}{3} \sum (Q_{rr} = Q_{LL})_k (Z_k^3 - Z_{k-1}^3) = 29484 \ N \times m \quad (309)$$

$$D_{\theta\theta} = \frac{1}{3} \sum (Q_{\theta\theta} = Q_{TT})_k (Z_k^3 - Z_{k-1}^3) = 29484 \ N \times m \quad (310)$$

$$D_{r\theta} = \frac{1}{3} \sum (Q_{r\theta} = Q_{LT})_k (Z_k^3 - Z_{k-1}^3) = 4615 \ N \times m \quad (311)$$

Shell Laminate Moduli

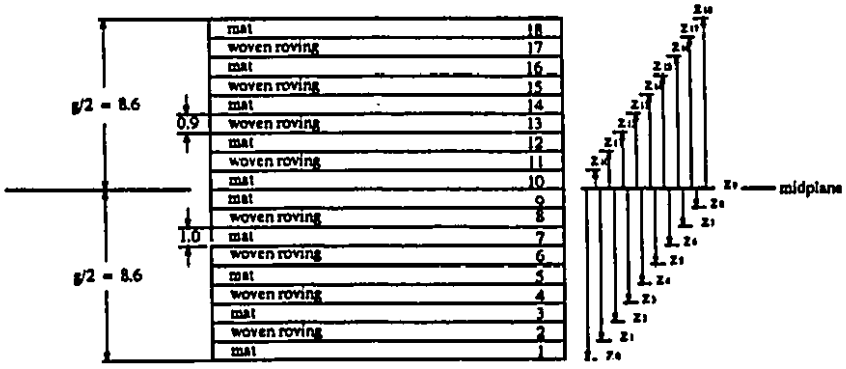

Figure 24: General Laminate for Shell

The in-plane modulus components are

$$A_{xx} = \sum (Q_{xx} = Q_{LL})_k (Z_k - Z_{k-1}) = 2.15 \times 10^8 \ N/m \tag{312}$$

$$A_{\theta\theta} = \sum (Q_{\theta\theta} = Q_{TT})_k (Z_k - Z_{k-1}) = 2.15 \times 10^8 \ N/m \tag{313}$$

$$A_{x\theta} = \sum (Q_{x\theta} = Q_{LT})_k (Z_k - Z_{k-1}) = 3.38 \times 10^7 \ N/m \tag{314}$$

The coupling modulus components are

$$B_{xx} = \frac{1}{2} \sum (Q_{xx} = Q_{LL})_k (Z_k^2 - Z_{k-1}^2) = 0 \ N \tag{315}$$

$$B_{\theta\theta} = \frac{1}{2} \sum (Q_{\theta\theta} = Q_{TT})_k (Z_k^2 - Z_{k-1}^2) = 0 \ N \tag{316}$$

$$B_{x\theta} = \frac{1}{2} \sum (Q_{x\theta} = Q_{LT})_k (Z_k^2 - Z_{k-1}^2) = 0 \ N \tag{317}$$

The flexural modulus components are

$$D_{xx} = \frac{1}{3} \sum (Q_{xx} = Q_{LL})_k (Z_k^3 - Z_{k-1}^3) = 5190 \ N \times m \tag{318}$$

7.4 Flange Moments

Effective gasket diameter

$$K = \frac{A}{B} = 1.6 \tag{319}$$

$$G = \frac{2B^2}{3} \sin(\frac{1}{B})[1 + \frac{K^2}{1+K}] = 0.397 \ m \tag{320}$$

Moment arms

$$h_D = \frac{1}{2}(G - B - g) = 0.040 \ m \tag{321}$$

$$h_T = \frac{1}{4}(2G - B - C + D) = 0.022\ m \quad (322)$$

$$h_G = \frac{B^2}{4}\sin(\frac{1}{B})(1 + \frac{3k^2}{1+2k}) - \frac{G}{2} = 0.014\ m \quad (323)$$

$$h_{GS} = \frac{1}{2}(C - G) = 0.014\ m \quad (324)$$

Flange loads and moments are calculated for operating and gasket seating conditions:

Operating moment

$$H_D = \frac{\pi}{4}B^2 p = 24386\ N \quad (325)$$

$$H_T = \frac{\pi}{4}[(C - D)^2 - B^2]p = 20277\ N \quad (326)$$

$$M_D = H_D h_D = 972\ N \times m \quad (327)$$

$$M_T = H_T h_T = 445\ N \times m \quad (328)$$

$$M_B = (H_D + H_T)h_{GS} = 627\ N \times m \quad (329)$$

Gasket seating moment

$$A_b = na = 12 \times 137 = 1.644 \times 10^{-3}\ m^2 \quad (330)$$

$$H_{GS} = A_b S_a = 282768\ Pa \quad (331)$$

$$M_{GS} = H_{GS} h_{GS} = 3969.73\ N \times m \quad (332)$$

Flange coefficients

$$l_1 = \frac{B^3}{2(A_{r\theta} + A_{rr})(A^2 - B^2)} = 2.0997445E - 10 \quad (333)$$

$$l_2 = \frac{A^2 B}{2(A_{r\theta} - A_{rr})(A^2 - B^2)} = -7.3249756E - 10 \quad (334)$$

$$l_3 = \frac{1}{2\varepsilon^3 D_{xx}} = 5.5515343E - 09 \quad (335)$$

$$l_4 = -\varepsilon l_3 = -1.4372191E - 07 \quad (336)$$

$$l_5 = \frac{l_3}{2\varepsilon}(1 - \frac{1}{2}\frac{A_{x\theta}}{A_{xx}}) = 9.8796644E - 11 \quad (337)$$

$$l_6 = B \ln \frac{B}{2} - \frac{B}{2} = -0.7191361 \quad (338)$$

$$l_7 = \frac{1}{4(A - B)\pi D_{rr}} l_6 = -1.0783044E - 05 \quad (339)$$

$$l_8 = \frac{B}{2A^2}(2 \ln \frac{B}{2} + 2\frac{D_{r\theta}}{D_{rr}} \ln \frac{B}{2} + 1 - \frac{D_{r\theta}}{D_{rr}}) = -2.307766 \quad (340)$$

$$l_9 = \frac{1}{2B}(2 \ln \frac{A}{2} + 2\frac{D_{r\theta}}{D_{rr}} \ln \frac{A}{2} + 1 - \frac{D_{r\theta}}{D_{rr}}) = -4.095953 \quad (341)$$

$$l_{10} = \frac{A^2 B^3}{8(B^2 - A^2)(D_{rr} + D_{r\theta})} = -1.6242068E - 07 \quad (342)$$

$$l_{11} = \frac{2}{(A - B)B\pi} = 11.78926 \quad (343)$$

$$l_{12} = \frac{A^2 B}{2(B^2 - A^2)(D_{rr} - D_{r\theta})} = -9.8981600E - 06 \quad (344)$$

$$l_{13} = \frac{B}{8} l_{11} = 0.4420971 \quad (345)$$

$$l_{14} = 2 \ln \frac{A}{2} - 2 \ln \frac{B}{2} + 2\frac{D_{r\theta}}{D_{rr}} \ln \frac{A}{2} - 2\frac{D_{r\theta}}{D_{rr}} \ln \frac{B}{2} = 1.087156 \quad (346)$$

$$l_{15} = -2\varepsilon l_4 = 7.4415411E - 06 \quad (347)$$

$$l_{16} = l_{10} l_{11} (l_8 - l_9) = -3.4240559E - 06 \quad (348)$$

$$l_{17} = \frac{4}{A^2} l_{10} = -2.8198033E - 06 \quad (349)$$

$$l_{18} = l_{12} l_{13} l_{14} = -4.7573367E - 06 \quad (350)$$

$$l_{19} = l_4 - \frac{t}{2} l_{17} = 4.9591144E - 08 \quad (351)$$

$$l_{20} = l_{15} - l_{17} = 2.0159505E - 05 \quad (352)$$

$$l_{21} = -l_7 + l_{16} - l_{18} = 1.2116325E-05 \quad (353)$$

$$l_{22} = l_3 + l_1 - l_2 = 6.4940062E-09 \quad (354)$$

$$l_{23} = tl_1 - tl_2 - l_5 = -7.0145494E-11 \quad (355)$$

$$l_{24} = \frac{-l_{20}l_{23}}{l_4l_{19} - l_{20}l_{22}} = -1.0243878E-02 \quad (356)$$

$$l_{25} = \frac{l_4l_{21}}{l_4l_{19} - l_{20}l_{22}} = 12.61475 \quad (357)$$

$$l_{26} = \frac{l_{19}l_{23}}{l_4l_{19} - l_{20}l_{22}} = 2.5199308E-05 \quad (358)$$

$$l_{27} = \frac{-l_{21}c_{22}}{l_4l_{19} - l_{20}l_{22}} = 0.5699914 \quad (359)$$

$$l_{28} = \frac{3}{1+2K}\frac{t_G}{G\pi E_G b^2 h_G} = 2.8194412E-07 \quad (360)$$

$$l_{29} = l_{21} + l_{27}(l_{12} + l_{17}) + \frac{t}{2}l_{25}(l_{12} + l_{17}) = 2.4285989E-06 \quad (361)$$

$$l_{30} = l_{26}(l_{12} + l_{17}) + \frac{t}{2}l_{24}(l_{12} + l_{17}) = 1.6597914E-09 \quad (362)$$

$$l_{31} = \frac{l_4l_{21}}{l_4l_{19} - l_{20}l_{22}} = 12.61475 \quad (363)$$

$$l_{32} = \frac{-l_{21}l_{22}}{l_4l_{19} - l_{20}l_{22}} = 0.5699914 \quad (364)$$

$$l_{33} = l_{21} + (l_{12} + l_{17})l_{32} + \frac{t}{2}(l_{12} + l_{17})l_{31} = 2.4285989E-06 \quad (365)$$

$$l_{34} = \frac{l_{33}}{l_{28} + l_{33}} = 0.8959824 \quad (366)$$

7.5 Results in Graphic Form

7.5.1 Flange Stresses

The rotation of the flange ring has caused tension in the flange upper laminate layers, and compression in the lower layers. Constrained by the shell, both maximum absolute tangential and radial flange stress values occur at the junction for both operating and gasket seating conditions.

Shown in Figures 25 and 26, for both operating and gasket seating conditions, the absolute surface flange radial stress values decrease rapidly outward along the direction of the flange radius. The values finally drop to zero at the flange outside free edge. Shown in Figures 27 and 28 , the tangential stress values also decrease, but with a gentler slope, with finite values at the outside edge. When approaching the junction, the stress curves are almost constant which implies that stress values are reduced by the constraining connecting shell which limits the rotation in the flange ring.

After all, the upper layers near the flange-and-shell junction are critical in FRP flange design. Excessive tension at this location often results in ply failure. On the other hand, high compression in the lower layers will not damage the flange.

Excessive bolting force may crush FRP on the outer faces of the flanges around the bolt holes during the bolting up precedure. These contact stresses cannot be predicted by analytical methods formulated in this study. In practice, a steel washer is usually placed under the bolt head in order to eliminate both the turning friction and the concentrated bolt load.

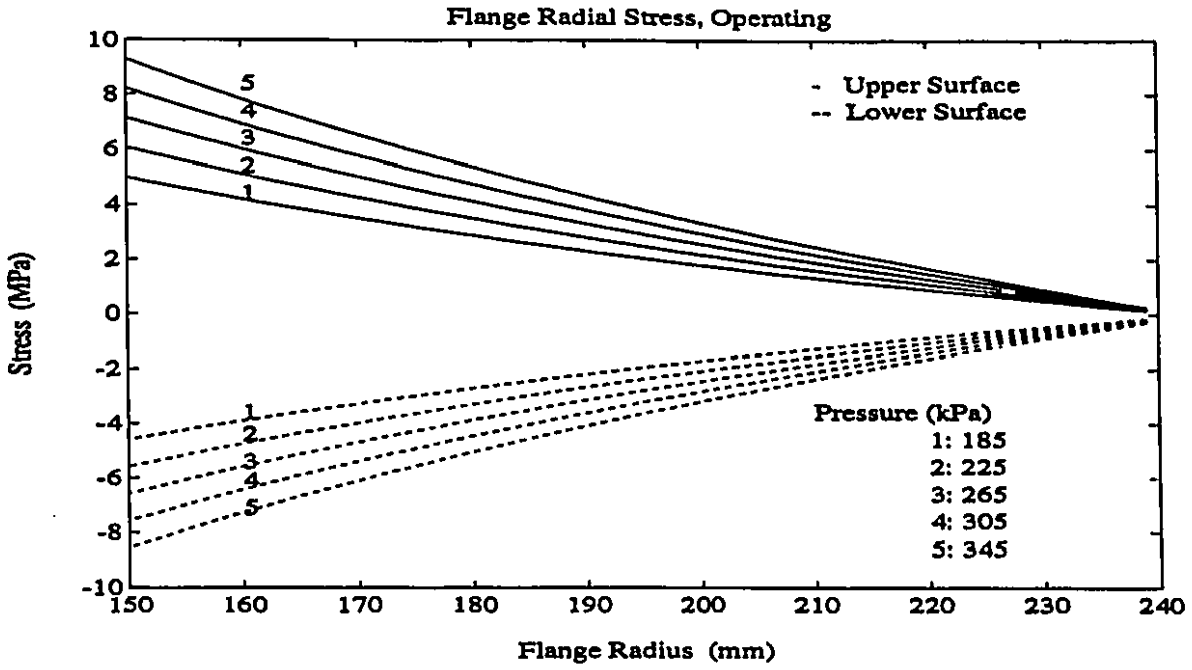

Figure 25: Flange Radial Stress, Operating

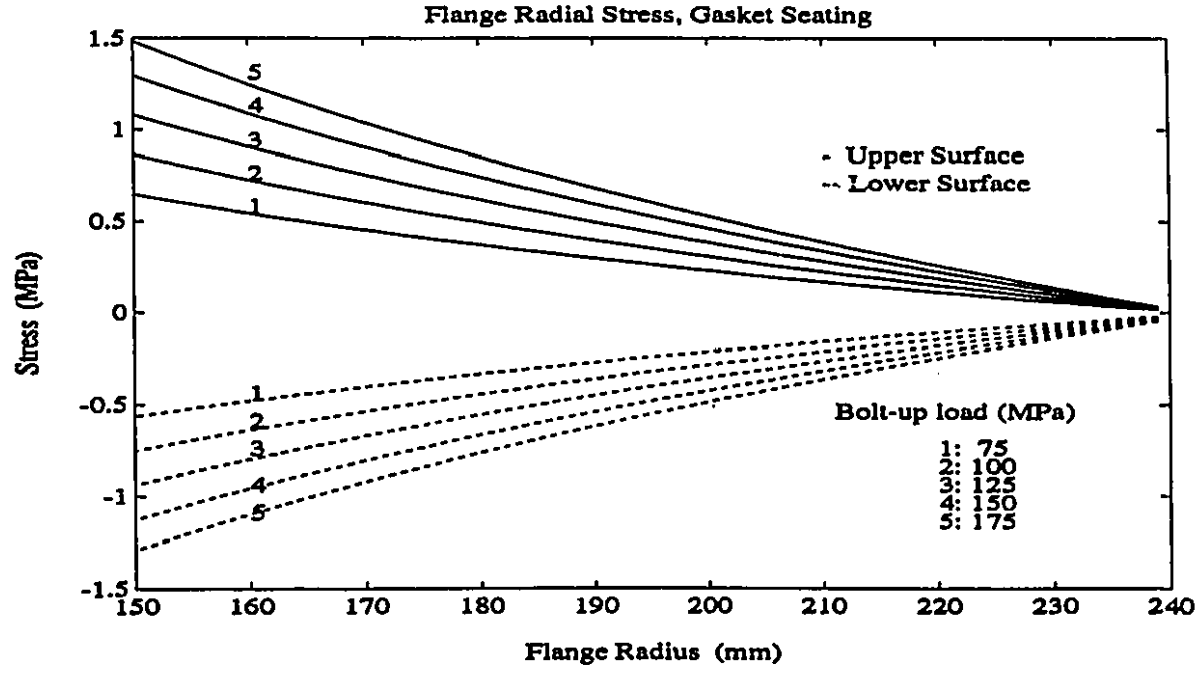

Figure 26: Flange Radial Stress, Gasket Seating

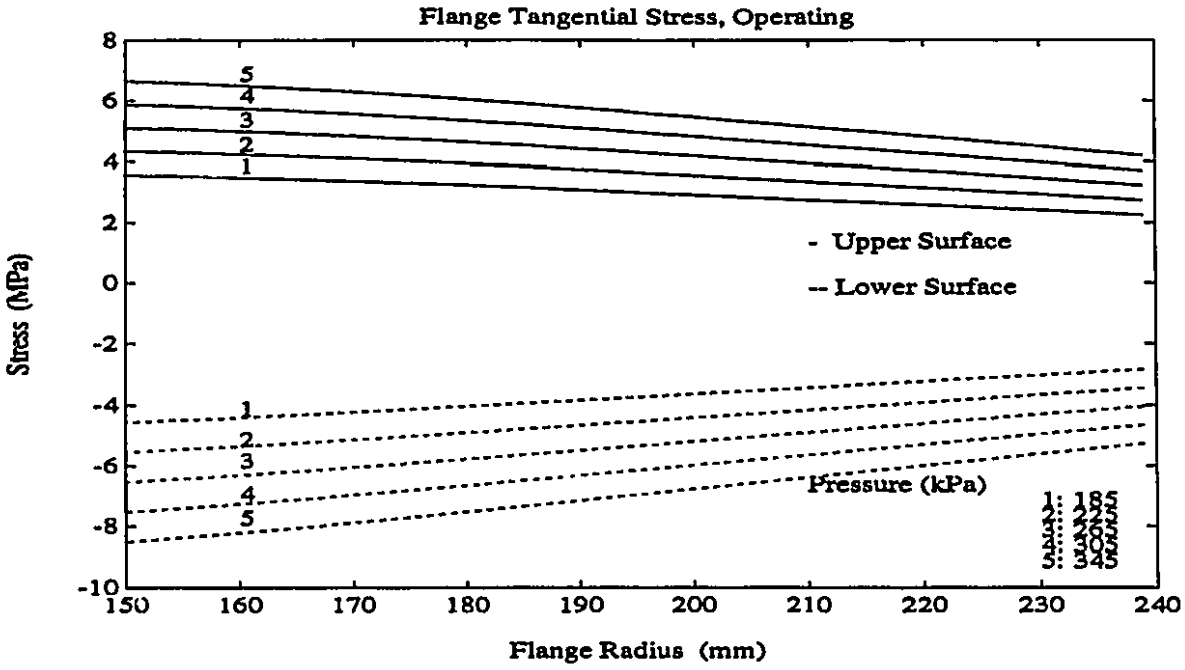

Figure 27: Flange Tangential Stress, Operating

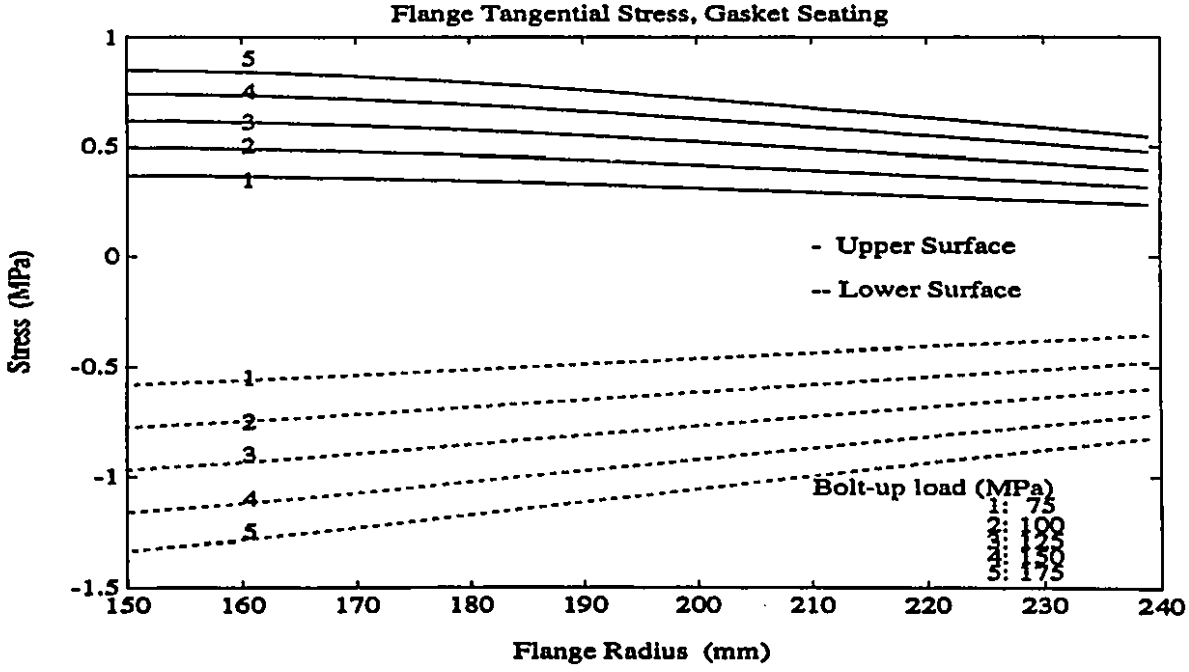

Figure 28: Flange Tangential Stress, Gasket Seating

7.5.2 Shell Stresses

Due to the constraint of the flange ring which limits the radial expansion of the shell, for both, operating and gasket seating conditions, the absolute shell longitudinal stresses reach their maximum values at the junction in the outer layers (tension) and the inner layers (compression), respectively. Also for operating and gasket seating conditions the maximum tensile tangential stresses in the outer layers occur at a certain distance from the junction, while the maximum compressive tangential stresses in the inner layers remain at the junction.

For an FRP shell, failure is usually caused by tension unless the shell is very thin in which case longitudinal compression may cause buckling. However, the shell concerned here is thick enough to resist the tendency of buckling. The chance of failure caused by compression can thus be ruled out. Damage usually occurs in the shell outer layers at the sharp corner of the flange-and-shell junction if no fillet is provided, where the positive longitudinal stress reaches its highest value, and a small distance from the junction where the positive tangential stress reaches its maximum.

Outer layers of the shell will fail first if the strength limit is surpassed by the loading. Such situation should be avoided in the design.

The longitudinal stresses are shown along the length of the shell in Figures 29 and 30. For both, operating and gasket seating conditions, the absolute shell surface longitudinal stress value decreases for locations away from the junction. After it goes through the lowest point, the stress curves stabilize at a nonzero value which are not readable from the figures shown here. The tangential stresses are shown in Figures 31 and 32. The tangential stresses reach maximum values a short distance away from the junction. Further beyond the junction, the stress values decline to a constant value which is twice the longitudinal stress value of the same location.

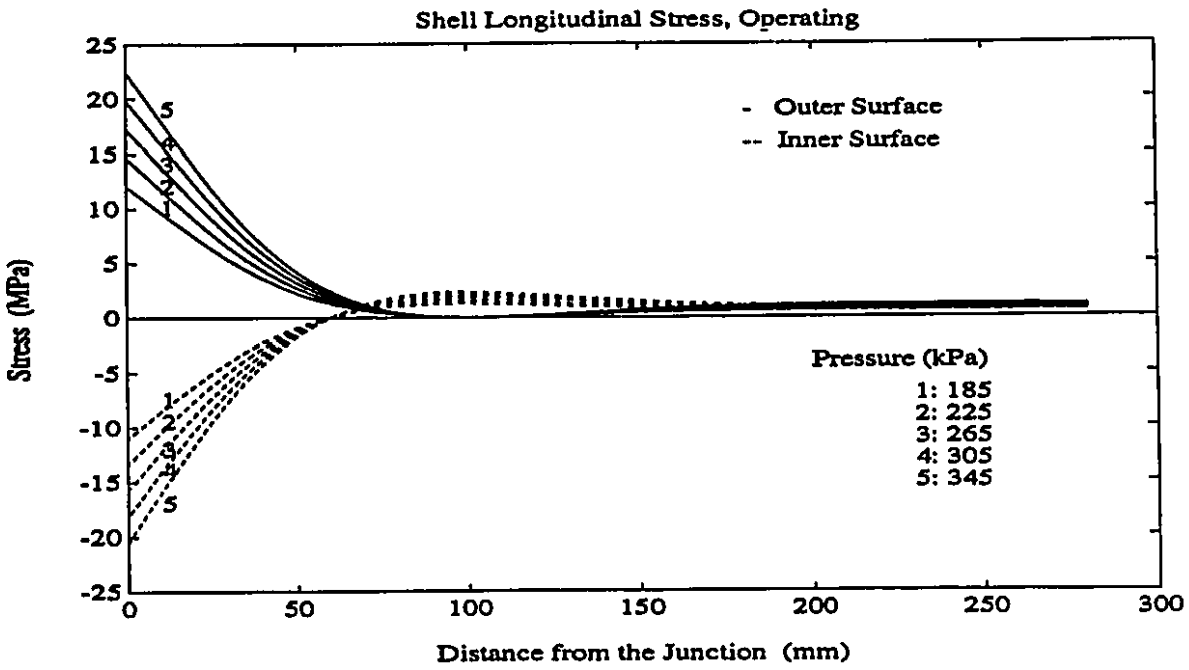

Figure 29: Shell Longitudinal Stress, Operating

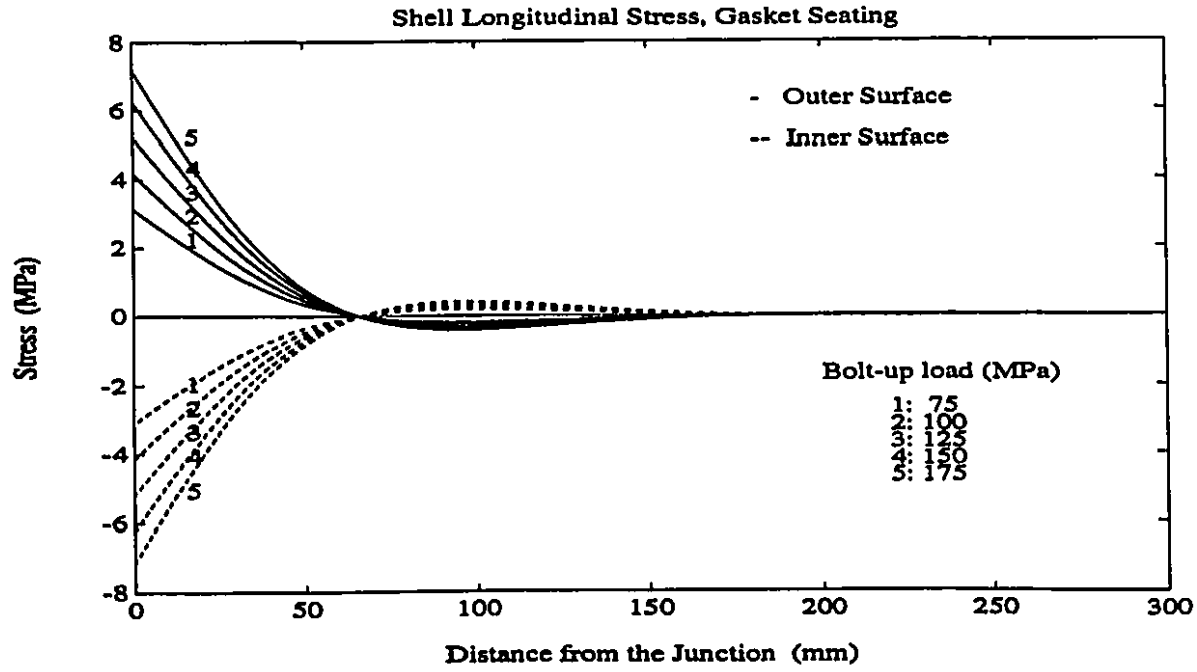

Figure 30: Shell Longitudinal Stress, Gasket Seating

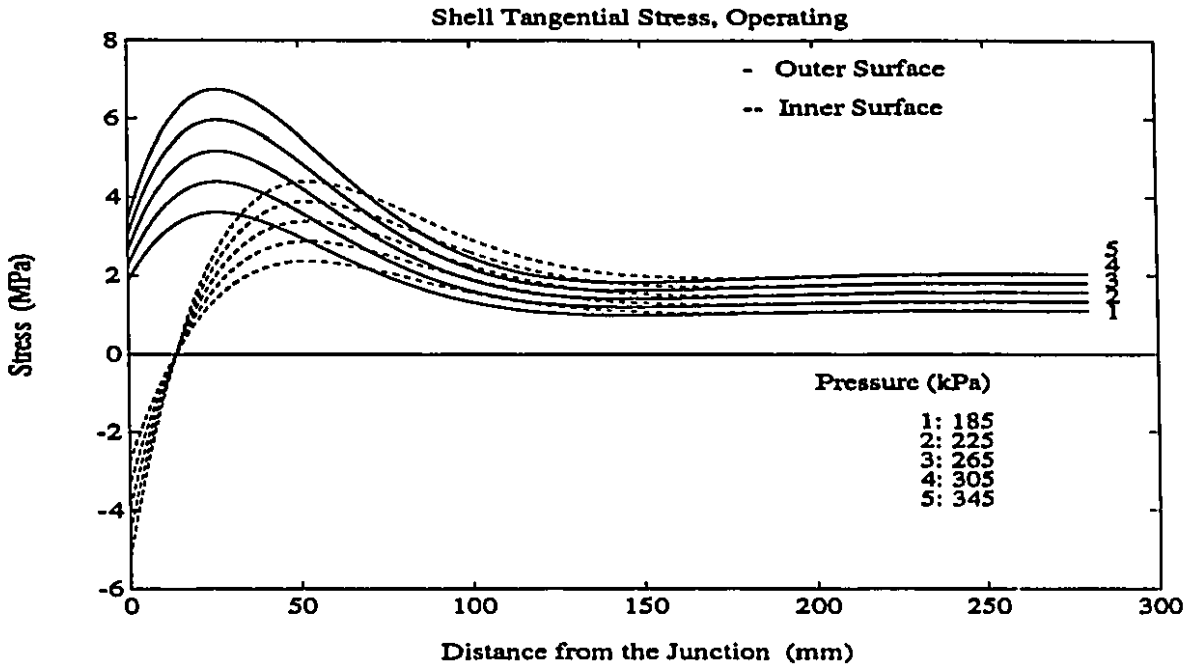

Figure 31: Shell Tangential Stress, Operating

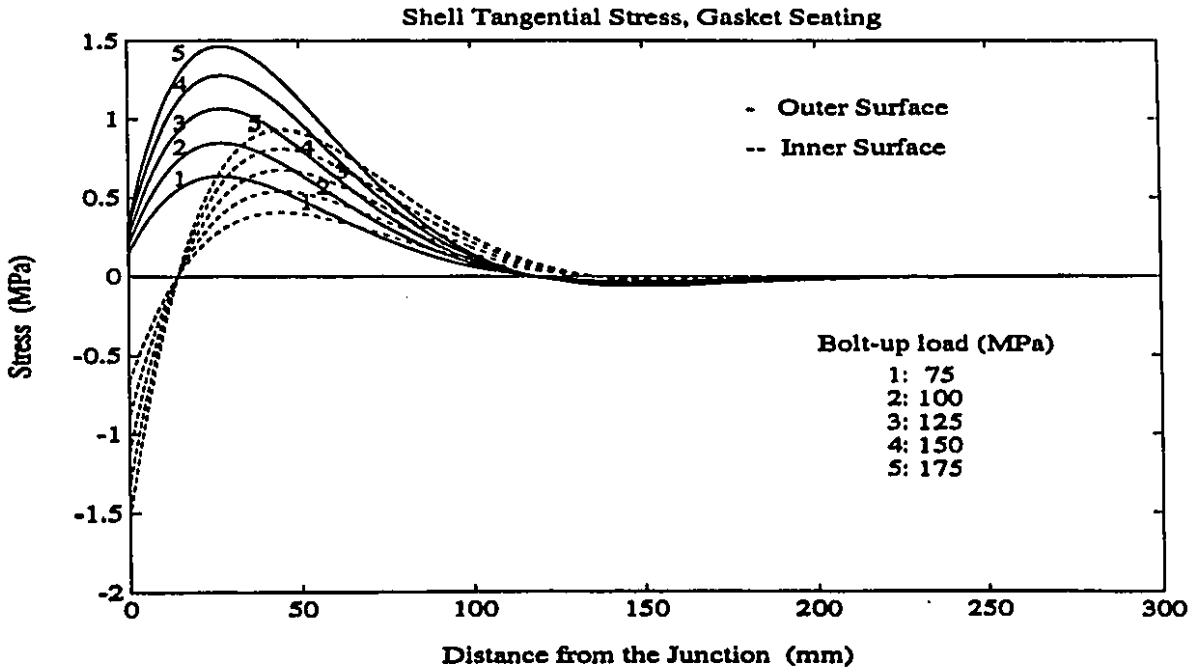

Figure 32: Shell Tangential Stress, Gasket Seating

7.6 Results in Tabular Form

For the upper surface of ply No. 32 (see Fig. 23), in the flange laminate at the inner radius at operating conditions

$$\varepsilon_r = \varepsilon_r^0 + zk_r = 0.996 \times 10^{-3} \tag{367}$$

$$\varepsilon_\theta = \varepsilon_\theta^0 + zk_\theta = 0.597 \times 10^{-3} \tag{368}$$

and

$$\sigma_r = Q_{rr}\varepsilon_r + Q_{r\theta}\varepsilon_\theta = 9.30\ MPa \tag{369}$$

$$\sigma_\theta = Q_{r\theta}\varepsilon_r + Q_{\theta\theta}\varepsilon_\theta = 6.64\ MPa \tag{370}$$

For all 32 plies of the flange at operating conditions, the strains are as shown in Tables 3 and 4, the stresses in Tables 5,6,7,8.

For the upper surface of ply No. 18 in the shell laminate at the junction at operating conditions

$$\varepsilon_x = \varepsilon_x^0 + zk_x = 2.710 \times 10^{-3} \tag{371}$$

$$\varepsilon_\theta = \varepsilon_\theta^0 + zk_\theta = -0.126 \times 10^{-3} \tag{372}$$

and

$$\sigma_x = Q_{xx}\varepsilon_x + Q_{x\theta}\varepsilon_\theta = 22.37\ MPa \tag{373}$$

$$\sigma_\theta = Q_{x\theta}\varepsilon_x + Q_{\theta\theta}\varepsilon_\theta = 3.46\ MPa \tag{374}$$

For all 18 plies of the flange at operating conditions, the strains are as shown in Tables 9 and 10, the stresses in Tables 11,12,13,14.

The strains change linearly across the laminate thickness. However, because of higher moduli of woven roving layers, the stresses in adjacent woven roving layers are comparatively higher than those in mat layers. Unlike the strains, the stresses change dramatically across the thickness.

Both flange and shell are subjected to midplane streching or compression, these smaller values of strains are given in the following tables. Shell tangential strain remains the same across the thickness, due to the shell axial symmetry.

7.7 Failure Criteria

There are three commonly used failure criteria for composite material, namely maximum strain failure criterion, maximum stress failure criterion, and Tsai-Wu failure criterion. For FRP materials, calculated strain values are more convenient to predict damage, since damage occurs at the same strains, irrespective of the glass fiber content, modulus and hence stresses. Also in a laminate, stresses change dramatically from layer to layer, depending on the layers' moduli, whereas strains are more consistently distributed.

For FRP materials, there are five strain limits as well as five strength constants. They are tensile and compressive stresses or strains in the direction of the fiber and transverse to the fiber direction, and the in-plane shear stress or strain. The definition of these limits and methods for their determination can be found in [40], p.21-30.

The strength of the flange and shell laminates can be examined in terms of five strength constants or strain limits using one of three criteria mentioned here, but they are not included in this dissertation.

7.8 Summary

Both strain and stress results are given in this chapter. The choice of a failure criterion is largely based on the observation with FRP flange in service. It is reported that flanges are often damaged at the flange-shell junction during bolt-up. This is consistent with the results we obtained in this chapter.

$\epsilon_r(\mu\epsilon)$	Radius, r(mm)						
z(mm)	150	165	180	195	210	225	240
15.2	996	737	522	339	181	42	-80
14.2	935	692	490	319	171	40	-74
13.3	880	651	461	300	161	39	-69
12.3	819	606	430	280	151	37	-63
11.4	764	566	401	262	141	35	-58
10.4	703	521	369	241	131	34	-52
9.5	649	480	341	223	121	32	-46
8.5	588	435	309	203	111	30	-40
7.6	533	395	281	184	101	29	-35
6.6	472	350	249	164	91	27	-29
5.7	417	309	220	146	81	25	-23
4.7	356	264	189	125	71	23	-17
3.8	301	224	160	107	61	22	-12
2.8	240	179	128	86	51	20	-6
1.9	185	138	100	68	41	18	-1
0.9	124	93	68	48	31	17	4
0	70	53	40	29	21	15	10
-0.9	15	12	11	11	12	13	15
-1.9	-45	-32	-20	-8	2	12	21
-2.8	-100	-72	-48	-27	-7	10	26
-3.8	-161	-117	-80	-47	-17	8	32
-4.7	-216	-158	-108	-65	-27	7	38
-5.7	-277	-203	-140	-86	-37	5	44
-6.6	-332	-244	-169	-104	-47	3	49
-7.6	-393	-289	-200	-124	-57	1	55
-8.5	-447	-329	-229	-143	-67	0	61
-9.5	-508	-374	-261	-163	-77	-1	67
-10.4	-563	-415	-289	-181	-87	-3	72
-11.4	-624	-460	-321	-202	-97	-4	78
-12.3	-679	-500	-349	-220	-107	-6	83
-13.3	-740	545	-381	-240	-117	-8	89
-14.2	-795	-586	-410	-259	-127	-9	95
-15.2	-856	-631	-441	-279	-137	-11	101

Table 3: Flange Radial Strain at Inter-Layer, z = Distance from Mid-Plane

$\epsilon_\theta(\mu\epsilon)$	Radius, r(mm)						
z(mm)	150	165	180	195	210	225	240
15.2	597	621	622	607	582	550	515
14.2	550	573	574	561	538	509	476
13.3	507	530	532	520	499	473	442
12.3	459	482	485	474	456	432	404
11.4	416	439	442	433	417	395	369
10.4	369	390	395	388	373	354	331
9.5	326	347	352	347	334	317	297
8.5	278	299	305	301	291	276	258
7.6	235	256	262	260	252	239	224
6.6	188	208	215	214	208	198	186
5.7	145	164	173	173	169	161	151
4.7	97	116	125	128	125	120	113
3.8	54	73	83	87	86	83	78
2.8	6	25	35	41	43	42	40
1.9	-35	-17	-6	0	4	6	6
0.9	-83	-66	-53	-45	-39	-34	-32
0	-126	-109	-96	-86	-78	-71	-66
-0.9	-169	-152	-138	-127	-117	-108	-101
-1.9	-216	-200	-186	-173	-160	-149	-139
-2.8	-259	-244	-228	-214	-200	-186	-173
-3.8	-307	-292	-276	-259	-243	-227	-212
-4.7	-350	-335	-318	-300	-282	-264	-246
-5.7	-398	-383	-365	-346	-326	-305	-284
-6.6	-440	-426	-408	-387	-365	-342	-319
-7.6	-488	-474	-455	-433	-408	-383	-357
-8.5	-531	-518	-498	-474	-447	-420	-391
-9.5	-579	-566	-545	-519	-491	-461	-430
-10.4	-621	-609	-588	-560	-530	-497	-464
-11.4	-669	-657	-635	-606	-573	-538	-502
-12.3	-712	-701	-677	-647	-612	-575	-537
-13.3	-760	-749	-725	-693	-656	-616	-575
-14.2	-802	-792	-767	-734	-695	-653	-610
-15.2	-850	-840	-815	-779	-739	-694	-648

Table 4: Flange Tangential Strain at Inter-Layer

$\sigma_r(mat)$	Radius, r(mm)						
z(mm)	150	165	180	195	210	225	240
15.2	9.30	7.17	5.38	3.84	2.48	1.27	0.18
14.2	8.71	6.72	5.04	3.59	2.32	1.19	0.17
13.3	8.18	6.31	4.73	3.37	2.17	1.11	0.15
12.3	7.59	5.85	4.39	3.12	2.01	1.03	0.14
11.4	7.06	5.44	4.08	2.90	1.87	0.95	0.13
10.4	6.48	4.99	3.74	2.66	1.71	0.87	0.11
9.5	5.95	4.58	3.43	2.44	1.57	0.79	0.10
8.5	5.36	4.12	3.08	2.19	1.41	0.71	0.09
7.6	4.83	3.71	2.78	1.97	1.26	0.64	0.07
6.6	4.24	3.26	2.43	1.72	1.10	0.55	0.06
5.7	3.72	2.85	2.12	1.50	0.96	0.48	0.05
4.7	3.13	2.39	1.78	1.26	0.80	0.40	0.03
3.8	2.60	1.98	1.47	1.03	0.66	0.32	0.02
2.8	2.01	1.53	1.13	0.79	0.50	0.24	0.01
1.9	1.48	1.12	0.82	0.57	0.35	0.16	0
0.9	0.90	0.66	0.48	0.32	0.19	0.08	-0.01
0	0.37	0.25	0.17	0.10	0.05	0	-0.02
-0.9	-0.15	-0.15	-0.13	-0.11	-0.09	-0.06	-0.03
-1.9	-0.74	-0.60	-0.47	-0.36	-0.25	-0.14	-0.05
-2.8	-1.27	-1.01	-0.78	-0.58	-0.39	-0.22	-0.06
-3.8	-1.85	-1.47	-1.13	-0.82	-0.55	-0.30	-0.07
-4.7	-2.38	-1.88	-1.43	-1.04	-0.69	-0.38	-0.09
-5.7	-2.97	-2.33	-1.78	-1.29	-0.85	-0.46	-0.10
-6.6	-3.50	-2.74	-2.09	-1.51	-1.00	-0.53	-0.11
-7.6	-4.09	-3.20	-2.43	-1.76	-1.16	-0.62	-0.13
-8.5	-4.61	-3.61	-2.74	-1.98	-1.30	-0.69	-0.14
-9.5	-5.20	-4.06	-3.08	-2.22	-1.46	-0.78	-0.15
-10.4	-5.73	-4.47	-3.39	-2.44	-1.61	-0.85	-0.16
-11.4	-6.32	-4.93	-3.73	-2.69	-1.77	-0.93	-0.18
-12.3	-6.85	-5.34	-4.04	-2.91	-1.91	-1.01	-0.19
-13.3	-7.43	-5.79	-4.38	-3.16	-2.07	-1.09	-0.21
-14.2	-7.96	-6.20	-4.69	-3.38	-2.21	-1.17	-0.22
-15.2	-8.55	-6.66	-5.04	-3.62	-2.37	-1.25	-0.23

Table 5: Flange Radial Stress in Mat Layer (MPa)

$\sigma_r(W.R.)$	Radius, r(mm)						
z(mm)	150	165	180	195	210	225	240
14.2	18.43	14.03	10.34	7.17	4.41	1.96	-0.23
13.3	17.33	13.19	9.72	6.74	4.14	1.84	-0.21
12.3	16.10	12.25	9.03	6.26	3.85	1.71	-0.20
11.4	14.99	11.41	8.40	5.83	3.58	1.59	-0.18
10.4	13.76	10.47	7.71	5.35	3.29	1.46	-0.16
9.5	12.66	9.62	7.08	4.91	3.02	1.35	-0.14
8.5	11.43	8.68	6.39	4.43	2.72	1.22	-0.12
7.6	10.32	7.84	5.77	4.00	2.46	1.10	-0.11
6.6	9.09	6.90	5.07	3.52	2.16	0.97	-0.09
5.7	7.98	6.06	4.45	3.08	1.90	0.85	-0.07
4.7	6.76	5.12	3.76	2.60	1.60	0.72	-0.05
3.8	5.65	4.27	3.13	2.17	1.33	0.60	-0.04
2.8	4.42	3.33	2.44	1.69	1.04	0.47	-0.02
1.9	3.31	2.49	1.82	1.25	0.77	0.36	0
0.9	2.08	1.55	1.12	0.77	0.48	0.23	0.01
0	0.98	0.71	0.50	0.34	0.21	0.11	0.02
-0.9	-0.12	-0.13	-0.11	-0.08	-0.05	0	0.04
-1.9	-1.35	-1.07	-0.81	-0.57	-0.34	-0.13	0.06
-2.8	-2.45	-1.91	-1.43	-1.00	-0.61	-0.25	0.08
-3.8	-3.68	-2.85	-2.12	-1.48	-0.90	-0.38	0.09
-4.7	-4.79	-3.70	-2.75	-1.91	-1.17	-0.49	0.11
-5.7	-6.02	-4.63	-3.44	-2.40	-1.46	-0.62	0.13
-6.6	-7.13	-5.48	-4.07	-2.83	-1.73	-0.74	0.15
-7.6	-8.36	-6.42	-4.76	-3.31	-2.03	-0.87	0.17
-8.5	-9.46	-7.26	-5.38	-3.74	-2.29	-0.99	0.18
-9.5	-10.69	-8.20	-6.08	-4.23	-2.59	-1.12	0.20
-10.4	-11.80	-9.05	-6.70	-4.66	-2.85	-1.24	0.22
-11.4	-13.03	-9.98	-7.39	-5.14	-3.15	-1.37	0.24
-12.3	-14.13	-10.83	-8.02	-5.57	-3.42	-1.48	0.25
-13.3	-15.36	-11.77	-8.71	-6.05	-3.71	-1.61	0.27
-14.2	-16.47	-12.61	-9.33	-6.49	-3.98	-1.73	0.29

Table 6: Flange Radial Stress in Woven Roving Layer (MPa)

$\sigma_\theta(mat)$	Radius, r(mm)						
z(mm)	150	165	180	195	210	225	240
15.2	6.64	6.41	6.05	5.62	5.15	4.66	4.15
14.2	6.14	5.93	5.60	5.21	4.77	4.31	3.85
13.3	5.69	5.50	5.20	4.83	4.43	4.00	3.57
12.3	5.19	5.03	4.75	4.42	4.05	3.66	3.26
11.4	4.74	4.60	4.35	4.05	3.71	3.35	2.98
10.4	4.24	4.12	3.91	3.63	3.33	3.00	2.67
9.5	3.79	3.69	3.50	3.26	2.99	2.69	2.39
8.5	3.30	3.22	3.06	2.85	2.61	2.35	2.08
7.6	2.85	2.79	2.65	2.47	2.26	2.04	1.81
6.6	2.35	2.31	2.21	2.06	1.89	1.70	1.50
5.7	1.90	1.88	1.81	1.69	1.54	1.39	1.22
4.7	1.40	1.41	1.36	1.27	1.16	1.04	0.91
3.8	0.95	0.98	0.96	0.90	0.82	0.73	0.63
2.8	0.45	0.50	0.51	0.49	0.44	0.39	0.32
1.9	0.01	0.08	0.11	0.11	0.10	0.08	0.04
0.9	-0.48	-0.39	-0.33	-0.29	-0.27	-0.26	-0.25
0	-0.93	-0.82	-0.73	-0.66	-0.61	-0.57	-0.53
-0.9	-1.38	-1.25	-1.13	-1.04	-0.95	-0.88	-0.81
-1.9	-1.88	-1.72	-1.58	-1.45	-1.33	-1.22	-1.12
-2.8	-2.33	-2.15	-1.98	-1.82	-1.67	-1.53	-1.40
-3.8	-2.83	-2.63	-2.43	-2.24	-2.05	-1.88	-1.71
-4.7	-3.28	-3.05	-2.83	-2.61	-2.40	-2.19	-1.98
-5.7	-3.77	-3.53	-3.28	-3.03	-2.78	-2.53	-2.29
-6.6	-4.22	-3.96	-3.68	-3.40	-3.12	-2.84	-2.57
-7.6	-4.72	-4.43	-4.13	-3.81	-3.50	-3.19	-2.88
-8.5	-5.17	-4.86	-4.53	-4.19	-3.84	-3.50	-3.16
-9.5	-5.67	-5.34	-4.98	-4.60	-4.22	-3.84	-3.47
-10.4	-6.12	-5.77	-5.38	-4.97	-4.56	-4.15	-3.75
-11.4	-6.62	-6.24	-5.83	-5.39	-4.94	-4.49	-4.06
-12.3	-7.06	-6.67	-6.23	-5.76	-5.28	-4.80	-4.33
-13.3	-7.56	-7.15	-6.67	-6.17	-5.66	-5.15	-4.64
-14.2	-8.01	-7.58	-7.08	-6.55	-6.00	-5.46	-4.92
-15.2	-8.51	-8.05	-7.52	-6.96	-6.38	-5.80	-5.23

Table 7: Flange Tangential Stress in Mat Layer (MPa)

$\sigma_\theta(W.R.)$	Radius, r(mm)						
z(mm)	150	165	180	195	210	225	240
14.2	12.29	12.15	11.69	11.04	10.27	9.43	8.55
13.3	11.38	11.26	10.84	10.24	9.53	8.75	7.93
12.3	10.36	10.27	9.90	9.36	8.71	8.00	7.25
11.4	9.44	9.38	9.05	8.56	7.97	7.32	6.63
10.4	8.43	8.39	8.11	7.68	7.15	6.56	5.94
9.5	7.51	7.50	7.27	6.88	6.41	5.88	5.32
8.5	6.49	6.52	6.32	6.00	5.59	5.13	4.64
7.6	5.58	5.63	5.48	5.20	4.85	4.45	4.02
6.6	4.56	4.64	4.54	4.32	4.03	3.70	3.33
5.7	3.65	3.75	3.69	3.52	3.29	3.02	2.71
4.7	2.63	2.76	2.75	2.64	2.47	2.26	2.03
3.8	1.71	1.87	1.90	1.85	1.73	1.58	1.41
2.8	0.70	0.88	0.96	0.96	0.91	0.83	0.72
1.9	-0.21	0	0.11	0.17	0.17	0.15	0.11
0.9	-1.23	-0.98	-0.82	-0.71	-0.64	-0.59	-0.57
0	-2.14	-1.87	-1.66	-1.50	-1.38	-1.27	-1.19
-0.9	-3.06	-2.76	-2.51	-2.30	-2.12	-1.95	-1.81
-1.9	-4.08	-3.75	-3.45	-3.18	-2.94	-2.71	-2.49
-2.8	-4.99	-4.64	-4.30	-3.98	-3.67	-3.39	-3.11
-3.8	-6.01	-5.63	-5.24	-4.86	-4.50	-4.14	-3.80
-4.7	-6.92	-6.51	-6.09	-5.66	-5.23	-4.82	-4.42
-5.7	-7.94	-7.50	-7.03	-6.54	-6.06	-5.57	-5.10
-6.6	-8.86	-8.39	-7.88	-7.34	-6.79	-6.25	-5.72
-7.6	-9.88	-9.38	-8.82	-8.22	-7.61	-7.01	-6.41
-8.5	-10.79	-10.27	-9.66	-9.02	-8.35	-7.69	-7.03
-9.5	-11.81	-11.26	-10.61	-9.90	-9.17	-8.44	-7.71
-10.4	-12.72	-12.15	-11.45	-10.70	-9.91	-9.12	-8.33
-11.4	-13.74	-13.13	-12.39	-11.58	-10.73	-9.87	-9.02
-12.3	-14.66	-14.02	-13.24	-12.38	-11.47	-10.55	-9.63
-13.3	-15.67	-15.01	-14.18	-13.26	-12.29	-11.31	-10.32
-14.2	-16.59	-15.90	-15.03	-14.06	-13.03	-11.99	-10.94

Table 8: Flange Tangential Stress in Woven Roving Layer (MPa)

$\epsilon_x(\mu\varepsilon)$	Shell distance aparting from the junction,x(mm)									
z(mm)	0	20	40	60	80	100	120	140	160	180
8.6	2710	1555	675	174	-32	-68	-32	17	56	79
7.6	2411	1380	599	158	-22	-52	-19	25	60	80
6.7	2142	1221	531	143	-13	-37	-7	32	63	81
5.7	1843	1046	455	127	-2	-21	6	40	67	82
4.8	1574	887	387	112	6	-6	18	48	70	82
3.8	1275	712	311	96	16	9	31	55	73	83
2.9	1006	554	243	82	25	24	43	63	77	84
1.9	708	378	167	66	35	40	56	71	80	85
1	439	220	99	51	55	68	78	83	85	85
0	140	44	23	35	55	71	81	86	87	86
-1	-158	-131	-52	19	65	88	94	94	90	87
-1.9	-427	-289	-120	4	74	102	106	101	93	88
-2.9	-726	-465	-196	-11	84	119	120	109	97	89
-3.8	-995	-623	-264	-25	94	133	132	116	100	89
-4.8	-1294	-799	-340	-42	104	150	145	124	104	90
-5.7	-1563	-957	-409	-56	113	164	157	131	107	91
-6.7	-1862	-1132	-484	-72	123	181	170	139	110	92
-7.6	-2131	-1291	-553	-87	132	195	182	146	113	92
-8.6	-2430	-1466	-628	-103	143	212	195	154	117	93

Table 9: Shell Longitudinal Strain at Inter-Layer

$\epsilon_\theta(\mu\epsilon)$	Shell distance aparting from the junction, x(mm)									
z(mm)	0	20	40	60	80	100	120	140	160	180
8.6	-126	482	617	540	413	308	245	217	210	213
7.6	-126	482	617	540	413	308	245	217	210	213
6.7	-126	482	617	540	413	308	245	217	210	213
5.7	-126	482	617	540	413	308	245	217	210	213
4.8	-126	482	617	540	413	308	245	217	210	213
3.8	-126	482	617	540	413	308	245	217	210	213
2.9	-126	482	617	540	413	308	245	217	210	213
1.9	-126	482	617	540	413	308	245	217	210	213
1	-126	482	617	540	413	308	245	217	210	213
0	-126	482	617	540	413	308	245	217	210	213
-1	-126	482	617	540	413	308	245	217	210	213
-1.9	-126	482	617	540	413	308	245	217	210	213
-2.9	-126	482	617	540	413	308	245	217	210	213
-3.8	-126	482	617	540	413	308	245	217	210	213
-4.8	-126	482	617	540	413	308	245	217	210	213
-5.7	-126	482	617	540	413	308	245	217	210	213
-6.7	-126	482	617	540	413	308	245	217	210	213
-7.6	-126	482	617	540	413	308	245	217	210	213
-8.6	-126	482	617	540	413	308	245	217	210	213

Table 10: Shell Tangential Strain at Inter-Layer

$\sigma_x(mat)$	Shell distance aparting from the junction,x(mm)									
z(mm)	0	20	40	60	80	100	120	140	160	180
8.6	22.37	13.76	6.65	2.35	0.41	-0.05	0.13	0.51	0.82	1.01
7.6	19.88	12.30	6.02	2.21	0.50	0.07	0.25	0.57	0.85	1.02
6.7	17.64	10.98	5.45	2.09	0.57	0.20	0.34	0.63	0.88	1.03
5.7	15.15	9.52	4.82	1.96	0.66	0.33	0.46	0.70	0.91	1.03
4.8	12.91	8.20	4.25	1.84	0.74	0.46	0.55	0.76	0.93	1.04
3.8	10.42	6.73	3.62	1.70	0.82	0.59	0.67	0.82	0.96	1.05
2.9	8.18	5.42	3.05	1.58	0.90	0.71	0.76	0.88	0.99	1.05
1.9	5.68	3.95	2.42	1.45	0.98	0.85	0.87	0.95	1.02	1.06
1	3.44	2.63	1.85	1.32	1.06	0.97	0.97	1.01	1.04	1.07
0	0.95	1.17	1.22	1.19	1.14	1.11	1.08	1.07	1.07	1.07
-1	-1.53	-0.28	0.59	1.06	1.23	1.24	1.20	1.14	1.10	1.08
-1.9	-3.77	-1.60	0.02	0.93	1.31	1.37	1.29	1.20	1.13	1.09
-2.9	-6.26	-3.07	-0.61	0.80	1.39	1.50	1.41	1.27	1.16	1.09
-3.8	-8.50	-4.30	-1.17	0.68	1.47	1.62	1.50	1.33	1.18	1.10
-4.8	-10.99	-5.85	-1.81	0.54	1.55	1.76	1.62	1.39	1.21	1.11
-5.7	-13.24	-7.17	-2.37	0.42	1.63	1.88	1.71	1.45	1.24	1.11
-6.7	-15.73	-8.63	-3.01	0.29	1.71	2.02	1.83	1.52	1.27	1.12
-7.6	-17.97	-9.95	-3.58	0.17	1.79	2.14	1.92	1.58	1.29	1.13
-8.6	-20.46	-11.41	-4.21	0.03	1.88	2.28	2.03	1.64	1.32	1.13

Table 11: Shell Longitudinal Stress in Mat Layer (MPa)

$\sigma_x(W.R.)$	Shell distance aparting from the junction,x(mm)									
z(mm)	0	20	40	60	80	100	120	140	160	180
7.6	43.85	26.41	12.44	4.18	0.57	-0.21	0.23	0.98	1.60	1.98
6.7	38.93	23.51	11.19	3.91	0.74	0.04	0.45	1.12	1.66	1.99
5.7	33.46	20.30	9.81	3.61	0.93	0.34	0.69	1.26	1.73	2.01
4.8	28.53	17.40	8.56	3.35	1.09	0.61	0.91	1.39	1.78	2.02
3.8	23.06	14.18	7.17	3.05	1.28	0.91	1.15	1.54	1.85	2.03
2.9	18.13	11.29	5.92	2.79	1.45	1.18	1.37	1.67	1.91	2.05
1.9	12.66	8.07	4.53	2.49	1.64	1.48	1.61	1.81	1.97	2.06
1	7.73	5.17	3.28	2.22	1.80	1.75	1.83	1.94	2.03	2.08
0	2.26	1.96	1.89	1.93	1.99	2.04	2.08	2.09	2.09	2.09
-1	-3.20	-1.25	0.50	1.63	2.18	2.34	2.32	2.23	2.16	2.11
-1.9	-8.13	-4.15	-0.74	1.37	2.35	2.61	2.54	2.37	2.21	2.12
-2.9	-13.60	-7.36	-2.13	1.07	2.53	2.91	2.78	2.51	2.28	2.13
-3.8	-18.53	-10.26	-3.38	0.81	2.70	3.18	3.00	2.64	2.34	2.15
-4.8	-24.00	-13.48	-4.77	0.51	2.89	3.48	3.24	2.79	2.40	2.16
-5.7	-28.93	-16.37	-6.01	0.24	3.06	3.75	3.46	2.92	2.46	2.18
-6.7	-34.40	-19.59	-7.40	-0.04	3.24	4.04	3.70	3.06	2.52	2.19
-7.6	-39.32	-22.49	-8.65	-0.31	3.41	4.31	3.92	3.19	2.58	2.21

Table 12: Shell Longitudinal Stress in Woven Roving Layer (MPa)

$\sigma_\theta(mat)$	Shell distance aparting from the junction,x(mm)									
z(mm)	0	20	40	60	80	100	120	140	160	180
8.6	3.46	6.61	6.26	4.79	3.38	2.45	1.99	1.83	1.84	1.91
7.6	2.96	6.32	6.14	4.76	3.40	2.48	2.01	1.85	1.85	1.91
6.7	2.51	6.05	6.02	4.74	3.42	2.50	2.03	1.86	1.85	1.91
5.7	2.01	5.76	5.90	4.71	3.43	2.53	2.05	1.87	1.86	1.91
4.8	1.57	5.50	5.78	4.69	3.45	2.55	2.07	1.88	1.87	1.91
3.8	1.07	5.20	5.66	4.66	3.46	2.58	2.09	1.90	1.87	1.91
2.9	0.62	4.94	5.54	4.64	3.48	2.61	2.11	1.91	1.88	1.91
1.9	0.12	4.65	5.42	4.61	3.50	2.63	2.13	1.92	1.88	1.91
1	-0.32	4.38	5.30	4.58	3.51	2.66	2.15	1.94	1.89	1.92
0	-0.82	4.09	5.18	4.56	3.53	2.69	2.18	1.95	1.89	1.92
-1	-1.31	3.80	5.05	4.53	3.55	2.71	2.20	1.96	1.90	1.92
-1.9	-1.76	3.53	4.94	4.51	3.56	2.74	2.22	1.97	1.90	1.92
-2.9	-2.26	3.24	4.81	4.48	3.58	2.76	2.24	1.99	1.91	1.92
-3.8	-2.71	2.98	4.70	4.45	3.59	2.79	2.26	2.00	1.92	1.92
-4.8	-3.21	2.68	4.57	4.43	3.61	2.82	2.28	2.01	1.92	1.92
-5.7	-3.65	2.42	4.46	4.40	3.63	2.84	2.30	2.02	1.93	1.93
-6.7	-4.15	2.13	4.33	4.38	3.64	2.87	2.32	2.04	1.93	1.93
-7.6	-4.60	1.86	4.22	4.35	3.66	2.89	2.34	2.05	1.94	1.93
-8.6	-5.10	1.57	4.09	4.33	3.68	2.92	2.37	2.06	1.94	1.93

Table 13: Shell Tangential Stress in Mat Layer (MPa)

$\sigma_\theta(W.R.)$	Shell distance aparting from the junction,x(mm)									
z(mm)	0	20	40	60	80	100	120	140	160	180
7.6	3.42	12.11	12.72	10.27	7.50	5.52	4.44	4.03	3.99	4.09
6.7	2.78	11.74	12.56	10.23	7.53	5.55	4.47	4.05	4.00	4.09
5.7	2.07	11.32	12.38	10.19	7.55	5.59	4.50	4.07	4.01	4.10
4.8	1.43	10.94	12.22	10.16	7.57	5.63	4.53	4.09	4.01	4.10
3.8	0.72	10.53	12.04	10.12	7.60	5.67	4.56	4.10	4.02	4.10
2.9	8.17	10.15	11.87	10.08	7.62	5.70	4.59	4.12	4.03	4.10
1.9	-0.62	9.73	11.69	10.05	7.64	5.74	4.62	4.14	4.04	4.10
1	-1.27	9.35	11.53	10.01	7.66	5.77	4.65	4.16	4.05	4.11
0	-1.98	8.94	11.35	9.97	7.69	5.81	4.68	4.18	4.05	4.11
-1	-2.69	8.52	11.17	9.93	7.71	5.85	4.71	4.20	4.06	4.11
-1.9	-3.33	8.14	11.01	9.90	7.74	5.89	4.74	4.21	4.07	4.11
-2.9	-4.04	7.72	10.83	9.86	7.76	5.93	4.77	4.23	4.08	4.11
-3.8	-4.68	7.35	10.66	9.83	7.78	5.96	4.80	4.25	4.09	4.12
-4.8	-5.39	6.93	10.48	9.79	7.81	6.00	4.83	4.27	4.09	4.12
-5.7	-6.03	6.55	10.32	9.75	7.83	6.03	4.86	4.28	4.10	4.12
-6.7	-6.74	6.13	10.14	9.72	7.85	6.07	4.89	4.30	4.11	4.12
-7.6	-7.38	5.76	9.98	9.68	7.87	6.11	4.92	4.32	4.12	4.12

Table 14: Shell Tangential Stress in Woven Roving Layer (MPa)

Chapter 8

FINITE ELEMENT ANALYSIS

8.1 Introduction

The Finite Element Method (FEM) has become a powerful technique for the analysis of various complicated structures which are difficult to handle analytically. In addition to the previous analytical analysis and experimental work, a finite element analysis was performed for the FRP flange connection.

8.2 Basic Knowledge

8.2.1 ANSYS 5.0

At the present software market, there are quite a few FEM commercial computer programs available, namely ANSYS, ABAQUS, NASTRAN, etc. The ANSYS [5] program is the only one supported by Computing Service Department at Concordia University. The program was first originated by Swanson in 1970. Since that time, the ANSYS program has been constantly updated with new features and enhancements. Up to now, the program can be used in all disciplines of engineering. The ANSYS software is available on all types of computers, from PCs to Mainframes, etc. The latest versions of ANSYS software are also available for Windows.

8.2.2 Choice of Elements

With the ANSYS program, the composite materials were modeled as layered elements. There are three types of layered elements available. They are SHELL91, SHELL99, and SOLID46 [3j.

SHELL99 element is an 8-node, 3-D shell element with six degrees of freedom at each node. It is developed to model thin to moderately thick plate and shell structures. The side-to-thickness ratio is roughly no smaller than 10. For those with smaller ratio, the SOLID46 is expected to yield better results.

SHELL91 can be used for the same purposes as SHELL99. The differences are that SHELL99 allows failure criterion calculation, whereas SHELL91 includes material nonlinear behavior such as plasticity, creep, large deflection, etc.Also, SHELL99 allows input of up to 100 layers of uniform thickness. If more than 100 layers are required, a user defined material matrix can be used. However, SHELL91 allows only an input of up to 16 layers.

SOLID46 is an 8-node, 3-D layered solid element with three degrees of freedom per node (UX,UY,XZ). It is developed to model layered solids and allows up to 100 uniform thickness layers per element. Several elements may be stacked across the plate or shell thickness.

SOLID46 is able to calculate non-zero stresses, strains and displacements in the transverse element z-direction. In order to yield results with same accuracy in comparison to using SHELL91 or SHELL99 elements, a finer SOLID46 element mesh is required. Through thickness effects can be obtained by using stacked SOLID46 element.

8.2.3 Assumptions and Restrictions

The assumptions and restrictions for SOLID46 are:

1) The bonding is perfect. No slippage is considered

2) Interlaminar shear stresses are calculated.

a) based on nodal forces

b) based on strain displacement relationships, average across layers.

Both methods are not exact.

8.2.4 Failure Criteria

With the ANSYS program, there are three kinds of commonly used failure criteria available. Also, the user is allowed to supply his own failure criterion, using a USER subroutine. The three in-program criteria are:

Maximum Strain Failure Criterion, which possesses nine failure strains

Maximum Stress Failure Criterion, which possesses nine failure stresses

Tsai-Wu Failure Criterion, which possesses nine failure stresses and three additional coupling coefficients

8.3 Data Input

In order to perform a finite element analysis, the object to be analyzed must be mathematically represented with a mesh of nodes and elements. This mesh can be created by two basic methods: Direct Node and Element Generation, and Solid Modeling/Meshing [4]. Direct node and element generation in the ANSYS program is accomplished by the use of the PREP7 node and element commands groups to build an analysis model. This method is easily understood, but cumbersome for large finite element models or objects with complex shapes. This thesis uses the second method: Solid modeling/meshing. This method uses high-level mathematical entities to describe an object. These entities can be automatically filled ("meshed") with nodes and elements. The solid modeling/meshing has several advantages over direct node/element generation:

1) It allows to work with a relatively small number of data items.

2) It allows geometric operations which cannot be done with nodes and elements.

3) It allows to easily modify the geometry.

4) It facilitates changes to element distribution. It is not committed to one analysis model.

5) It facilitates optimization procedures.

8.4 Examples

Problem

One FRP flange was modeled and a linear static FE analysis was performed. The flange dimensions are given in Figure 21, Chapter 7. Both flange and shell are

symmetrically layered up of woven roving and mat. In order to facilitate direct comparison between the results from a FE analysis and from an analytical method for a full face flange, the model was chosen to be identical to the flange which was studied using the analytical method in the previous chapters.

Two working conditions, bolt-up and operating, are analyzed here. The flanged connection is assumed to be sufficiently far from the end enclosures of the vessel, such that the longitudinal end bending is limited only to its small adjacent portions of the vessel compared to the overall length.

The material properties used for the problem are as follows:

Mat ply: (isotropic)

$$
\begin{aligned}
E_L &= 8.0\ GPa \\
E_T &= 8.0\ GPa \\
E_Z &= 3.0\ GPa \\
\nu_L &= 0.2 \\
E_S &= 3.33\ GPa
\end{aligned}
$$

Woven Roving ply: (polarly orthotropic)

$$
\begin{aligned}
E_L &= 18.0\ GPa \\
E_T &= 18.0\ GPa \\
E_Z &= 3.0\ GPa \\
\nu_L &= 0.13 \\
E_S &= 3.6\ GPa
\end{aligned}
$$

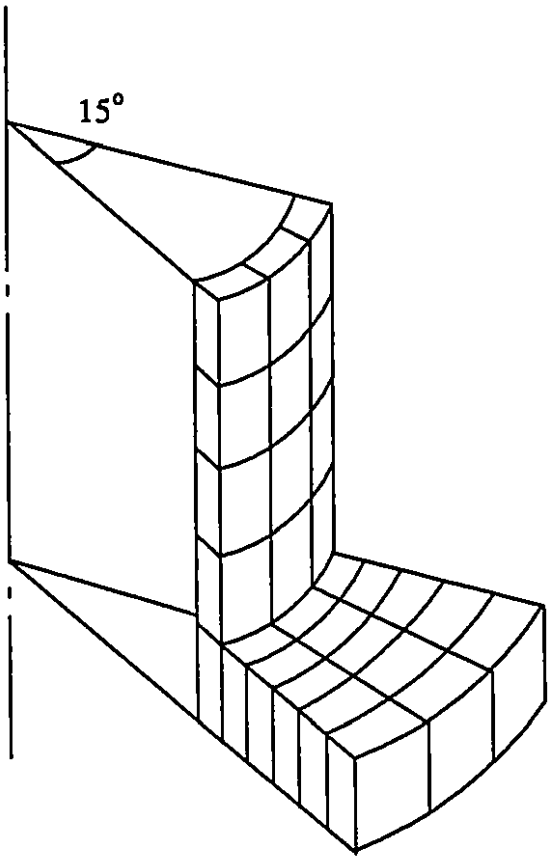

Figure 33: FEM Model

Finite Element Model

Axial symmetry is used to model a 15 degree section of the whole flange as shown in Figure 33. In this model, Solid46 elements are used for both the shell and flange sections.

Figure 34 shows the loads and constraints applied onto the finite element model.

Since the SOLID46 element has one degree of freedom (UY) per node along the model tangential direction, axial symmetrical boundary condition merely requires

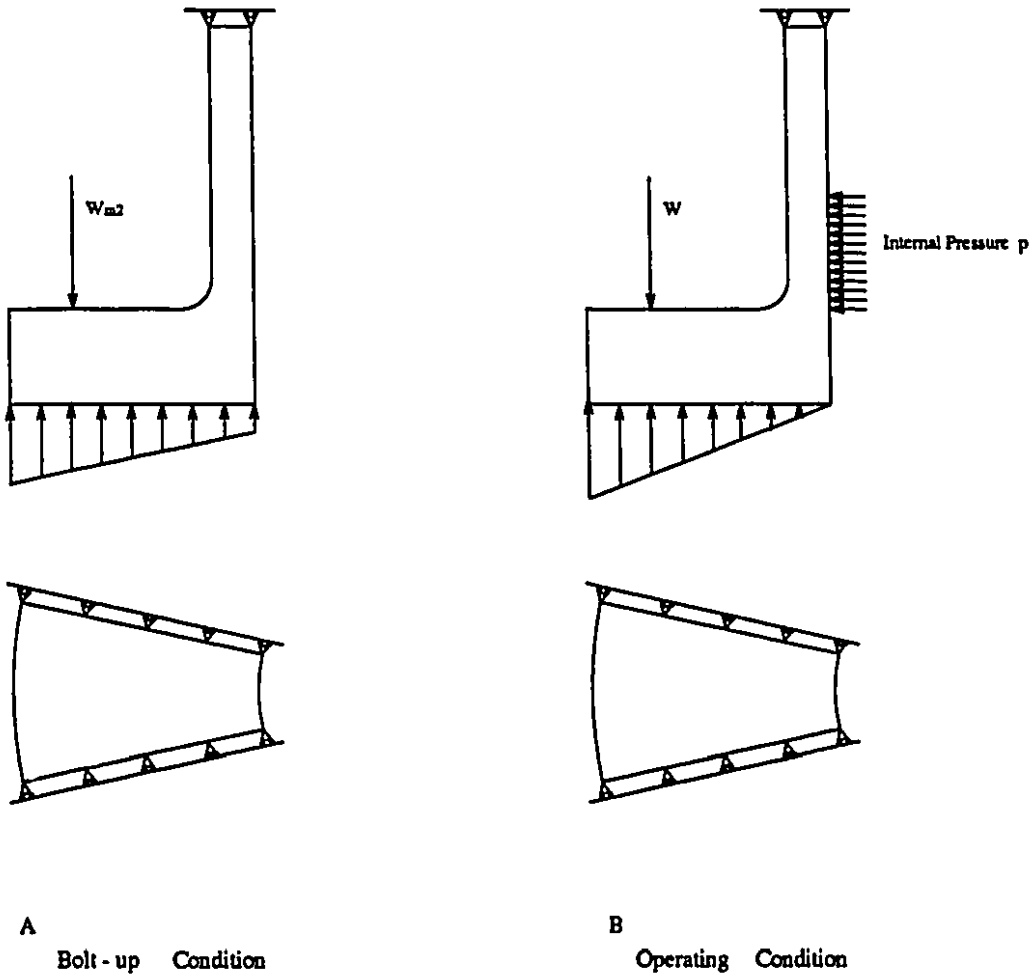

Figure 34: Model Loads and Constraints

zero displacement in this direction.

To keep the model from rigid body motion along the axial direction, the degree of freedom UZ in the shell section surface must be fixed. This will also give rise to bending near the shell boundary, balancing the rotation of the model once the loads are applied. Thus, in the model the shell length should be long enough to eliminate this local effect.

The front (lower) face of the flange is free from any boundary constraint. Flange rotation is expected to compress the gasket over the full face once the bolt load is applied.

The gasket load is assumed linearly distributed over the whole flange sealing surface for both operation and bolt-up condition. This assumption is consistent with previous analytical solutions.

For the purposes of modeling, the bolt load has been represented by a narrow circular ring shape surface load over the flange circumference so that equivalent bolt load in the bolts is regenerated.

However, this simulation of the actual bolt load situation can not reflect the accurate stress level in the area around the bolt hole. The failure of the flange body at or near the bolt holes will neither be predicted by this FE analysis, nor by the previous analytical analysis. Nevertheless, as the bolt hole area is relatively far away from the flange shell junction, this will not significantly affect the prediction of discontinuity stresses in that area.

Input Listing

The geometry, material properties and loads are defined, using parameters so that changes in the model can be conveniently made if required.

The layer stacking sequence is symmetric for both flange and shell laminates. Only half of laminates need to be defined, from the bottom up. The flange consists of 20 layers of mat and woven roving materials, whereas the shell consists of 10 layers. All layers are of constant thickness. Layer orientation angles are input as zero for both materials. A small value of E_z, equivalent to the resin's Young's modulus is specified for both mat and woven roving materials. Row-normalized values PRXY are used.

The loading input listing given in Appendix B is divided into two parts. Part 1 considers loads for the operating condition while part 2 of the input is for the bolt-up condition.

8.5 Results in Comparison with Analytical Method

The FEM may underestimate real stress levels at certain areas near the junction where high stress variations exist. Stresses at these areas are averaged over the element. In such a case, a finer element meshing is needed.

8.5.1 Flange Stresses

The calculated flange stress values using the FEM come close to the analytical values only at the junction area. For other areas over the flange plate, the two results differ significantly from each other. The reason lies in the fact that the bolt load is replaced by a continuous circular ring type load at the bolt circle diameter on the back face of the flange in the finite element analysis, while in the analytical method the bolt load is absorbed into the flange overall bending moment. Thus using the analytical assumption, the bolt load has no direct impact over the flange front or back face. Due to this limit, the two calculated results will not converge on each other in these areas.

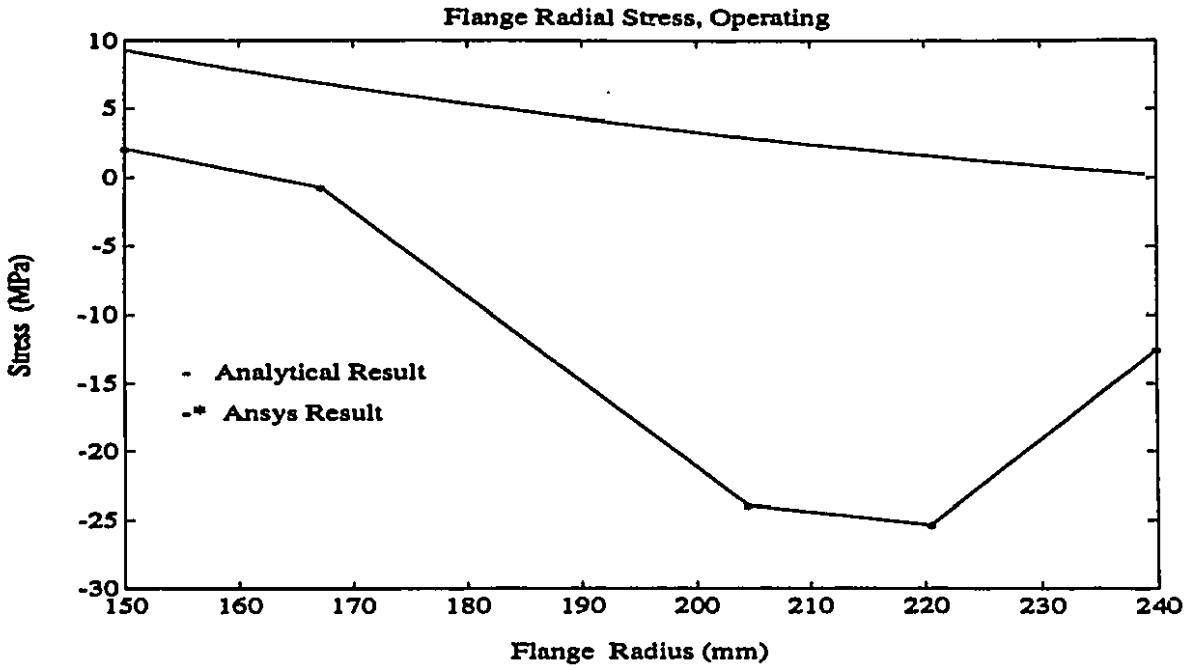

Figure 35: Flange Back Face Radial Stress, Operating

The results using the FEM are given in this section. Figures 35, 36, 37, 38 show the flange radial stress distributions over front and back face, for both operating and gasket seating conditions. The tangential stress distributions are shown in Figures 39, 40, 41, 42 for operating and gasket seating conditions.

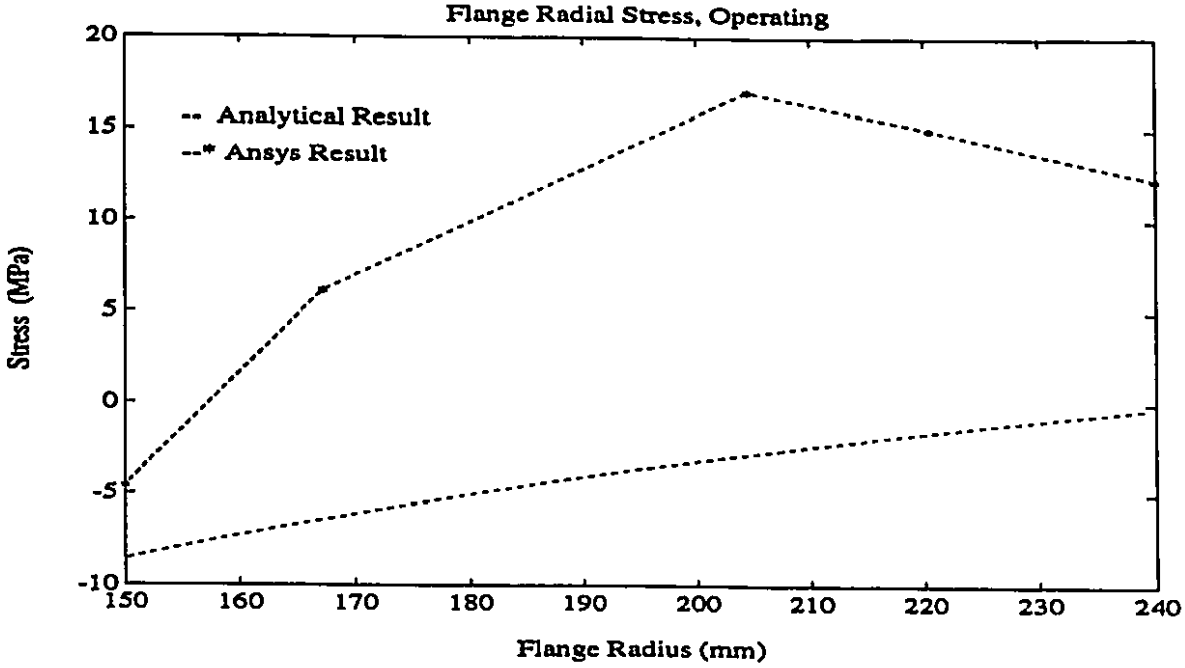

Figure 36: Flange Front Face Radial Stress, Operating

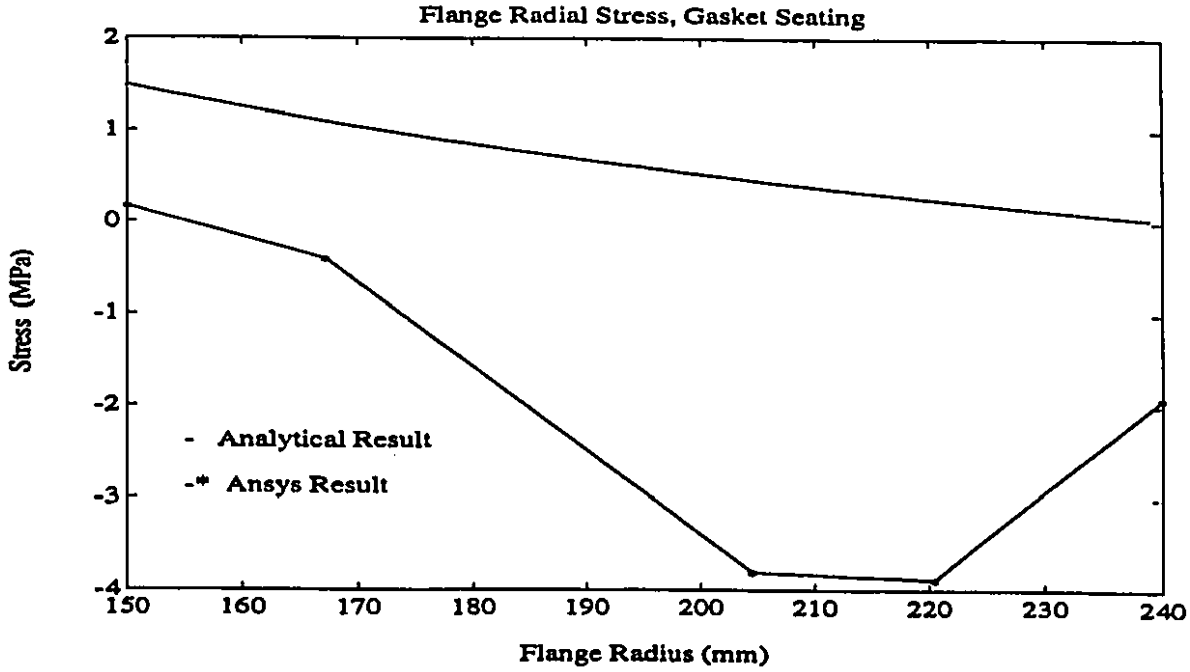

Figure 37: Flange Back Face Radial Stress, Gasket Seating

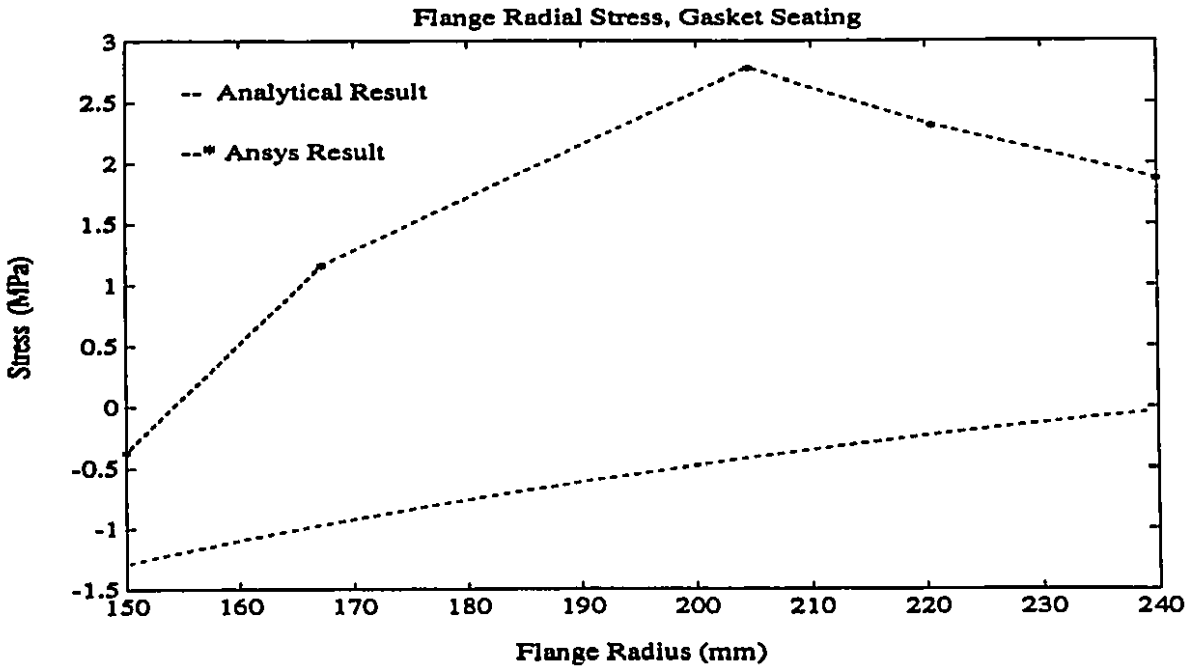

Figure 38: Flange Front Face Radial Stress, Gasket Seating

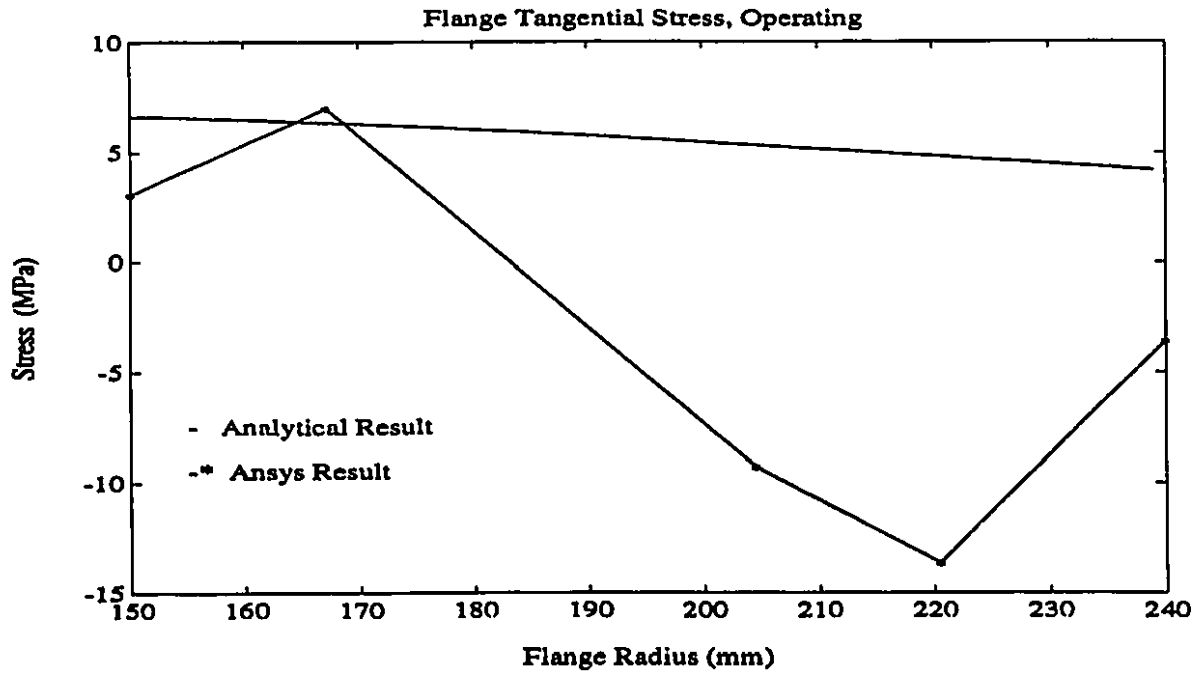

Figure 39: Flange Back Face Tangential Stress, Operating

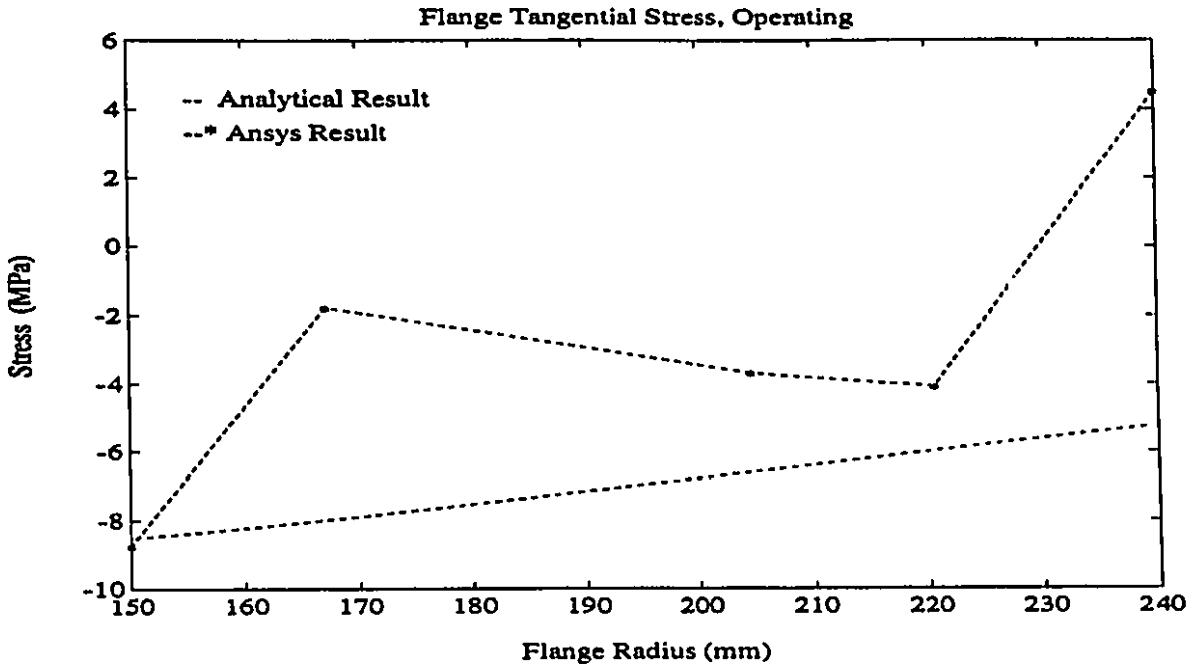

Figure 40: Flange Front Face Tangential Stress, Operating

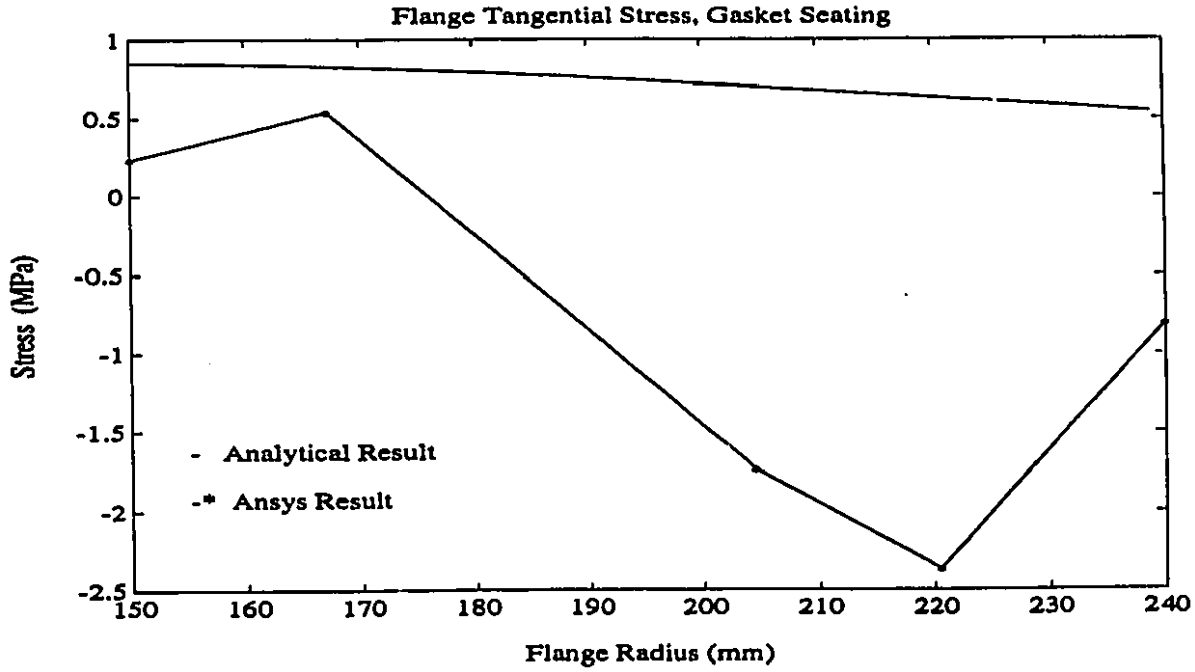

Figure 41: Flange Back Face Tangential Stress, Gasket Seating

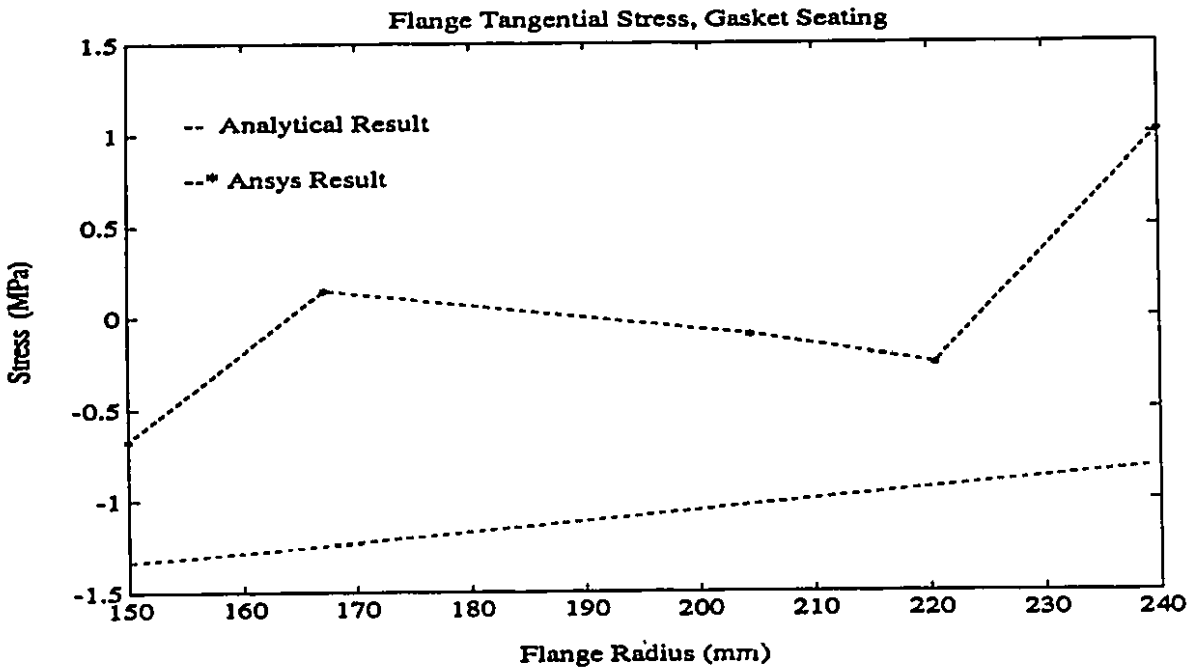

Figure 42: Flange Front Face Tangential Stress, Gasket Seating

8.5.2 Shell Stresses

For most part of the shell section shown here, the longitudinal stresses given by the FEM are very close to the analytical results, except at the areas near the junction, where some slight discrepancies exist. One reason of this is that over this section the stresses change dramatically where the elements will only give results based on medium values.

The FEM values of the shell tangential stresses are consistently close to their analytical values. At the junction adjacent area, the same tendency exist here as with the shell longitudinal stresses.

When looking at the figures shown here, we should also remember that the element used, Solid46, in the ANSYS software, includes shear deformation. Nevethless, the analytical results are based on no shear deformation. In return, the two results

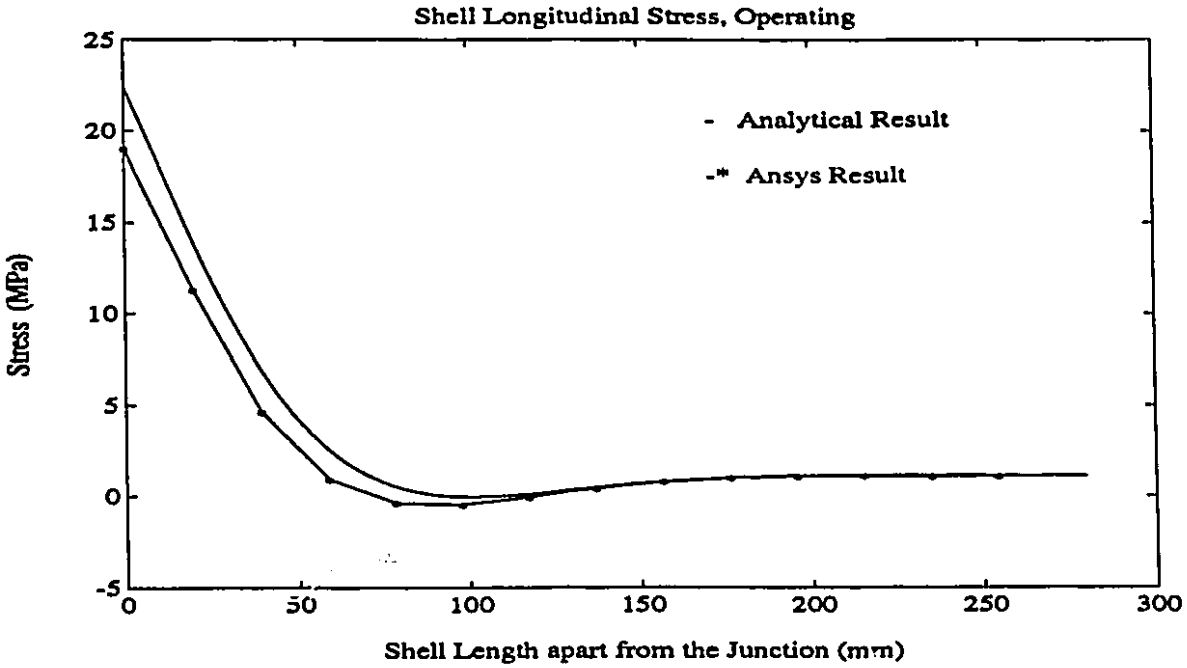

Figure 43: Shell Outer Surface Longitudinal Stress, Operating

obtained here are certainly showing certain differences, with a magnitude which cannot be predicted beforehand.

In the ANSYS, stress outputs can be listed on nodes as well as on Gauss points. The former output values are the average values of the latter one in adajecnt elements. On the point of the junction, because of different element coordinates assigned for the flange laminate and the shell laminate seperately, without appropriate coordinate transformations, the nodal stresses calculated by the ANSYS program are not the real values. Only the stresses given on Gauss point nearby are the true ones. Thus, junction nodal stress output should be avoided.

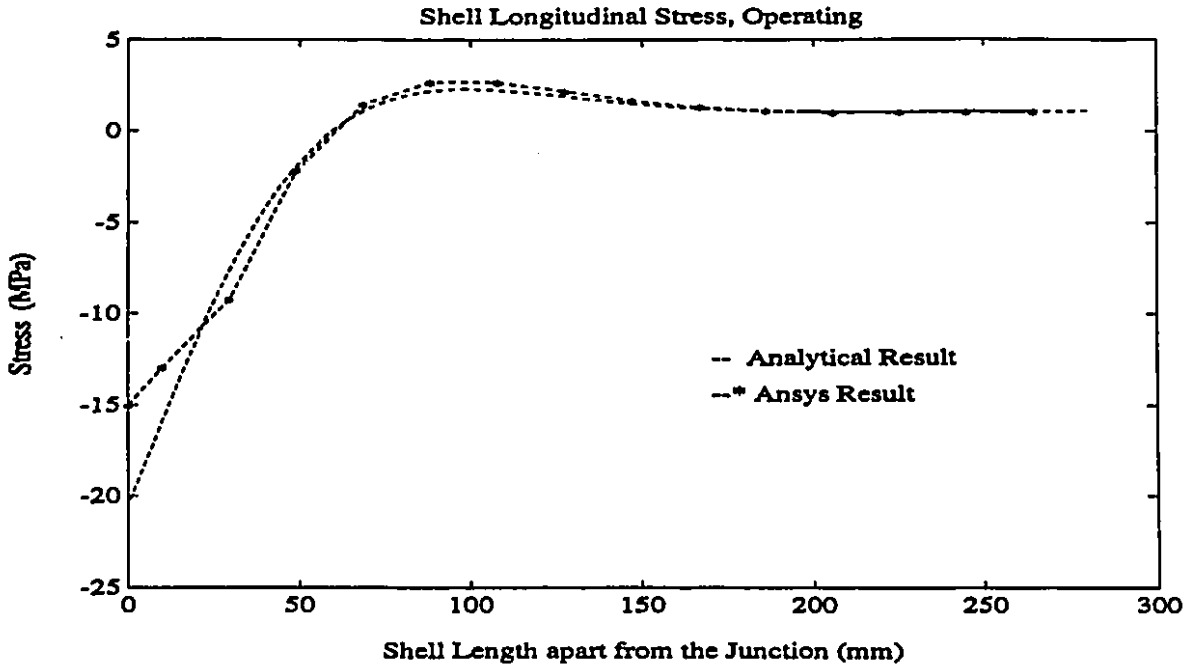

Figure 44: Shell Inner Surface Longitudinal Stress, Operating

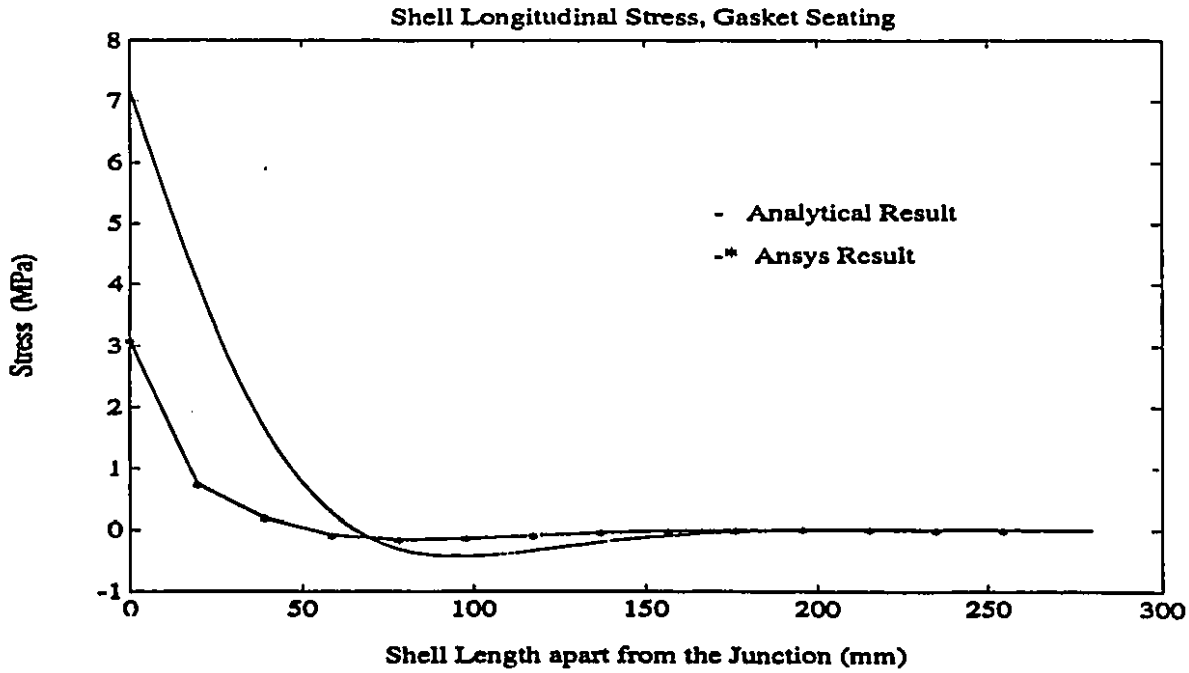

Figure 45: Shell Outer Surface Longitudinal Stress, Gasket Seating

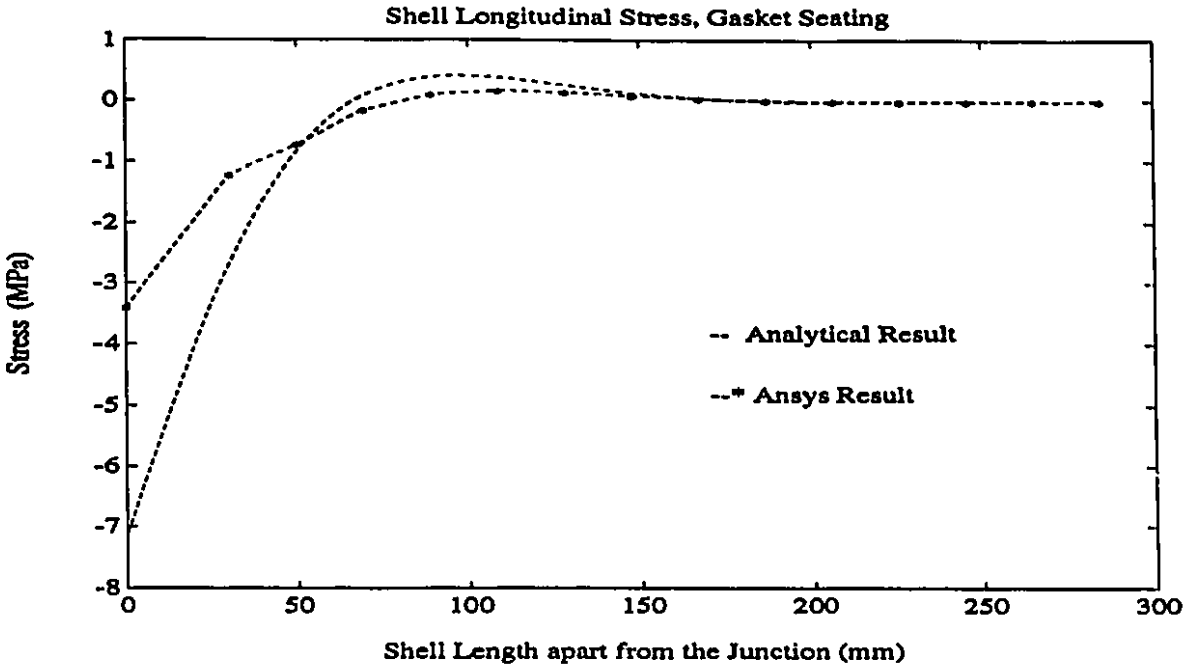

Figure 46: Shell Inner Surface Longitudinal Stress, Gasket Seating

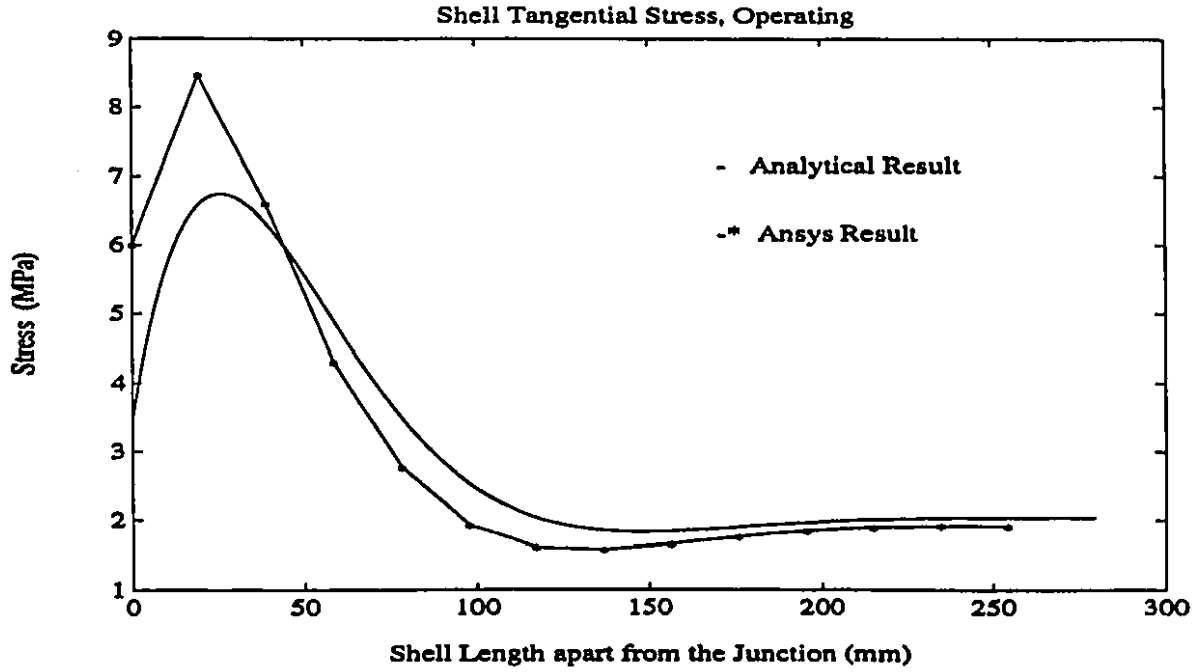

Figure 47: Shell Outer Surface Tangential Stress, Operating

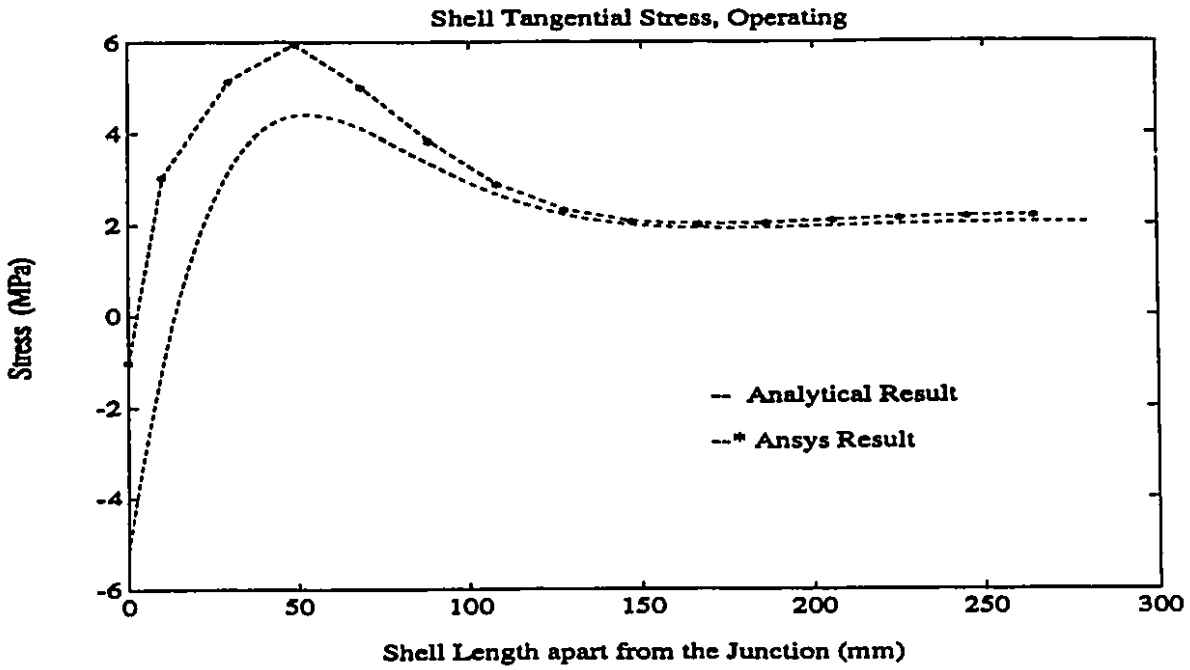

Figure 48: Shell Inner Surface Tangential Stress, Operating

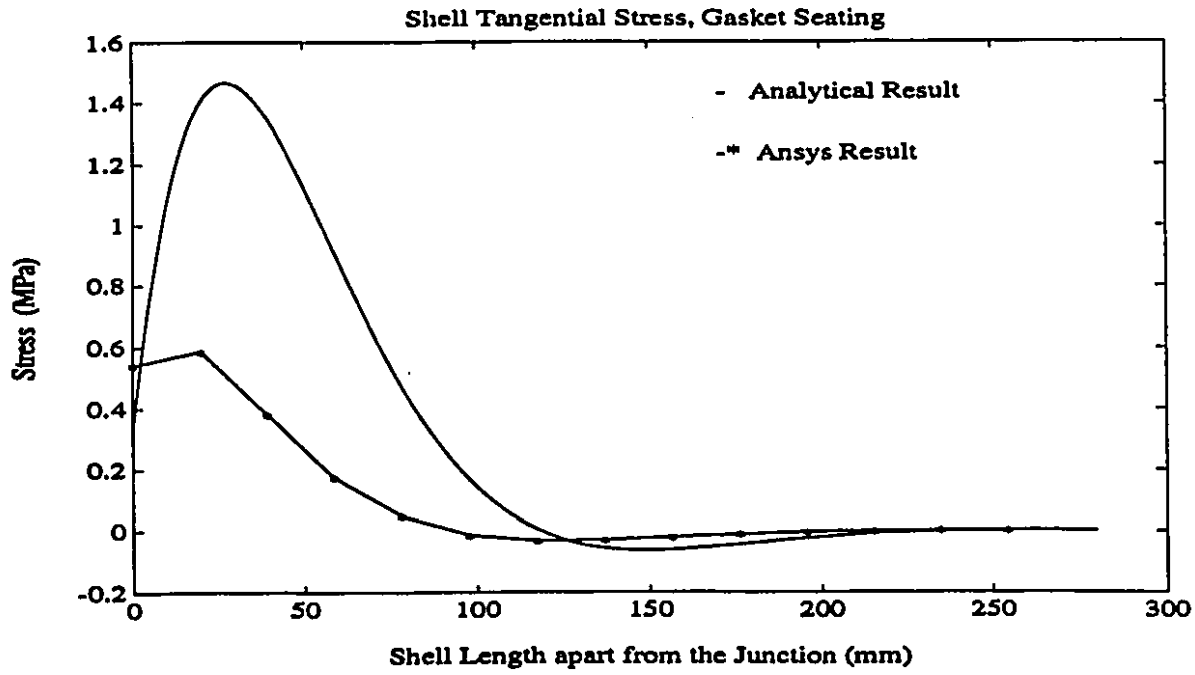

Figure 49: Shell Outer Surface Tangential Stress, Gasket Seating

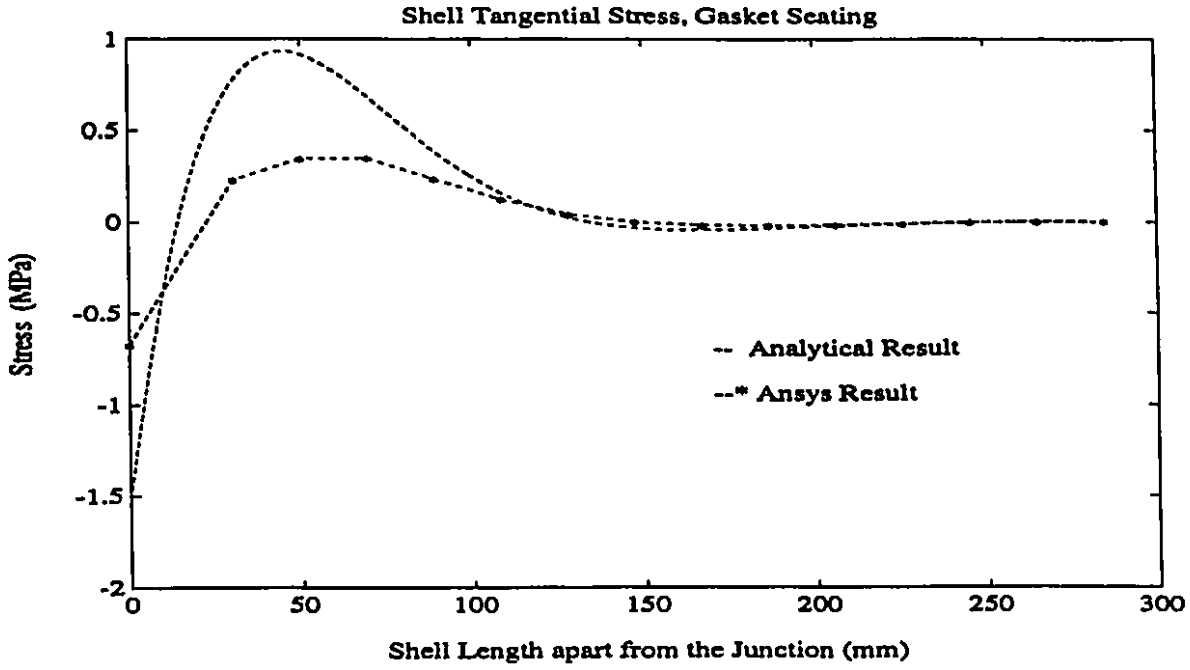

Figure 50: Shell Inner Surface Tangential Stress, Gasket Seating

8.6 Summary

It is generally observed here, that the FEM gives results very close to the results by an analytical method, given such a complex problem with many assumptions made in each calculation. However, due to the lack of sufficient experimental verification, it is not able to predict whether these two methods are on the safe side or not. In practice certain safety factors need to taken into consideration.

Chapter 9

EXPERIMENTAL WORK

9.1 Introduction

An FRP pressure vessel was tested as shown in Figure 51. This vessel has flanges of different thicknesses at its ends. To record the stresses and strains, strain gauges were mounted onto the flange surfaces. A close view of both top and bottom flanges is shown in Figures 52 and 53. The tests were conducted in both bolt-up and operating conditions. The operating pressure was gradually increased and data were collected during the pressurization cycle.

9.2 Description of the Tests

9.2.1 Test Set-Up

As shown in Figure 54, the vertically supported vessel was connected to a water pump and a drain line through its bottom nozzle. On the top nozzle, a vent line and pressure gage was installed. The vent could be connected to a pressurized air line in order to increase the test pressure beyond the pressure capacity of the water pump.

Figure 51: Test Pressure Vessel

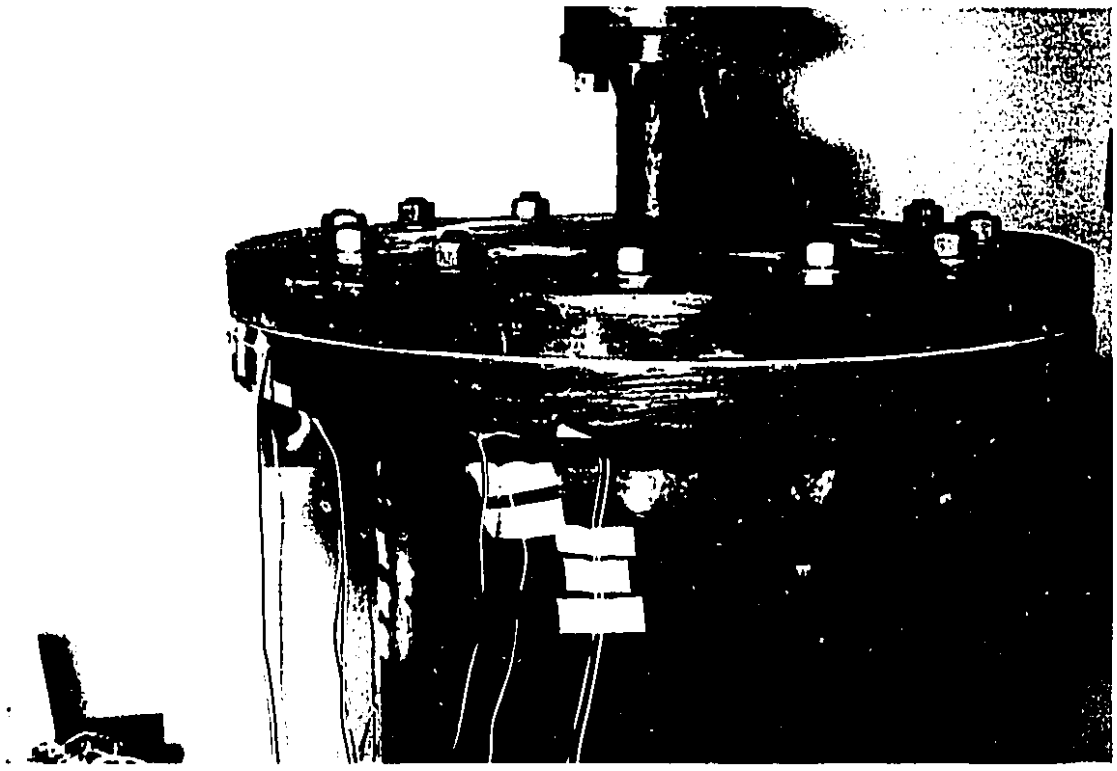

Figure 52: Top Flange

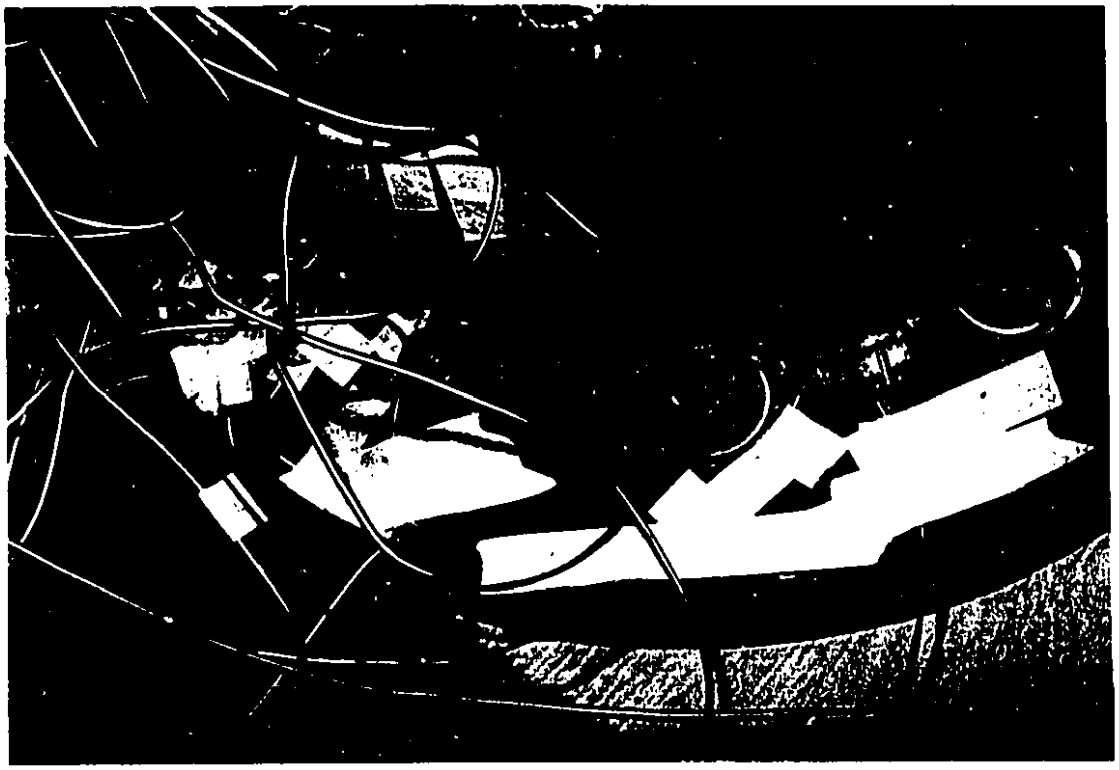

Figure 53: Bottom Flange

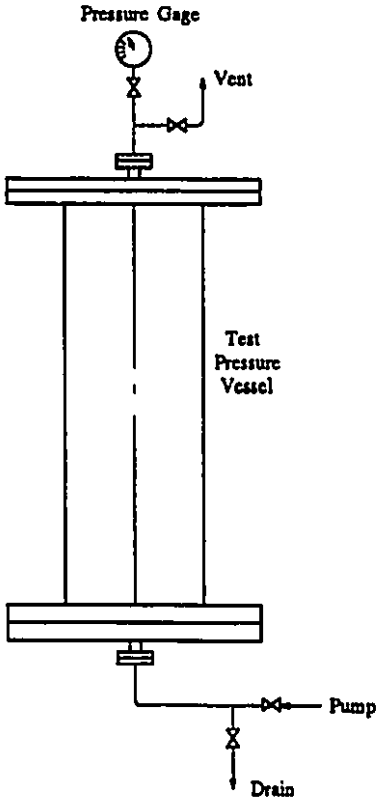

Figure 54: Test Set-Up

9.2.2 Test Pressure Vessel

The test pressure vessel was provided by C.P.F. Dualam Ltd. The flanges were made of glass mat and woven roving and were impregnated with the same resin. The polymer matrix is a vinyl ester. The resin is activated and cured with 1% MEK peroxide (max.) and 0.2 to 0.3% Cobalt Naphthenate. The vessel had a veil liner as a corrosive barrier. The outer surface is made of resin rich layer.

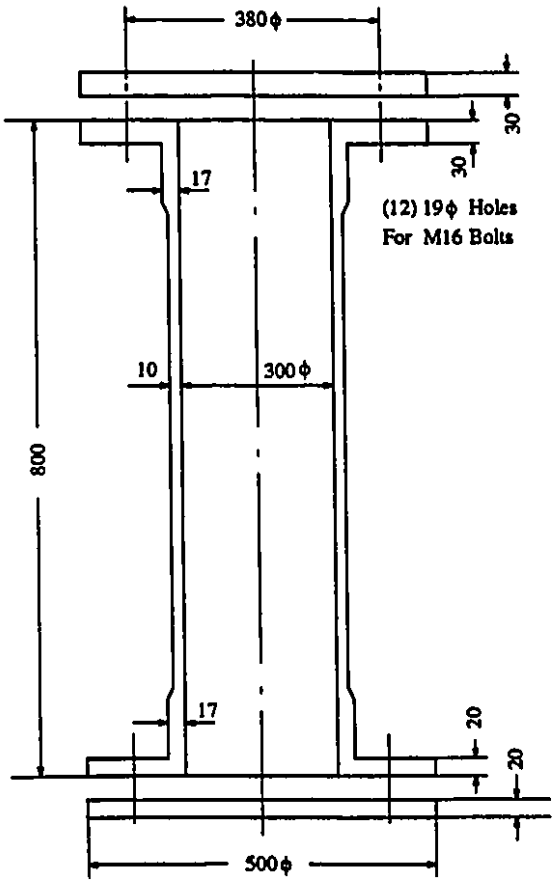

Figure 55: Dimensions of Test Vessel

The construction of the 30 mm flange laminate is

$$V/(M/WR/WR)_5/M/R$$

The 20 mm flange laminate is

$$V/(M/WR/WR)_3/M/R$$

The 17 mm shell laminate is

$$V/(M/WR/WR)_2M/WR/R$$

The 10 mm shell laminate is

V/M/WR/WR/M/R

where V = veil layer (2.0 mm thick), M = mat layer (1.0 mm thick), WR = woven roving layer (2.0 mm thick) and R = resin rich layer (2.0 mm thick).

Ten bi-axial strain gauges, CEA-06-125UW-120, were bonded with M-Bond 200 adhesive to the outside surface of the vessel as shown in Figure 56.

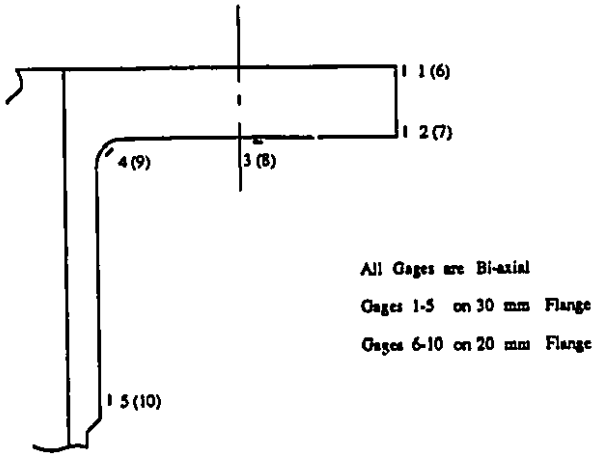

Figure 56: Strain Gage Locations

Two kinds of 3 mm thick full face gaskets were used. One was made of compressed asbestos, the other was made of synthetic rubber with a hardness of 75 durometer.

Water with a rust inhibitor was the test fluid.

There was considerable variation in the thickness of both flanges due to commercial fabrication tolerances. However, the effect was not taken into consideration, and the nominal values shown in Figure 55 will be used for subsequent stress analysis.

Since a change in test temperature would have had a severe impact on the accuracy of the test results, because of the large number of strain gauges involved in this test, a constant room temperature was maintained during the test.

The same test pressure vessel was also used to perform buckling tests, see Ouellette [59].

9.2.3 Test Parameters

The test parameters were:

Pressure (kPa) = 0, 138, 276, 414
Bolt load (MPa) = 50, 100, 150
Temperature = Room temperature (20^0 C)

9.3 Test Procedure

9.3.1 Bolt-up

A manual torque wrench was used. The bolts were lubricated with machine oil giving a nut factor of $K = 0.16$. This is an economical and practical way to control the load of a large number of bolts. The torque value required to apply on the bolts is calculated by

$$T = \frac{K}{0.2} \times \frac{\sigma}{172.4} \times T_T \tag{375}$$

Where

T	=	corrected torque (N-m)
K	=	nut factor for the application (see Table 5.1, p. 141, [14])
σ	=	average stress in thread region desired in the application (MPa)
T_T	=	torque value given in the reference (N-m)

When a bolt is tightened, it partially compresses the flange in its local area. When nearby bolts are tightened later, they also compress the flange in their region and thus reduce the preload of the first bolt. Tightening bolts on the opposite side of the flange, however, may increase the preload in some of the earlier bolts tightened on the near side. In order to tighten the flange bolts evenly, a torquing sequence for bolt-up shown in Figure 57 is usually employed. This bolt tightening sequence is called a "star pattern". Out of a total of 12 bolts, 2 were instrumented. This permitted a verification of calculated torque values.

In addition, to achieve a required preload, the bolts should be tightened gradually, in several cycles, in order to achieve the required preload. On the first pass, bolts are tightened to a value somewhat lower than the desired preload. After a few cycles of tightening in the star pattern, the desired uniform preload can be reached.

9.3.2 Pressurizing

Once the flange is bolted up, the test vessel can be pressurized. The pressure was generated by pumping water into the vessel. When the pressure reached the desired value each time, the corresponding strains were recorded.

After the first test was done, the flange outside diameter was cut down on lathe to a smaller value. The outer strain gauges were remounted on the area showing the

least amount of delamination due to machining the outside. A total of 5 tests were performed for 5 different flange outside diameters.

The purpose of this 5 tests was to define the effect of different outside to inside diameter ratios K on the flange stresses. It was considered useful for design purposes to examine the effect, of a varying ratio K on stresses and sealing characteristics.

The 5 different flange outside diameters are shown in Figure 58.

9.4 Stress Calculations

The formulae for calculating the stress from observed strains are

$$\sigma_x = mE(\varepsilon_x + \nu\varepsilon_y) \tag{376}$$

$$\sigma_y = mE(\nu\varepsilon_x + \varepsilon_y) \tag{377}$$

where

$$m = (1 - \nu^2)^{-1} \tag{378}$$

The outer resin rich layer of the test vessel is mainly vinyl ester resin. From Table 2.2, page 46 in Hoa [40], the properties for this material are taken as:

$$E_x = 4.0\ (GPa) \tag{379}$$

$$E_y = 4.0\ (GPa) \tag{380}$$

$$\nu_x = 0.35 \tag{381}$$

$$\nu_y = 0.35 \tag{382}$$

and also,

$$m = (1 - 0.35 \times 0.35)^{-1} = 1.140 \tag{383}$$

9.5 Interpretation of Test Data

There are some slight fluctuations in some strain measurements. This was caused by some drift in the strain gauges. The drift occurring spontaneously was easily detected and corrected by comparing the data recorded before the test and afterwards.

When a flange is clamped, there will be an angular distortion (rotation) of the flange under the influence of bolt and reaction forces. Thus bolts will bend accordingly. To compensate for bending, two strain gauges are usually positioned on the opposite sides of the unthreaded bolt shank diameter. Then the mean value of strain from these two gauges determines the preload of the bolt. Since we do not have full-field monitoring of all bolts (which would be best), there is a possibility that bolt bending may occur at some uninstrumented bolts. Thus using only a torque wrench, some of the uninstrumented bolts may be inaccurately loaded.

With these considerations in mind, experimental stress values for each of the five flange configurations are established.

9.6 Typical Results

9.6.1 Stress vs. Ratio of Diameters (K)

For the complex problem of FRP bolted flanged connections, it was shown that the width of flange and the location of the bolt circle have a profound effect on the performance of the bolted flanged connection. Figures 59 and 60 show that an increase in flange width results in lower stresses, and an attempt should be made to

place the bolt circle as much as practicable into the center of the flange cross section.

9.6.2 Stress vs. Fluid Pressure

Once the flange is bolted up, initial pressurizing of the flanged connection will relax the stresses in the flange. However, as further pressure is applied, the stresses are expected to reach higher levels, in which case the operating stresses will govern the vessel strength.

In this test, no leakage was observed with an increase of pressure. However, when the pressure was increased above 400 kPa, the sound of fiber cracking could be heard. Some damage is presumed to have occured within the laminate at the flange shell junction where the highest stresses were observed.

9.6.3 Stress vs. Bolt-Up Load

Stresses are very sensitive to bolt-up loads. Bolt sizes should be limited to the minimum bolt area necessary for gasket seating and operation. Overbolting must be avoided in order not to damage the relatively soft FRP material.

9.7 Results in Comparison with Analytical Method

For the most part of the flange and shell sections shown in Figures 65,66,67, and 68, both results are quite close, except at the junction. This is because the vessel tested had a slightly round corner at the junction. The tested shell values at this area were lower than that of a sharp corner.

The considerable variations in the thickness of flange and shell arising from resin curing process will also affect the agreement between the two methods. In order to

explain the existing discrepancy, a slight change of the layer's modulus can be used in calculating the analytical result, which will bring the two results closer.

9.8 Summary

In this study only two series of flanges, two kinds of gasket were tested, each series of flange differ in their outside diameters. Clearly the results must be used with caution in absence of a larger data base. More extensive testing might uncover discrepancies with the other analyses, which is of particular importance in improving the understanding of the FRP flange behavior.

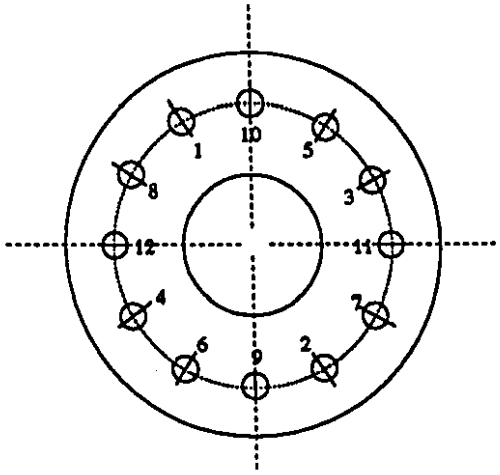

Figure 57: Bolt Torquing Sequence

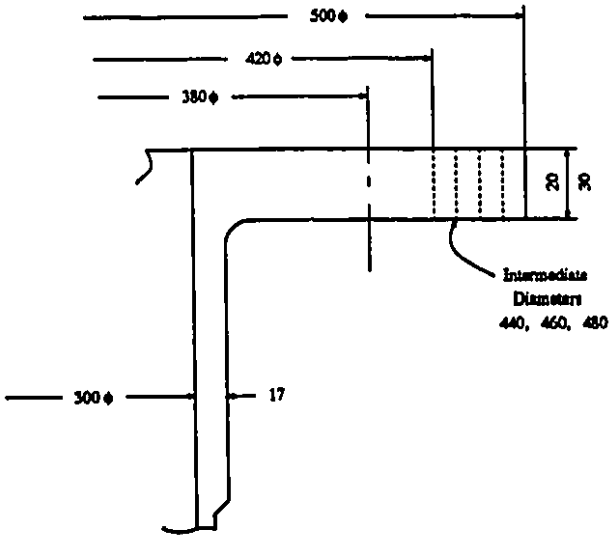

Figure 58: Flange Dimensions

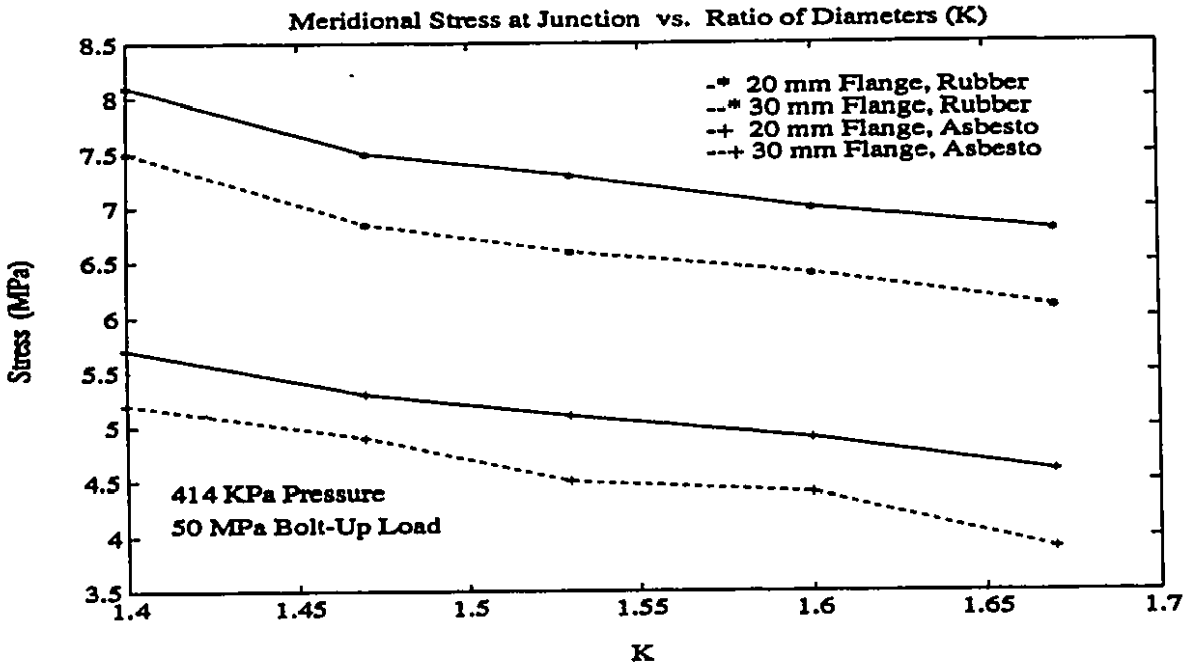

Figure 59: Flange Meridional Stress vs Ratio of Diameters K

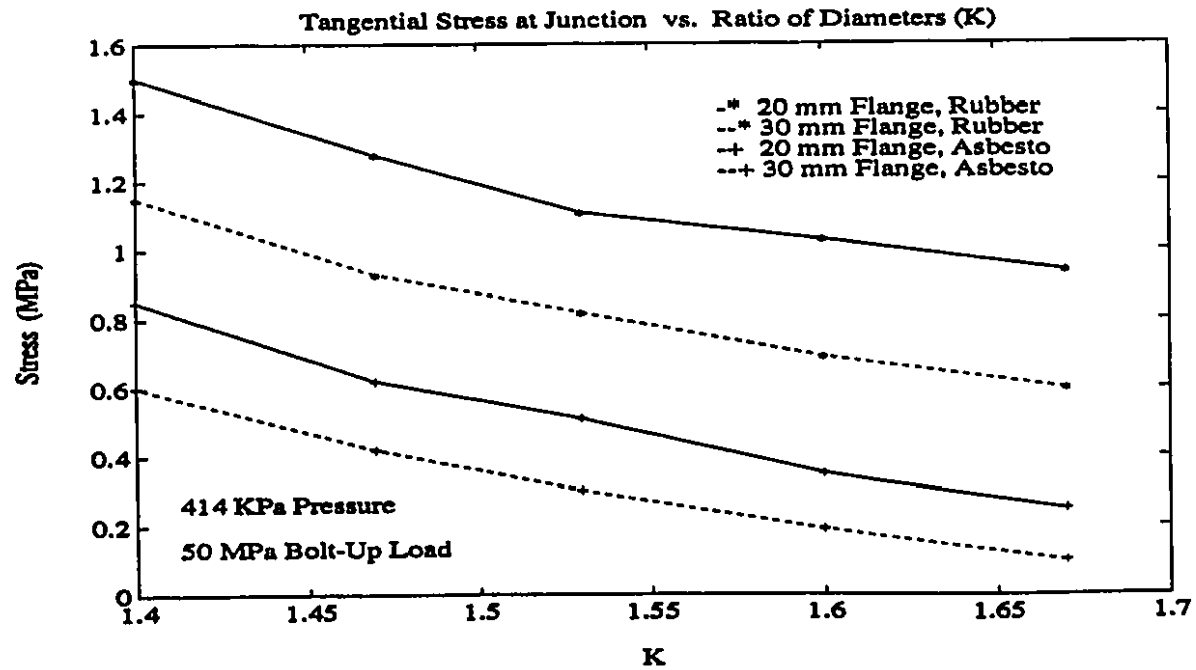

Figure 60: Flange Tangential Stress vs Ratio of Diameters K

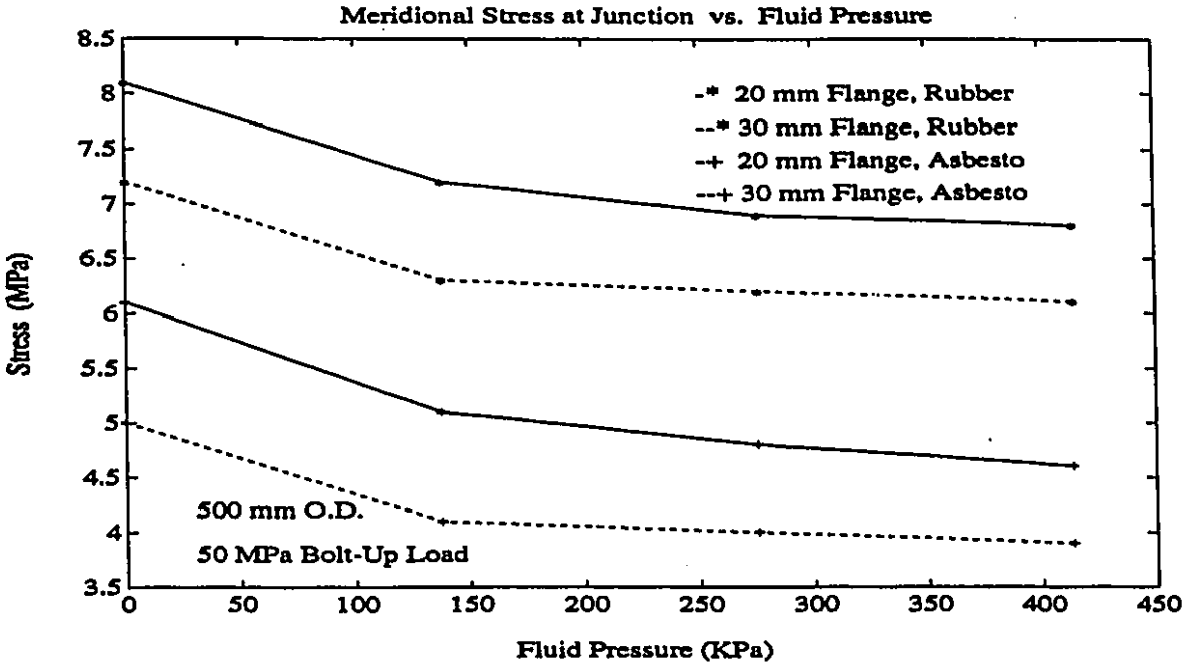

Figure 61: Flange Meridional Stress vs Fluid Pressure

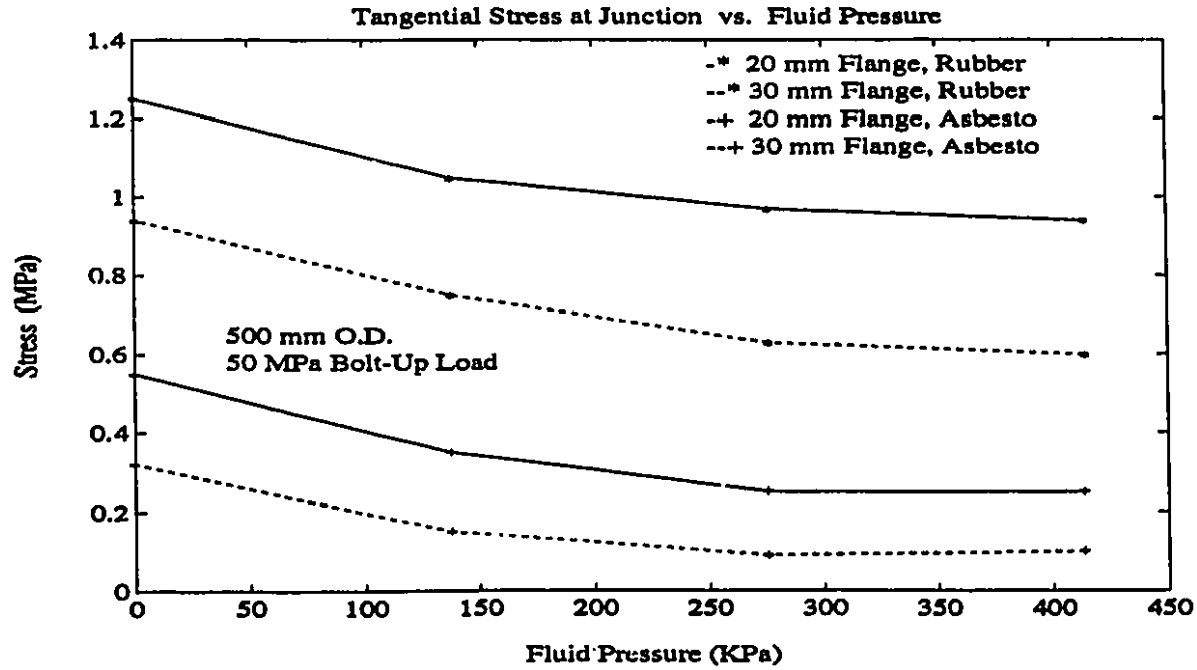

Figure 62: Flange Tangential Stress vs Fluid Pressure

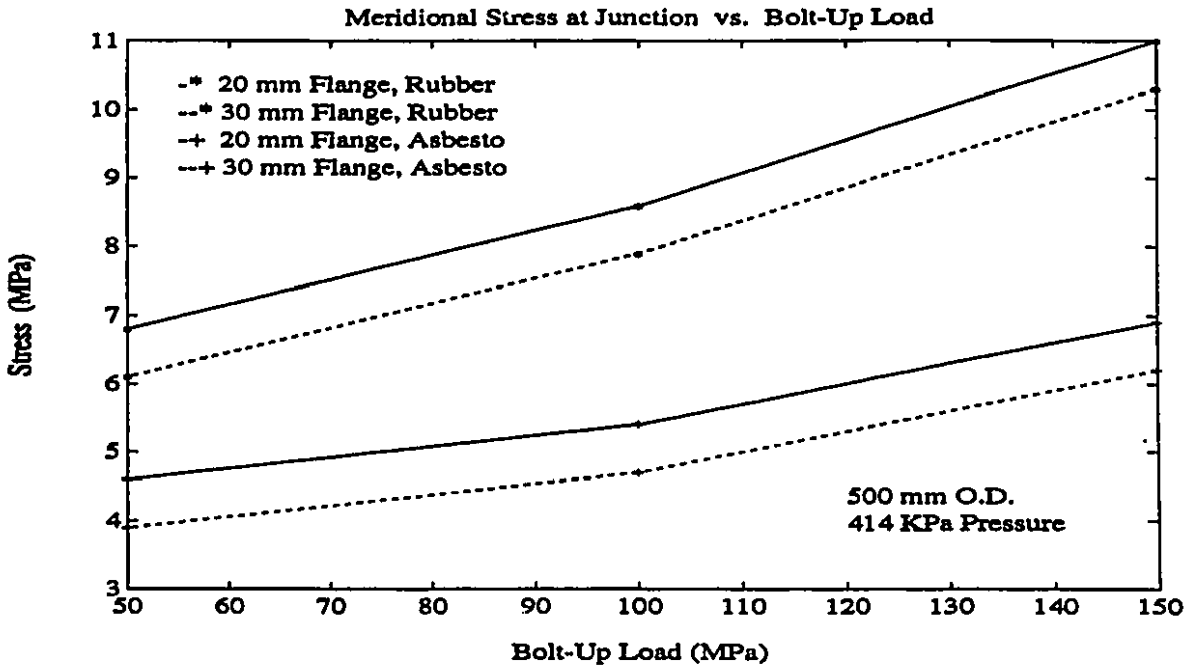

Figure 63: Flange Meridional Stress vs Bolt-Up Load

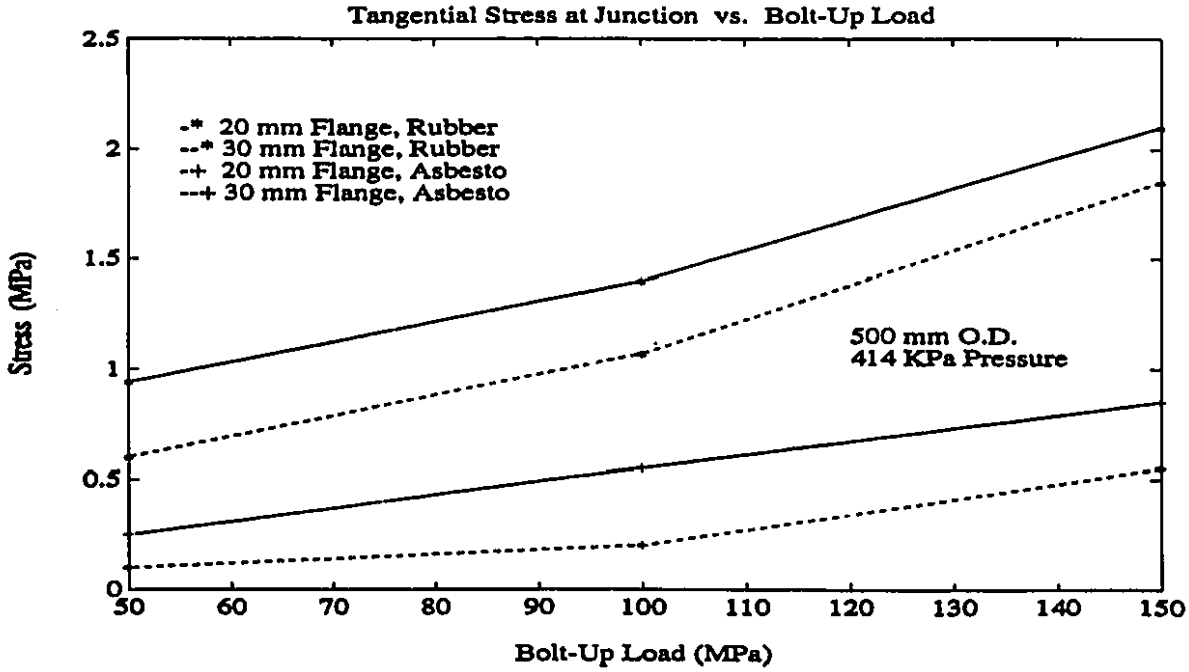

Figure 64: Flange Tangential Stress vs Bolt-Up Load

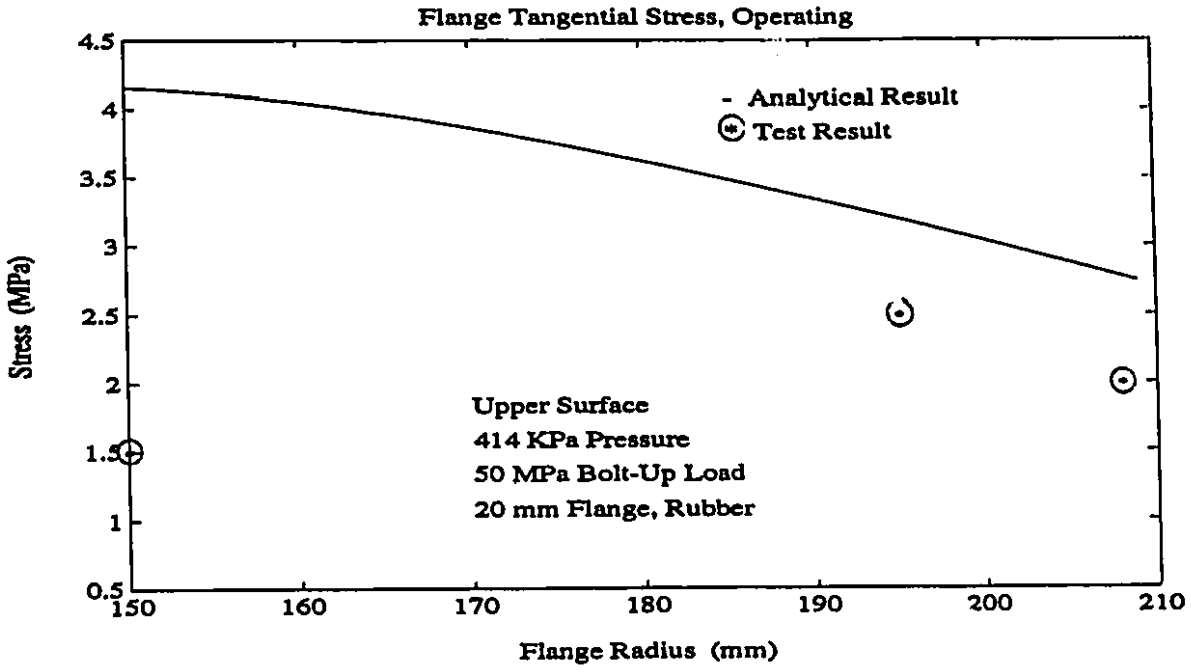

Figure 65: Comparison of Flange Tangential Stresses

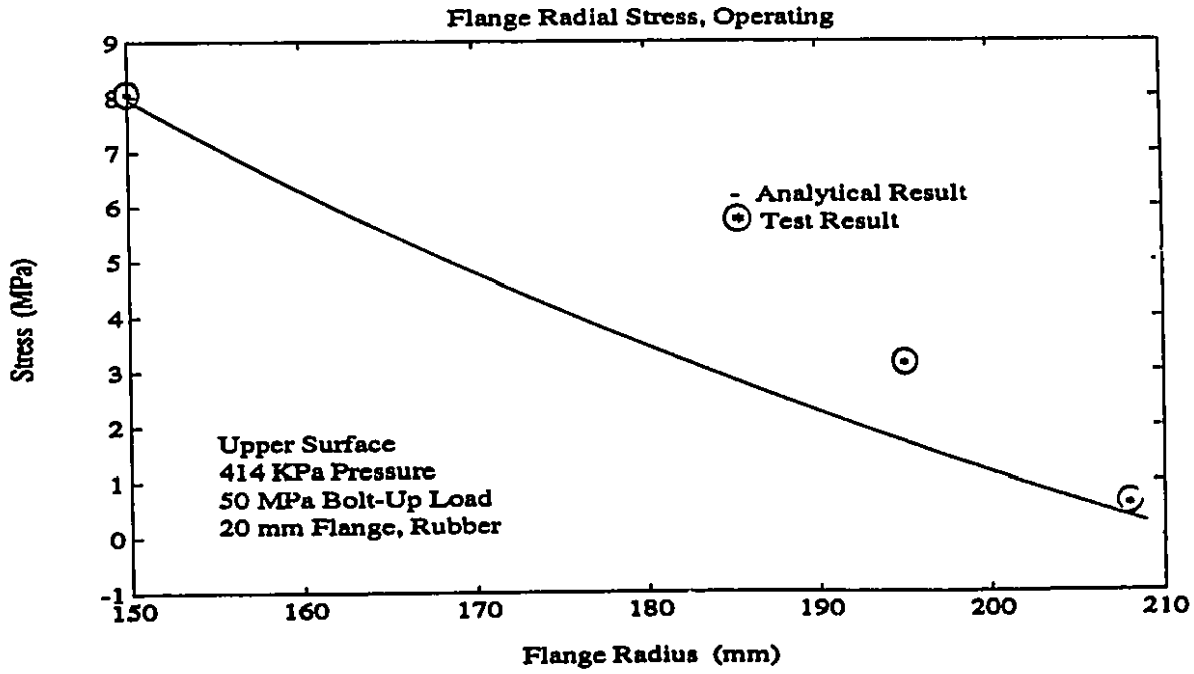

Figure 66: Comparison of Flange Radial Stresses

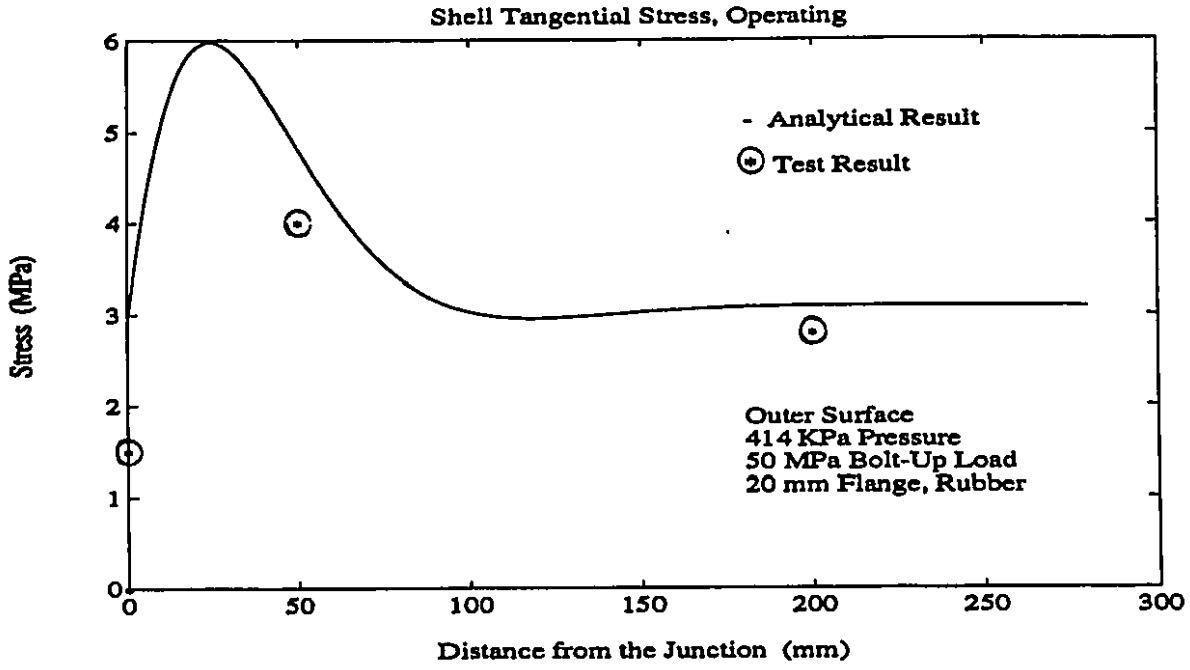

Figure 67: Comparison of Shell Tangential Stresses

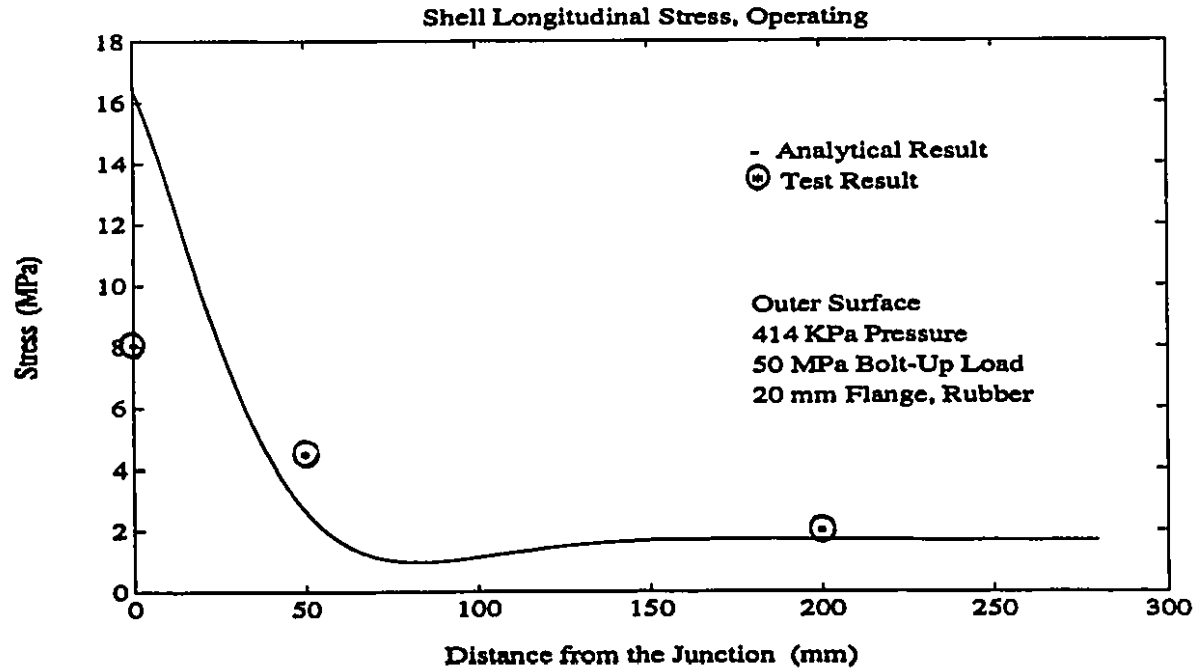

Figure 68: Comparison of Shell Longitudinal Stresses

Chapter 10

FINAL REMARKS

10.1 Conclusions

It is the purpose of this dissertation to provide a new, more accurate method to be used in the design of FRP bolted flanged connections. The method given is based on a rigorous mathematical analysis of the problem, using as few simplifying assumptions as possible. Due to the complexity of the laminate problem, not all of the physical constraints could be satisfied, however, results are much more accurate than those obtained in using any of the greatly simplified customary design methods, based on metallic flanges.

The method as presented, using infinite series expansion in the solution, is obviously not really suitable for everyday use by flange designers. It may, however, serve as a "yardstick" on which improved simplified design methods may be evaluated.

Thus, the strength of identical pairs of flanges was analyzed, using two methods, the classical and shear deformable laminated plate and shell theory. The calculated result was compared with the data generated from a FEM analysis which showed their agreement. Furthermore for non-identical pairs of flanges, including blind flanges, the effect of outside-to-inside diameter was also experimentally investigated. The experimental result was compared with the analytical solution.

The results of the above investigations have lead to the following conclusions:

All design rules based on metallic flange design experience must be validated using the laminate theory and FRP failure criteria. The analytical solution developed in this dissertation is simple to implement, inexpensive to use, and effective. A designer with some basic knowledge of the laminate theory can correctly apply the proposed method. For standard flanges, the results have shown consistency with other methods such as FEM, and;

Due to the similarity of nomenclature and basic concept used with ASME metallic flange design methods, no new problems are encountered in the implementation of the proposed design procedure. In the event that the design method be accepted for use, it would fill a gap which presently exists in the design of FRP pressure vessels and pipe flanges.

10.2 Recommendations for Future Work

It is clear that more experimental investigation of FRP flanged connections is needed. The test in this dissertation was on 300 mm diameter non-identical pairs with blind flanges. It is important to understand the performance of identical FRP flange pairs and dissimilar flange pairs of other sizes as well. An experimental verification of the proposed design method is desired for various sizes and dimensions, and also under various operating conditions such as pressure, temperature and moisture.

The concepts put forward in this dissertation should be used to obtain a simplified method of analysis, which retains the basic ideas but reduces some of the tedious calculations required with the shear deformation theory.

Advanced design methods for flanged connections should also be based on the

concept of joint tightness. The strength behavior of the flange is studied in this dissertation. This method should be extended to include flange rotation, gasket performance, and leak rate. A defined leakage level can thus be controlled in this elastic interactive gasket/bolt/flange system.

The FEM model in this dissertation was meshed with single solid element across model wall thickness. It would be interesting to see if the accuracy improves and if different results are provided by stacked elements across wall thickness.

Bibliography

[1] *ASME Boiler and Pressure Vessel Code, section VIII, Division 1, Pressure Vessels.* The American Society of Mechanical Engineers, New York, USA, 1989.

[2] *ASME Boiler and Pressure Vessel Code, section X, Fiberglass Reinforced Plastic Pressure Vessels.* The American Society of Mechanical Engineers, New York, USA, 1989.

[3] *Composite Structures, for Revision 4.4 Tutorial.* Swanson Analysis Systems, Inc., May 1989.

[4] *Solid Modelling Seminar, for Revision 4.4*, volume 1–4. Swanson Analysis Systems, Inc., April 1991.

[5] *ANSYS 5.0 Revision, User's Manuals*, volume 1–4. Swanson Analysis Systems, Inc., December 1992.

[6] Anonymous. Design of flanges for full face gaskets. *Engineering Department Bulletin*, (45):6, 1951. Taylor Forge and Pipe Works, Chicago.

[7] J.E. Ashton, J.C. Halpin, and P.H. Petit. *Primer on Composite Materials: Analysis.* Technomic Publishing Co., Inc., Stamford, Connecticut, USA, 1969.

[8] A. Bazergui and H.D. Marchand, L.and Raut. Development of a production test procedure for gaskets. *Weld Research Council Bulletin*, (309), November 1985.

[9] A. Bazergui and L. Marchand. PVRC milestone gasket tests - first results. *Weld Research Council Bulletin*, (292), February 1984.

[10] A. Bazergui and L. Marchand. Development of tightness test procedure for gaskets in elevated temperature service. *Weld Research Council Bulletin*, (339), December 1988.

[11] G.E. Bibel. Thermal gradients in large diameter pipe flanges. In *4th Int ANSYS conf Exhi Part 2*, pages 11.32–11.41. ANSYS, Houston, PA, USA, 1989.

[12] J.H. Bickford. Advances in bolting technology, nuclear engineering and design. In *8th int conf on Stuct Mech in React Technol, Brussels, Belg*, volume 90, pages 307–315, August 1985.

[13] J.H. Bickford. Bolted technology council and the search for more accurate preload. In *American Society of Mechanical Engineers, Pressure Vessels and Piping Division (Publication) PVP*, volume 158, pages 1–6. ASME, New York, NY, USA, 1989.

[14] J.H. Bickford. *An Introduction to the Design and Behavior of Bolted Joints.* Marcel Dekker,Inc., USA, Second Edition, 1990.

[15] J.H. Bickford, K Hayashi, A.T. Chang, and J.R. Winter. Preliminary evaluation of the elevated temperature behavior of a bolted flanged connection. *Welding Research Council Bulletin*, (341), May 1989.

[16] A.E. Blach. *Bolted Flanged Connections With Full Face Gaskets.* Ph.d. dissertation, University of Montreal, Quebec, Canada, 1983.

[17] A.E. Blach. Bolted flanged connections for non-circular pressure vessels. In *American Society of Mechanical Engineers, Pressure Vessels and Piping Division (Publication) PVP*, volume 158, pages 97–104. ASME, New York, NY, USA, 1989.

[18] A.E. Blach and A. Bazergui. Method of analysis of bolted flanged connections - a review. *Welding Research Council Bulletin*, (271), 1981.

[19] A.E. Blach, A. Bazergui, and R. Baldur. Full face gasketed bolted flanged connections. *Welding Research Council Bulletin*, (314), May 1986.

[20] A.E. Blach and S.V. Hoa. Bolted flanged connections for glass fiber reinforced plastic pipes and pressure vessels. *Design Engineering*, 1987. UK.

[21] A.E. Blach and S.V. Hoa. The effects of pull back on stresses in FRP flanges. *Experimental Techniques, Supplement*, pages 12–1 , November 1988.

[22] A.E. Blach and L. Sun. Fiber reinforced plastic bolted flanged connections. In *Proc. 2nd International Symposium on Fluid Sealing of Static Gasketed Joints*, 1990.

[23] A.E. Blach and L. Sun. Bolted flanged connections with longitudinal bending moments. In *Design and Analysis of Pressure Vessels, Piping, and Components - 1992 American Society of Mechanical Engineers, Pressure Vessels and Piping Division (Publication) PVP*, volume 235, pages 3–8. ASME, New York, NY, USA, 1992.

[24] A.E. Blach and L. Sun. Bolted flanged connections with longitudinal bending moments: Experimental results. In *Power Plant Equipment Design: Bolted Joints, Pumps, Valves, Pipe and Duct Supports - 1993 American Society of Mechanical Engineers, Pressure Vessels and Piping Division (Publication) PVP*, volume 255, pages 97–103. ASME, New York, NY, USA, 1993.

[25] S. Blach. Kinetics of curing of a vinyl ester resin. Master's thesis, Concordia University, Canada, September 1993.

[26] A. Bouzid and A. Chaaban. Flanged joint analysis: A simplified method based on elastic interaction. *Transactions of the Canadian Society for Mechanical Engineering*, 17(2):181–196, 1993.

[27] J.A. Brydson. *Plastics Materials.* The Whitefriars Press Ltd.,London and Tonbridge, 1977.

[28] A.U. Bugov and G.V. Isaev. Stressed state of rectangular flanges at static axial load. *Soviet Energy Technology(English Translation of Energomashinostroenie)*, (4):27–30, 1989.

[29] J.M. Campbell. FRP flanges for process pipe and tanks. In *Proc. FRP SYMPOSIUM,National Association of Corrosion Engineers, Niagara Frontier Section, USA*, September 1990.

[30] J. Cao and A.J. Bell. Elastic analysis of a circular flange joint subjected to axial force. *International Journal of Pressure Vessels and Piping*, 55(3):435–449, 1993.

[31] D.H. Cascales, C. Militello, and W. J. Mulhall. Bolted flanged joint leakage analysis with non-linear gasket behaviour. *International Journal of Pressure Vessels and Piping*, 30(3):205–215, 1987.

[32] N.P. Cheremisinoff and P.N. Cheremisinoff. *Fiberglass-reinforced Plastics Deskbook.* Ann Arbor Science Publishers, Inc., 1978.

[33] M.A. Crabb, R.O. Case, and T.E. Shoup. Development of a computer integrated design system for bolted flange connections. In *Computers in Engineering, Proceedings of the International Computers in Engineering Conference and Exhibit*, volume 2, pages 361–363. ASME, New York, NY, USA, 1986.

[34] D.E. Czernik and F.L. Miszczak. Real time gasket stress measurement. *Automotive Engineering*, 100(1):9–13, January 1992.

[35] A.I. Efremov, S.D. Kerimbaev, and K.A. Chimchikov. Heat-exchange body-to-closure bolted flanged connection. *Soviet Energy Technology(English Translation of Energomashinostroenie)*, (5):28–30, 1989.

[36] J. R. Fowler. Combined bending, tension, and pressure capacity of API flanges. *American Society of Mechanical Engineers (Paper).* ASME, New York, NY, USA, PET3 12.

[37] G A. Ghoneim and K. G. Haverty. Capabilities of API flanges under combined pressure, tension and bending moment. *American Society of Mechanical Engineers (Paper).* ASME, New York, NY, USA, 7p PET24.

[38] E.W. Godwin, F.L. Matthews, and P.F. Kilty. The design of bolted flange joints in GRP pipes. *Plastics and Rubber Processing and Applications*, 6(2), 1986.

[39] T.E. Graham. FRP flanges for process pipe and tanks. In *Managing Corrosion with Plastics.* National Association of Corrosion Engineers, November 1989.

[40] S.V. Hoa. *Analysis for Design of Fiber Reinforced Plastic Vessels and Piping.* Technomic Publishing Co.,Inc.,USA, 1991.

[41] K.H. Hsu and J.R. Payne. PVRC research program on bolted flanged connections. In *Valves, Bolted Joints, Pipe Supports, and Restraints - 1992 American Society of Mechanical Engineers, Pressure Vessels and Piping Division (Publication) PVP*, volume 236, pages 79–85. ASME, New York, NY, USA, 1992.

[42] K.H. Hsu, J.R. Payne, and M. Derenne. Recent development in PVRC elevated temperature gasket testing. In *Power Plant Equipment Design: Bolted Joints,Pumps,Values,Pipe and Duct Supports - 1993 American Society of Mechanical Engineers, Pressure Vessels and Piping Division (Publication) PVP*, volume 255. ASME, New York, NY, USA, 1993.

[43] R.M. Jones. *Mechanics of Composite Materials.* McGraw-Hill Book Company, New York, USA, 1980.

[44] H. Kimura and K. Murata. Study of the flexural rigidity of annular flanged connections. *Bulletin of the JSME*, 29(257):3928–3933, November 1986.

[45] S. Kohmura. Design of aluminium bolted flanged connections (2nd report relationship between stresses and bending flexibility in integral hub flanges). *Bulletin of the JSME*, 29(249):1026–1032, March 1986.

[46] E. Kreyszig. *Advanced Engineering Mathematics.* John Wiley & Sons, Inc., USA, sixth edition, 1988.

[47] H.L. Langhaar. *Energy Methods in Applied Mechanics.* Wiley, New York,USA, 1962.

[48] S.G. Lekhnitskii. *Anisotropic Plates.* Gordon and Breach Science Publishers, New York, USA, 1968.

[49] G.F. Leon. Design methods for plastic bolted flanged connections. In *Seventh Int. Conference on Pressure Vessel Technology, Duesseldorf, Germany, Design Analysis Materials*, volume 1, pages 90–104, June 1992.

[50] A. Lifson and A.J. Smalley. Bending flexibility of bolted flanges and its effect on dynamical behavior of structures, loading. *Journal of Vibration, Acoustics, Stress, and Reliability in Design*, 111(4):392–398, October 1989.

[51] D.W. Lindstrom. *Series Solution for a Cylindrical Composite Shell Subject to Axisymmetric Loadings.* Ph.d. dissertation, University of Ottawa, Canada, 1990.

[52] E.D. Lowthian. Experimental evaluation of full faced fiber reinforced plastic flanges. PVRC grant 83-21, December 1984.

[53] G. Lubin. *Handbook of Composites.* Van Nostrand Rheinhold, 1982.

[54] F.L. Matthews, D.M. Foulkes, E.W. Godwin, and P.F. Kilty. The strength of bolted flange joints in GRP pipes. In *Proc. 14th Reinforced Plastics Congress.* British Plastics Federation, 1984.

[55] J.L. McLarty. *Design Details of Integral Flanges for the Ends of Very Large Composite Fiber Structures.* Elsevier Applied Science Publ, London, Engl and New York, NY, USA, 1985.

[56] R.V. Modestova, V.V. Gudkov, G.I. Kasyanchuk, and O.P. Samofalov. Flange joints of vessels and apparatus made of aluminum. *Chemical and Petroleum Engineering (English translation of Khimicheskoe i Neftyanoe Mashinostroenie)*, 21(11–12):572–573, November–December 1985.

[57] T. Morohoshi, T. Sawa, K. Maruyama, and K. Yamamoto. Characteristics of bolted joints subjected to external bending moments. (analysis of the case where clamped parts are pipe flanges with gaskets by three-dimensional theory of elasticity). *JSME International Journal, Series 1: Solid Mechanics, Strength of Materials*, 32(4):477–484, October 1989.

[58] B.S. Nau. Computer modelling of the sealing behaviour of gaskets in flanged joints. *Nuclear Engineering and Design*, 90(2):181–191, December 1985.

[59] P. Ouellette. Buckling of glass-reinforced plastic filament-wound pressure vessels under hydrostatic external pressure. Master of engineering thesis, Concordia University, Canada, 1985.

[60] W.J. Palmer, R.J. Tomawski, L.I. Ezekoye, and M. L. Lacey. Design of a bolted flange subjected to severe nuclear system thermal transients - a case study. In *American Society of Mechanical Engineers, Pressure Vessels and Piping Division (Publication) PVP*, volume 109, pages 95–98. ASME, New York, NY, USA.

[61] B. Parkyn. *Glass Reinforced Plastics.* Butterworth & Co (Canada) Ltd., 1970.

[62] J.R. Payne. Traditional vs new bolt load calculations. In *ASME Pressure Vessel and Piping Conference*, San Diego, June 1991.

[63] L.P. Pertsev, P.S. Marchenko, and V.N. Stognii. Calculation of rectangular flanged joints. *Chemical and Petroleum Engineering (English translation of Khimicheskoe i Neftyanoe Mashinostroenie)*, 23(9–10):501–506, May 1988.

[64] D. G. Rao, V. Ramamurti, and S. Narayanan. Stress analysis of ribbed flanges. *Computers and Structures*, 22(4):725–735, 1986.

[65] J.N. Reddy. *Energy and Variational Methods in Apllied Mechanics.* John Wiley and Sons, Inc., 1984.

[66] J.N. Reddy. A simple higher-order theory for laminated composite plates. *Journal of Applied Mechanics*, 51:745–752, December 1984.

[67] T.H. Richards. *Energy Methods in Stress Analysis.* Ellis Horwood/Wiley, New York, 1977.

[68] M. Riemer, R. Taschner, and V. Pavelic. Analysis of a bolted flange with eccentric loading. *Journal of Vibration, Acoustics, Stress, and Reliability in Design*, 108(3):369–376, July 1986.

[69] D.B. Rossheim and A.R.C. Markl. Gasket loading constants. *Mechanical Engineering*, 65:647, 1943.

[70] H. T. Salem. *Finite Element Stress Analysis of Prestressed Bolted Connections.* Cahners Exposition Group, Stamford, CT, USA.

[71] T. Sawa, N. Higurashi, and H. Akagawa. Stress analysis of pipe flange connections. In *American Society of Mechanical Engineers, Pressure Vessels and Piping Division (Publication) PVP*, volume 173, pages 51–57. ASME, New York, NY, USA, 1989.

[72] T. Sawa, T. Hirose, and H. Kumano. Behavior of pipe flange connection in transient temperature field. *Journal of Pressure Vessel Technology, Transactions of the ASME*, 115(2):142–146, May 1993.

[73] T. Sawa, T. Morohoshi, H. Kumano, and A. Shimizu. Analysis of circular bolted flanged joints on solid round bars subjected to external bending moments. In *Power Plant Equipment Design : Bolted Joints, Pumps, Valves, Pipe and Duct Supports, American Society of Mechanical Engineers, Pressure Vessels and Piping Division (Publication) PVP*, volume 255, pages 55–63. ASME, New York, NY, USA, 1993.

[74] T. Sawa, T. Morohoshi, and K. Yamamoto. Charateristics of bolted joints subjected to external bending moments: (analysis of the case where clamped parts are pipe flanges by three dimensional theory of elasticity). *JSME International Journal*, 30(270):2018–2026, December 1987.

[75] T. Sawa, R. Sasaki, and M. Yoneno. Analysis of pipe flange connections used adhesives instead of gaskets. In *Power Plant Equipment Design : Bolted Joints, Pumps, Valves, Pipe and Duct Supports, American Society of Mechanical Engineers, Pressure Vessels and Piping Division (Publication) PVP*, volume 255, pages 83–91. ASME, New York, NY, USA, 1993.

[76] T.H. Shames and C.L. Dym. *Energy and Finite Element Methods in Structural Mechanics.* Hemisphere Publishing Co.,USA, 1985.

[77] L. Sun and A.E. Blach. Analysis for design of bolted flanged connections made of fiber reinforced plastic. In *Proc. 3rd International Symposium on Fluid Sealing of Static Gasketed Joints*, Biarritz, France, September 1993.

[78] L. Sun and A.E. Blach. Design of bolted flanged connections made of fiber reinforced plastic materials with FEM result. In *Proc. International Conference on Design and Manufacturing Using Composite*, Montreal, Canada, August 1994.

[79] R.T. Tenchev. Including bolt bending stiffness in finite-element analysis of flanged connections. *Communications in Applied Numerical Methods*, 7(2):123–129, Feburary 1991.

[80] S.P. Timoshenko. *Strength of Material*, volume II. Van Nostrand Company, Princeton, N.J.,USA, 1956. Article 28: Twisting of Circular Ring by Couples Uniformly Distributed along its Center Line.

[81] S.W. Tsai. *Composites Design.* Think Composites, Dayton, Ohio, USA, third edition, 1987.

[82] S.W. Tsai and H.J. Hahn. *Introduction to Composite Materials.* Technomic Publishing Company, USA, 1980.

[83] J.R. Vinson and T.W. Chou. *Composite Materials and Their Use in Structures.* Applied Science, USA, 1975.

[84] J.R. Vinson and R.L. Sierakowski. *The Behavior of Structures Composed of Composite Materials.* Kluwer Academic Publishers, USA, 1986.

[85] I.E. Vyakhkhi. Stiffness of flanged joints subjected to a bending moment. *Soviet Engineering Research*, 7(9):28–31, September 1987.

[86] E.O. Waters, D.B. Wesstrom, D.B. Rossheim, and F.S.G. Williams. Development of general formulas for bolted flanges. *Taylor Forge and Pipe Works, 1937, Chicago, Reprinted by Welding Research Council as PVRC Monograph in 1979.*, 59:161–169, 1937.

[87] E.O. Waters, D.B. Wesstrom, D.B. Rossheim, and F.S.G. Williams. Formulas for stresses in bolted flanged connections. *ASME-Trans*, 60:267–278, april 1938.

[88] E. S. Widder and G. J. Novak. Gasketed joint analysis using computer aided engineering techniques. *Automotive Sealing SAE Special Publications*, (921):1–9, 1992. SAE, Warrendale, PA, USA, 920131.

[89] E. Zahavi. A finite element analysis of flange connections. *ASME Journal of Pressure Vessel Technology*, 115:327–330, August 1993.

[90] J. Zheng, R. Cai, and Z. Wu. Integral analysis and calculation of flange system. *Huagong Jixie/Chemical Engineering and Machinery*, 16(4):206–210, 1989. Chinese.

Nomenclature

A	m	flange outside diameter
A_b	m^2	bolt area provided
A_{ij}	N/m	in-plane laminate modulus
a	-	coefficient in differential equation
B	m	flange inside diameter
B_{ij}	N	coupling laminate modulus
b	m	width of gasket
C	m	bolt circle diameter
c_1, c_2	-	integration coefficients
D	m	bolt hole diameter
D_{ij}	N-m	flexural laminate modulus
Δ	-	coefficient
δ	m	gasket compression at outer edge
E_G	Pa	gasket modulus
E_i	Pa	Young's modulus
E_{ij}	N-m^2	3rd order laminate modulus
η	-	moment arm coefficient
F	N	flange rotation force
F_{ij}	N-m^3	4th order laminate modulus
$f(r)$	-	function in differential equation
G	m	effective gasket diameter

G_{ij}	Pa	shear modulus
g	m	shell hub thickness
γ	rad	rotation of normal to the midplane, shell
H_D	N	hydrostatic end force
H_G	N	gasket compression force, operation
H_{GS}	N	gasket compression force, bolt-up
H_{ij}	N-m^5	5th order laminate modulus
H_T	N	hydrostatic force under gasket
h_D	m	moment arm of hydrostatic end force
h_G	m	moment arm for gasket force, operation
h_{GS}	m	moment arm for gasket force, bolt-up
h_T	m	moment arm for hydrostatic force under gasket
K	-	ratio outside to inside diameter
k_i	-	coefficient in differential equation
L	-	fiber direction
M	N-m/m	discontinuity moment
M_D	N-m	moment due to hydrostatic end force
M_G	N-m	moment due to gasket compression, operation
M_G^*	N-m	moment due to gasket compression, bolt-up
M_{GS}	N-m	moment due to bolt load, bolt-up
M_i	N-m/m	stress resultant, moment
M_0	N-m	total flange moment, operation
M_0^*	N-m	total flange moment, bolt-up
M_T	N-m	moment due to hydrostatic force under gasket
m	-	coefficient
m_1, m_2	-	coefficients
N_i	N/m	stress resultant, force
ν	-	Poisson's ratio
p	Pa	internal pressure
P_i	N-m	stress resultant
Π	N-m	total potential energy

ψ	rad	rotation of normal to the midplane, flange
Q	N/m	discontinuity force
Q_{ij}	N/m	stress resultant, force
Q_{ij}	Pa	elastic constants
R	m	radius
R_{ij}	N-m	stress resultant
r	m	coodinate along radial direction, flange
S_a	Pa	allowable bolt stress, gasket seating
σ	Pa	stress
σ_G	Pa	gasket compression stress
T	-	transverse to the fiber direction
t	m	flange thickness
t_G	m	gasket thickness
θ	rad	flange rotation
θ	rad	coordinate perpendicular to radius direction, flange and shell
U	N-m	strain energy
u^f	m	displacement in r direction, flange
u^s	m	displacement in x direction, shell
u_0^f	m	midplane displacement in r direction, flange
u_0^s	m	midplane displacement in x direction, shell
V	N-m	work done by force
v^f	m	displacement in θ direction, flange
v^s	m	displacement in θ direction, shell
ε	-	strain
W	N	total bolt load on flange
W_{m2}	N	bolt load, gasket seating
w^f	m	displacement in z direction, flange
w^s	m	displacement in z direction, shell
w_0^f	m	midplane displacement in z direction, flange
w_0^s	m	midplane displacement in z direction, shell
x	m	coordinate along length direction

x_0	m	location of centroid
$\bar{x}$	m	location of centroid
ξ	$1/m^2$	function in higher order displacement field
z	m	coordinate along thickness direction, flange and shell
ζ	$1/m^2$	function in higher order displacement field

Appendix A: Program for Analytical Solution

```
************************************************************************
 ANALYTICAL PROGRAM
 FOR FIBER REINFORCED PLASTIC FLANGED CONNECTIONS
 BASED ON CLASSICAL LAMINATE THEORY
************************************************************************

The program was used in calculating strains and stresses in Chapter 7.
It contains both operating and gasket seating condition.

REAL K,MD,MT,MB,MG,MO,M,MGS,MGG,MOG
REAL 11,12,13,14,15,16,17,18,19,110,111,112,113,114,
     *  115,116,117,118,119,120,121,122,123,124,125,126,
     * 127,128,129,130,131,132,133,134

c Parameter
PI=3.141592654

c Design pressure
P=345000.0
```

```
c Flange and shell dimensions
A=0.48
B=0.30
C=0.425
D=0.019

c Gasket data
TG=0.003
EG=55.0e6

c Laminae elastic constants
c Mat(1.5oz)
ERM=8.0E9
URM=0.2
UEM=0.2
c Woven roving
ERW=18.0E9
URW=0.13
UEW=0.13

c Lamina modulus components
QRRM=ERM/(1.0-URM*UEM)
QEEM=QRRM
QREM=UEM*ERM/(1.0-URM*UEM)
QRRW=ERW/(1.0-URW*UEW)
QEEW=QRRW
QREW=UEW*ERW/(1.0-URW*UEW)

c Flange laminate
Z10=0.0
```

```
Z11=0.0009
Z12=0.0019
Z13=0.0028
Z14=0.0038
Z15=0.0047
Z16=0.0057
Z17=0.0066
Z18=0.0076
Z19=0.0085
Z20=0.0095
Z21=0.0104
Z22=0.0114
Z23=0.0123
Z24=0.0133
Z25=0.0142
Z26=0.0152

c Flange thickness
t=z26*2.0

c Flange laminate moduli

c In-plane modulus components
ARR=2.0*(QRRM*(Z12-Z11+Z14-Z13+Z16-Z15+Z18-Z17
     *  +Z20-Z19+Z22-Z21+Z24-Z23+Z26-Z25)+QRRW*(Z11-Z10+
     * Z13-Z12+Z15-Z14+Z17-Z16+Z19-Z18+Z21-Z20+Z23-Z22+
     * Z25-Z24))

ARE=2.0*(QREM*(Z12-Z11+Z14-Z13+Z16-Z15+Z18-Z17
     *  +Z20-Z19+Z22-Z21+Z24-Z23+Z26-Z25)+QREW*(Z11-Z10+
     *  Z13-Z12+Z15-Z14+Z17-Z16+Z19-Z18+Z21-Z20+Z23-Z22+
```

```
     * Z25-Z24))

AEE=2.0*(QEEM*(Z12-Z11+Z14-Z13+Z16-Z15+Z18-Z17
     *  +Z20-Z19+Z22-Z21+Z24-Z23+Z26-Z25)+QEEW*(Z11-Z10+
     * Z13-Z12+Z15-Z14+Z17-Z16+Z19-Z18+Z21-Z20+Z23-Z22+
     * Z25-Z24))

c Flexural modulus
Drr=2.0/3.0*(QRRM*(Z12**3-Z11**3+z14**3-Z13**3
     * +z16**3-Z15**3+z18**3-Z17**3+Z20**3-Z19**3
     *  +Z22**3-Z21**3+Z24**3-Z23**3+Z26**3-Z25**3)
     *  +QRRW*(Z11**3-z10**3+Z13**3-z12**3+Z15**3-z14**3
     * +Z17**3-Z16**3+Z19**3-Z18**3+Z21**3-Z20**3
     * +Z23**3-Z22**3+Z25**3-Z24**3))

DrE=2.0/3.0*(QREM*(Z12**3-Z11**3+z14**3-Z13**3
     * +z16**3-Z15**3+z18**3-Z17**3+Z20**3-Z19**3
     *  +Z22**3-Z21**3+Z24**3-Z23**3+Z26**3-Z25**3)
     *  +QREW*(Z11**3-z10**3+Z13**3-z12**3+Z15**3-z14**3
     * +Z17**3-Z16**3+Z19**3-Z18**3+Z21**3-Z20**3
     * +Z23**3-Z22**3+Z25**3-Z24**3))

DEE=DRR

c Shell laminate
sz5=0.0
sz6=0.001
sz7=0.0019
SZ8=0.0029
SZ9=0.0038
SZ10=0.0048
```

```
SZ11=0.0057
SZ12=0.0067
SZ13=0.0076
SZ14=0.0086

c Shell thickness
gg=sz14*2.0

c Shell laminate moduli

c In-plane modulus components
SAEE=2.0*(QRRM*(SZ6-SZ5+SZ8-SZ7+SZ10-SZ9
     * +SZ12-SZ11+SZ14-SZ13)
     * +QRRW*(SZ7-SZ6+SZ9-SZ8+SZ11-SZ10+SZ13-SZ12))

SAXX=SAEE

SAXE=2.0*(QREM*(SZ6-SZ5+SZ8-SZ7+SZ10-SZ9
     * +SZ12-SZ11+SZ14-SZ13)
     * +QREW*(SZ7-SZ6+SZ9-SZ8+SZ11-SZ10+SZ13-SZ12))

c Flexural modulus components
SDXX=2.0/3.0*(QRRM*(sZ6**3-sZ5**3+sz8**3-sZ7**3
     * +sZ10**3-sz9**3+SZ12**3-SZ11**3+SZ14**3-SZ13**3)
     *  +QRRW*(sZ7**3-sz6**3+sZ9**3-sz8**3+SZ11**3-SZ10**3
     * +SZ13**3-SZ12**3))

c Operating condition

c Location of entroid of sector of unit width
K=A/B
```

```
SB=(A-B)/2.0
G=2.0*B**2/3.0*SIN(1.0e-3/B)*(1.0+K**2/(K+1.0))
G=G*1.0e3

c Flange moment arms, loads and moments: part 1
SHGG=B**2/4.0*SIN(1.0e-3/B)*(1.0+3.0*K**2/(1.0+2.0*K))
        SHGG=SHGG*1.0E3
SHG=SHGG-G/2.0
SHG2=SHGG*2.0
HD=PI/4.0*B**2*P
SHD=(G-B-gg)/2.0
MD=HD*SHD
HT=PI/4.0*((C-D)**2-B**2)*P
SHT=(2.0*G-B-C+D)/4.0
MT=HT*SHT
SHGS=0.5*(C-G)
MB=(HD+HT)*SHGS
XII=1.0-SHGS/SHG
EPSILON=(SAEE*SAXX-SAXE**2)/B**2/SDXX/SAXX
EPSILON=SQRT(SQRT(EPSILON))

c Flange coefficients
l1=B**3/2.0/(ARE+ARR)/(A**2-B**2)
l2=A**2*B/2.0/(ARE-ARR)/(A**2-B**2)
l3=1.0/2.0/EPSILON**3/SDXX
l4=-epsilon*l3
l5=l3*(1.0-SAXE/SAXX/2.0)/2.0/EPSILON
l6=B*ALOG(B/2.0)-B/2.0
l7=l6/4.0/(A-B)/pi/DRR
l8=B*(2.0*ALOG(B/2.0)+2.0*ALOG(B/2.0)*DRE/DRR+
     * 1.0-DRE/DRR)/2.0/A**2
```

```
l9=(2.0*ALOG(A/2.0)+2.0*ALOG(A/2.0)*DRE/DRR+1.0
     * -DRE/DRR)/2.0/B
l10=A**2*B**3/8.0/(DRE+DRR)/(B**2-A**2)
l11=2.0/(A-B)/B/PI
l12=A**2*B/2.0/(-DRE+DRR)/(B**2-A**2)
l13=B/8.0*l11
l14=-2.0*ALOG(B/2.0)-2.0*ALOG(B/2.0)*DRE/DRR+
     * 2.0*ALOG(A/2.0)+2.0*ALOG(A/2.0)*DRE/DRR
l15=-2.0*epsilon*l4
l16=l10*l11*(l8-l9)
l17=4.0/A**2*l10
l18=l12*l13*l14
l19=l4-t/2.0*l12-t/2.0*l17
l20=-l12+l15-l17
l21=-l7+l16-l18
l22=l1-l2+l3
l23=t*l1-t*l2-l5
l24=-l20*l23/(l4*l19-l20*l22)
l25=l4*l21/(l4*l19-l20*l22)
l26=l19*l23/(l4*l19-l20*l22)
l27=-l21*l22/(l4*l19-l20*l22)
l28=3.0/(1.0+2.0*K)*TG/G/PI/EG/SB**2/SHG
l29=l21+l27+(l12+l17)+t/2.0*l25*(l12+l17)
l30=l26*(l12+l17)+t/2.0*l24*(l12+l17)
l31=l4*l21/(l4*l19-l20*l22)
l32=-l21*l22/(l4*l19-l20*l22)
l33=l21+(l12+l17)*l32+T/2.0*(l12+l17)*l31
l34=l33/(l28+l33)

c Flange moment arms, loads and moments: part 2
MG=((MD+MT+MB)*l29+P*l30)/(XII*l29+l28)
```

```
MO=MD+MT+MB-XII*MG
HG111=MG/SHG
W111=HD+HT+HG111
w112=HD+HG111
Q=l24*P+l25*MO
M=l26*P+l27*MO
F1=(MO/PI/B)*2.0/(A-B)
C1=-4.0/B*l10*(F1*(l8-l9)+M*4.0/A**2+Q*T*2.0/A**2)
C2=B/2.0*l12*(B*F1*l14/8.0-M-Q*T/2.0)
C3=-C1/4.0*(A/2.0)**2-C2*ALOG(A/2.0)-B*F1/8.0/
     * DRR*(A/2.0)**2*(ALOG(A/2.0)-1.0)

c Flange upper surface
zz=t/2.0
s=zz
DO 211 x=B/2.0,A/2,0.001
UO=(P*T-Q)*2.0/B*l1*x+(-P*T+Q)*B/2.0*l2/x
DUODR=(P*T-Q)*2.0/B*l1-(-P*T+Q)*B/2.0*l2/x**2
PSI=-B*F1/8.0/DRR*(2.0*X*ALOG(X)-X)-C1/2.0*X-C2/X
dpsidr=-B*F1/8.0/DRR*(2.0*ALOG(X)+1.0)-C1/2.0+C2/X**2
c Flange strain values
ERR=DUODR+s*DPSIDR
EEE=u0/x+s*psi/x
c Flange stress values
SIGMArw=QRRW*ERR+QREW*EEE
SIGMAew=QREW*ERR+QEEW*EEE
SIGMArm=QRRM*ERR+QREM*EEE
SIGMAem=QREM*ERR+QEEM*EEE
c Convert Unit Pa to MPa for Matlab Graphing
SIGMArw=SIGMARW*1.0E-6
SIGMAew=SIGMAEW*1.0E-6
```

```
SIGMArm=SIGMARM*1.0E-6
SIGMAem=SIGMAEM*1.0E-6

OPEN(1,FILE='FRP1.DAT',STATUS='NEW')
WRITE(1,*)x,err,eee
CLOSE(1)

OPEN(2,FILE='FRP2.DAT',STATUS='NEW')
WRITE(2,*)X,SIGMArw,SIGMAew,sigmarm,sigmaem
CLOSE(2)
211 continue

c Flange lower surface
zz=-t/2.0
s=zz
do 411 x=B/2.0,A/2.0,0.001
U0=(P*T-Q)*2.0/B*11*x+(-P*T+Q)*B/2.0*12/x
DUODR=(P*T-Q)*2.0/B*11-(-P*T+Q)*B/2.0*12/x**2
PSI=-B*F1/8.0/DRR*(2.0*X*ALOG(X)-X)-C1/2.0*X-C2/X
dpsidr=-B*F1/8.0/DRR*(2.0*ALOG(X)+1.0)-C1/2.0+C2/X**2

c Flange strain values
ERR=DUODR+s*DPSIDR
EEE=u0/x+s*psi/x
c Flange stress values
SIGMArw=QRRW*ERR+QREW*EEE
SIGMAew=QREW*ERR+QEEW*EEE
SIGMArm=QRRM*ERR+QREM*EEE
SIGMAem=QREM*ERR+QEEM*EEE
c Convert Unit "Pa" to "MPa" for Matlab Graphing
SIGMArw=SIGMARW*1.0E-6
```

```
SIGMAew=SIGMAEW*1.0E-6
SIGMArm=SIGMARM*1.0E-6
SIGMAem=SIGMAEM*1.0E-6

OPEN(3,FILE='FRP3.DAT',STATUS='NEW')
WRITE(3,*)x,err,eee
CLOSE(3)

OPEN(4,FILE='FRP4.DAT',STATUS='NEW')
WRITE(4,*)x,SIGMArw,SIGMAew,sigmarm,sigmaem
CLOSE(4)
411 continue

c Shell

sztt=gg/2.0
c Outer surface
ztt=sztt
do 611 x=0,0.281,0.001
sw=(Q-epsilon*M)*l3*exp(-epsilon*x)*cos(epsilon*x)
     *  -M*l4*exp(-epsilon*x)*sin(epsilon*x)+p*l5
seee=sw*2.0/B
sexx1=(B*P/4.0-2.0*sw/B*SAXE)/SAXX
sexx12=epsilon*exp(-epsilon*x)*cos(epsilon*x)*(l15*M)
     * +epsilon*exp(-epsilon*x)*sin(epsilon*x)*(2*l4*Q+l15*M)
sexx=sexx1+ztt*sexx12
c Shell stress values
sSIGMAxw=QRRW*sExx+QREW*seEE
sSIGMAew=QREW*sExx+QEEW*seEE
sSIGMAxm=QRRM*sExx+QREM*sEEE
sSIGMAem=QREM*sExx+QEEM*sEEE
```

```
c Convert Unit "Pa" to "MPa" for Matlab Graphing
sSIGMAxw=SSIGMAXW*1.0E-6
sSIGMAew=SSIGMAEW*1.0E-6
sSIGMAxm=SSIGMAXM*1.0E-6
sSIGMAem=SSIGMAEM*1.0E-6

OPEN(5,FILE='FRP5.DAT',STATUS='NEW')
write(5,*)x,sexx,seee
CLOSE(5)

OPEN(6,FILE='FRP6.DAT',STATUS='NEW')
write(6,*)X,SSIGMAXM,SSIGMAEM,sSIGMAxw,sSIGMAew
CLOSE(6)
611 CONTINUE

c Inner surface
ztt=-sztt
do 811 x=0,0.281,0.001
sw=(Q-epsilon*M)*l3*exp(-epsilon*x)*cos(epsilon*x)
     *  -M*l4*exp(-epsilon*x)*sin(epsilon*x)+p*l5
c Shell strain values
seee=sw*2.0/B
sexx1=(B*P/4.0-2.0*sw/B*SAXE)/SAXX
sexx12=epsilon*exp(-epsilon*x)*cos(epsilon*x)*(l15*M)
     * +epsilon*exp(-epsilon*x)*sin(epsilon*x)*(2*l4*Q+l15*M)
sexx=sexx1+ztt*sexx12
c Shell stress values
sSIGMAxw=QRRW*sExx+QREW*seEE
sSIGMAew=QREW*sExx+QEEW*seEE
sSIGMAxm=QRRM*sExx+QREM*sEEE
sSIGMAem=QREM*sExx+QEEM*sEEE
```

```
c Convert Unit "Pa" to "MPa" for Matlab Graphing
sSIGMAxw=SSIGMAXW*1.0E-6
sSIGMAew=SSIGMAEW*1.0E-6
sSIGMAxm=SSIGMAXM*1.0E-6
sSIGMAem=SSIGMAEM*1.0E-6

OPEN(7,FILE='FRP7.DAT',STATUS='NEW')
write(7,*)x,sexx,seee
CLOSE(7)

OPEN(8,FILE='FRP8.DAT',STATUS='NEW')
write(8,*)X,SSIGMAXM,SSIGMAEM,sSIGMAXW,sSIGMAEW
CLOSE(8)
811 CONTINUE

c End of Operating Condition

c Gasket Seating Condition

c Bolt-up load
Sa=172.17E6
Ab=1.644E-3
HGS=Sa*Ab
write(*,*)HGS

c Flange moment
MGS=HGS*SHGS
MGG=MGS*134
MOG=MGS-MGG
write(*,*)Mgs,mog
```

```
Qg=l31*M0G
Mg=l32*M0G
F2=2.0*(M0G/B/PI)/(A-B)

C1=-4.0/B*l10*(F2*(l8-l9)+Mg*4.0/A**2+Qg*T*2.0/A**2)
C2=B/2.0*l12*(B*F2*l14/8.0-Mg-Qg*T/2.0)

c Flange upper surface
zz=t/2.0
s=zz
do 1011 x=B/2.0,A/2.0,0.001
U0=(-Qg)*2.0/B*l1*x+(Qg)*B/2.0*l2/x
DUODR=(-Qg)*2.0/B*l1-(Qg)*B/2.0*l2/x**2
PSI=-B*F2/8.0/DRR*(2.0*X*ALOG(X)-X)-C1/2.0*X-C2/X
dpsidr=-B*F2/8.0/DRR*(2.0*ALOG(X)+1.0)-C1/2.0+C2/X**2

c Flange strain values
ERR=DUODR+s*DPSIDR
EEE=u0/x+s*psi/x

c Flange stress values
SIGMArw=QRRW*ERR+QREW*EEE
SIGMAew=QREW*ERR+QEEW*EEE
SIGMArm=QRRM*ERR+QREM*EEE
SIGMAem=QREM*ERR+QEEM*EEE
c Convert Unit "Pa" to "MPa" for Matlab Graphing
SIGMArw=SIGMARW*1.0E-6
SIGMAew=SIGMAEW*1.0E-6
SIGMArm=SIGMARM*1.0E-6
SIGMAem=SIGMAEM*1.0E-6
```

```
OPEN(9,FILE='FRP9.DAT',STATUS='NEW')
WRITE(9,*)x,err,eee
CLOSE(9)

OPEN(10,FILE='FRP10.DAT',STATUS='NEW')
WRITE(10,*)x,SIGMArw,SIGMAew,sigmarm,sigmaem
CLOSE(10)
1011 continue

c Flange lower surface
zz=-t/2.0
s=zz
do 1211 x=B/2.0,A/2.0,0.001
U0=(-Qg)*2.0/B*l1*x+(Qg)*B/2.0*l2/x
DU0DR=(-Qg)*2.0/B*l1-(Qg)*B/2.0*l2/x**2
PSI=-B*F2/8.0/DRR*(2.0*X*ALOG(X)-X)-C1/2.0*X-C2/X
dpsidr=-B*F2/8.0/DRR*(2.0*ALOG(X)+1.0)-C1/2.0+C2/X**2

c Flange strain values
ERR=DU0DR+s*DPSIDR
EEE=u0/x+s*psi/x

c Flange stress values
SIGMArw=QRRW*ERR+QREW*EEE
SIGMAew=QREW*ERR+QEEW*EEE
SIGMArm=QRRM*ERR+QREM*EEE
SIGMAem=QREM*ERR+QEEM*EEE
c Convert Unit Pa to MPa for Matlab Graphing
SIGMArw=SIGMARW*1.0E-6
SIGMAew=SIGMAEW*1.0E-6
SIGMArm=SIGMARM*1.0E-6
```

```
SIGMAem=SIGMAEM*1.0E-6


OPEN(11,FILE='FRP11.DAT',STATUS='NEW')
WRITE(11,*)x,err,eee
CLOSE(11)

OPEN(12,FILE='FRP12.DAT',STATUS='NEW')
WRITE(12,*)x,SIGMArw,SIGMAew,sigmarm,sigmaem
CLOSE(12)
1211 continue

c Shell

c Shell outer surface
sztt=gg/2.0
ztt=sztt
do 1411 x=0,0.281,0.001
sw=(Qg-epsilon*Mg)*l3*exp(-epsilon*x)*cos(epsilon*x)
     *  -Mg*l4*exp(-epsilon*x)*sin(epsilon*x)

c Shell strain values
seee=sw*2.0/B
sexx1=(-2.0*sw/B*SAXE)/SAXX
sexx12=epsilon*exp(-epsilon*x)*cos(epsilon*x)*(l15*Mg)
     * +epsilon*exp(-epsilon*x)*sin(epsilon*x)*(2*l4*Qg+l15*Mg)
sexx=sexx1+ztt*sexx12

c Shell stress values
sSIGMAxw=QRRW*sExx+QREW*seEE
sSIGMAew=QREW*sExx+QEEW*seEE
```

```
sSIGMAxm=QRRM*sExx+QREM*sEEE
sSIGMAem=QREM*sExx+QEEM*sEEE
c Convert Unit "Pa" to "MPa" for Matlab Graphing
sSIGMAxw=SSIGMAXW*1.0E-6
sSIGMAew=SSIGMAEW*1.0E-6
sSIGMAxm=SSIGMAXM*1.0E-6
sSIGMAem=SSIGMAEM*1.0E-6

OPEN(14,FILE='FRP14.DAT',STATUS='NEW')
write(14,*)X,sSIGMAxw,sSIGMAew,SSIGMAXM,SSIGMAEM
CLOSE(14)
1411 CONTINUE

c Shell inner surface
sztt=-gg/2.0
ztt=sztt
do 1611 x=0,0.281,0.001
sw=(Qg-epsilon*Mg)*l3*exp(-epsilon*x)*cos(epsilon*x)
     *  -Mg*l4*exp(-epsilon*x)*sin(epsilon*x)

c Shell strain values
seee=sw*2.0/B
sexx1=(-2.0*sw/B*SAXE)/SAXX
sexx12=epsilon*exp(-epsilon*x)*cos(epsilon*x)*(l15*Mg)
     * +epsilon*exp(-epsilon*x)*sin(epsilon*x)*(2*l4*Qg+l15*Mg)
sexx=sexx1+ztt*sexx12

c Shell stress values
sSIGMAxw=QRRW*sExx+QREW*seEE
sSIGMAew=QREW*sExx+QEEW*seEE
sSIGMAxm=QRRM*sExx+QREM*sEEE
```

```
sSIGMAem=QREM*sExx+QEEM*sEEE
c Convert Unit "Pa" to "MPa" for Matlab Graphing
sSIGMAxw=SSIGMAXW*1.0E-6
sSIGMAew=SSIGMAEW*1.0E-6
sSIGMAxm=SSIGMAXM*1.0E-6
sSIGMAem=SSIGMAEM*1.0E-6

OPEN(16,FILE='FRP16.DAT',STATUS='NEW')
write(16,*)X,sSIGMAxw,sSIGMAew,SSIGMAXM,SSIGMAEM
CLOSE(16)
1611 CONTINUE

c End of Gasket Seating Condition

STOP
END
```

Appendix B: Data Input for Finite Element Analysis

```
*****************************************************************************

ANSYS INPUT DATA

*****************************************************************************

The input data was used in calculating stresses in Chapter 8.
It contains operating and gasket seating condition.

$load_ansys50
$ansys
/batch ! Optional command (to run in batch mode)
/filename,a
/show,a,fig
/units,SI ! Input will be in meters, Newtons, seconds, etc.
c***.....................................................................***
c***  Preprocessing phase
c***.....................................................................***
/prep7
```

```
/TITLE, FRP FLANGE
c*** Define element type
ET,1,solid46,,,,,2, ! 8-node, 3-D layered solid element
pi=3.141592654
high=0.5
rad1=0.3/2.0
rad2=rad1+0.0096
rad3=0.48/2.0
c=0.425
c1=c/2.0-0.008
c2=c/2.0+0.008
HG=6358840.0 ! Gasket reaction force
valu=HG*(rad3-rad1)/2.0/pi
xx1=1.0/3.0*rad3**3
xx2=1.0/2.0*rad3**2*rad1
xx3=1.0/6.0*rad1**3
xx=xx1-xx2+xx3
valu=valu/xx
w=6359087.0 ! Bolt load
wpre=w/pi/(c2**2-c1**2)
thic=0.019
thet=15.0
lay1=0.001
lay2=0.0009
lay3=lay1
lay4=lay2
pree=3500.0 ! Internal pressure
esi1=0.0096
esi2=0.02
c*** Define  two real constant values
R,1,10,1
```

```
rmore
RMORE,1,0,lay1,2,0,lay2
RMORE,1,0,lay1,2,0,lay2
RMORE,1,0,lay1
R,2,20,1
RMORE
RMORE,1,0,lay3,2,0,lay4
RMORE,1,0,lay3,2,0,lay4
RMORE,1,0,lay3,2,0,lay4
RMORE,1,0,lay3,2,0,lay4
RMORE,1,0,lay3,2,0,lay4
c*** Define linear material property values
ex1=8.0e9 ! Elastic constants for mat(1.5 oz)
ey1=8.0e9
ez1=3.0e9 ! Assumed values between two layers
prxy1=0.2
gxy1=3.33e9
ex2=18.0e9 ! Elastic constants for woven roving
ey2=18.0e9
ez2=3.0e9 ! Assumed values between two layers
prxy2=0.13
gxy2=3.6e9
MP,EX,1,ex1 ! Define linear material property
MP,EY,1,ey1
MP,prXY,1,prxy1
MP,GXY,1,gxy1
MP,EX,2,ex2
MP,EY,2,ey2
MP,prXY,2,prxy2
MP,GXY,2,gxy2
c*** Define keypoints and volumes
```

```
local,13,1,,,,,-90
csys,13
k,1,rad1 ! Define keypoints
k,2,rad1,,high
k,3,rad2,,high
k,4,rad2,,thic
k,5,rad3,,thic
k,6,rad3
k,7,rad1,,thic
K,8,rad2
k,9,rad1,thet
k,10,rad1,thet,high
k,11,rad2,thet,high
k,12,rad2,thet,thic
k,13,rad3,thet,thic
k,14,rad3,thet
k,15,rad1,thet,thic
k,16,rad2,thet
k,17,c1
k,18,c2
k,19,c1,thet
k,20,c2,thet
k,21,c1,,thic
k,22,c2,,thic
k,23,c1,thet,thic
k,24,c2,thet,thic
v,10,2,7,15,11,3,4,12 ! Define volumes through previously defined
v,9,1,8,16,15,7,4,12    keypoints
v,16,8,17,19,12,4,21,23
v,19,17,18,20,23,21,22,24
v,20,18,6,14,24,22,5,13
```

```
/psymb,cs,1
esys,13
c*** Define element size
esize,esi1 ! Flange section
eshape
real,1
vmesh,1
esize,esi2 ! Shell section
eshape
real,2
vmesh,2,5,1

/view,1,3,2,1
/psymb,esys,1
/pnum,area,1
eplot

/PSYMB,NDIR,1
NPLOT

/PSYMB,ESYS
/PSYMB,LAYR,1
EPLOT

/pnum,area,0
/pnum,node,1
/pnum,kp,0
eplot

nsel,all
nrotat,all
```

```
c*** Define boundary specification
nSEL,S,LOC,Z,HIGH ! Fix shell in the axial direction
d,ALL,uz,0.0
nsel,all
nSEL,S,LOC,Y,0 ! Apply axial symmetry
D,ALL,uy,0.0
nsel,all
nSEL,S,LOC,Y,THET
D,ALL,uy,0.0
nsel,all
save
finish
c***.....***
c*** Solution phase
c***.....***
/solu
antype,static ! Static analysis
csys,13
DSYS,13
/pbc,defa
/psf,pres,,2

ASEL,S,LOC,X,RAD1 ! Apply internal pressure
SFA,ALL,,PRES,PREE
asel,all
sfalist,all,all ! List the surface loads

aSEL,S,LOC,Z,thic ! Apply bolt load
aSEL,R,LOC,X,c1,c2
sFa,ALL,,pres,wpre
asel,all
```

```
slze=rad1 ! Apply gasket reaction force, triangular
slop=valu/(rad3-rad1)   ! gasket force distribution
sfgrad,pres,13,x,slze,slop
nsel,all
nsel,s,loc,z,0
sf,all,pres,0.0
nsel,all

dsys,13
/pnum,node
EPLOT
/pBc,all,,1
/pbc,pres,norm,2
/view,1,3,2,1
eplot
solve
save
finish
c***.....................................................................***
c*** Post-processing phase
c***.....................................................................***
/post1
set,1,1
RSYS,13
Display results
pldisp,1,0
pldisp,2,0
/view,1,0,10,0

plnsOL,s,x
```

```
plnsOL,s,y
plnsOL,s,z
/view,1,3,2,1

plnsOL,s,x
plnsOL,s,y
plnsOL,s,z
/view,1,1,1,1

plnsOL,s,x
plnsOL,s,y
plnsOL,s,z
/view,1,0,0,0

plnsOL,s,x
plnsOL,s,y
plnsOL,s,z

/focus,1,8,8
/dist,1,3
plnsol,s,x
plnsol,s,y
plnsol,s,z

nsel,s,loc,y,6
nsel,r,loc,x,rad2
nlist,all
prnsol,s,comp
nsel,all

nsel,s,loc,y,6
```

```
nsel,r,loc,x,rad1
nlist,all
prnsol,s,comp
nsel,all

SAVE
finish
/exit
```

Appendix C: Experimental Data

****

STRAIN GAGE TEST DATA

5 different flange outside diameters

2 flange thicknesses

2 gaskets (compressed asbesto, synthetic rubber)

50 MPa Bolt-up Load

****

L represents longitudinal direction

T represents tangential direction

1A. Flange outside diameter: 500 mm, Flange thickness: 30 mm Flange
Gasket type:compressed asbesto

Pressure (kPa)	0	138	276	414
Gage no.	Stresses (MPa)			
1 L	-0.31	-0.20	-0.11	-0.10
T	-0.90	-0.80	-0.61	-0.61
2 L	0.32	0.23	0.15	0.16
T	0.93	0.80	0.61	0.61
3 L	1.62	1.23	1.15	1.06
T	0.87	0.48	0.27	0.29
4 L	5.09	4.16	4.05	3.98
T	0.32	0.15	0.09	0.10
5 L	1.02	0.87	0.45	0.41
T	1.09	0.56	0.56	0.77

1B. Flange outside diameter: 480 mm, Flange thickness: 30 mm Flange
Gasket type:compressed asbesto

Pressure (kPa)	0	138	276	414
Gage no.	Stresses (MPa)			
1 L	-0.73	-0.61	-0.41	-0.52
T	-1.31	-1.20	-1.10	-0.10
2 L	0.73	0.68	0.50	0.59
T	1.32	1.23	1.35	1.04
3 L	2.90	1.65	1.50	1.47
T	0.20	0.85	0.65	0.67
4 L	5.40	4.51	4.47	4.33
T	0.38	0.13	0.18	0.19
5 L	1.40	1.26	0.84	0.83
T	1.48	0.92	0.91	0.91

1C. Flange outside diameter: 460 mm, Flange thickness: 30 mm Flange
Gasket type:compressed asbesto

Gage no.	Pressure (kPa) 0	138	276	414
	Stresses (MPa)			
1 L	-0.80	-0.76	-0.66	-0.61
T	-1.76	-1.61	-1.43	-1.45
2 L	0.87	0.52	0.69	0.64
T	1.78	1.67	1.42	1.44
3 L	2.45	1.75	1.65	1.54
T	0.63	0.44	0.08	0.06
4 L	5.51	4.67	4.54	4.41
T	0.45	0.24	0.30	0.33
5 L	1.50	1.32	0.91	0.93
T	1.85	1.39	1.38	1.31

1D. Flange outside diameter: 440 mm, Flange thickness: 30 mm Flange
Gasket type:compressed asbesto

Gage no.	Pressure (kPa) 0	138	276	414
	Stresses (MPa)			
1 L	-1.22	-1.13	-1.06	-1.01
T	-2.10	-2.12	-1.87	-1.88
2 L	1.23	1.12	1.09	1.10
T	2.11	2.03	1.83	1.85
3 L	2.58	2.19	2.07	1.91
T	1.04	0.81	0.43	0.45
4 L	5.91	5.07	4.90	4.85
T	0.60	0.34	0.40	0.42
5 L	1.90	1.78	1.34	1.35
T	2.25	1.77	1.75	1.83

1E. Flange outside diameter: 420 mm, Flange thickness: 30 mm Flange
Gasket type:compressed asbesto

Gage no.	Pressure (kPa) 0	138	276	414
	Stresses (MPa)			
1 L	-1.23	-1.15	-1.09	-1.07
T	-2.61	-2.52	-2.38	-2.36
2 L	1.23	1.13	1.10	1.09
T	2.63	2.54	2.37	2.35
3 L	2.86	2.41	2.30	2.29
T	1.50	0.38	0.97	0.93
4 L	6.21	5.31	5.28	5.16
T	0.76	0.51	0.59	0.60
5 L	2.22	2.00	1.68	1.66
T	2.78	2.24	2.24	2.23

2A. Flange outside diameter: 500 mm, Flange thickness: 20 mm Flange
Gasket type:compressed asbesto

Gage no.	Pressure (kPa) 0	138	276	414
	Stresses (MPa)			
6 L	-0.50	-0.41	-0.32	-0.21
T	-1.32	-1.33	-0.91	-0.92
7 L	0.51	0.41	0.38	0.27
T	1.33	1.37	0.96	0.95
8 L	2.30	1.75	1.55	1.48
T	0.15	0.85	0.60	0.66
9 L	6.14	5.12	4.83	4.64
T	0.55	0.35	0.25	0.25
10L	2.01	1.21	1.15	1.07
T	2.17	1.09	1.02	1.08

2B. Flange outside diameter: 480 mm, Flange thickness: 20 mm Flange
Gasket type:compressed asbesto

Gage no.	Pressure (kPa). 0	138	276	414
	Stresses (MPa)			
6 L	-0.65	-0.52	-0.43	-0.33
T	-1.45	-1.42	-1.31	-1.32
7 L	0.66	0.54	0.43	0.33
T	1.41	1.42	1.33	1.34
8 L	2.44	1.85	1.65	1.50
T	0.55	0.25	0.06	0.05
9 L	6.21	5.23	4.97	4.71
T	0.64	0.45	0.36	0.35
10L	2.11	1.35	1.23	1.12
T	2.51	1.49	1.42	1.45

2C. Flange outside diameter: 460 mm, Flange thickness: 20 mm Flange
Gasket type:compressed asbesto

Gage no.	Pressure (kPa). 0	138	276	414
	Stresses (MPa)			
6 L	-0.81	-0.74	-0.63	-0.51
T	-1.82	-1.81	-1.72	-1.73
7 L	0.82	0.77	0.62	0.55
T	1.81	1.82	1.74	1.73
8 L	2.62	2.05	1.85	1.74
T	0.95	0.65	0.40	0.40
9 L	6.41	5.43	5.14	4.93
T	0.81	0.60	0.50	0.51
10L	2.32	1.55	1.41	1.34
T	2.97	1.99	1.82	1.85

2D. Flange outside diameter: 440 mm, Flange thickness: 20 mm Flange
Gasket type:compressed asbesto

Gage no.	Pressure (kPa). 0	138	276	414
	Stresses (MPa)			
6 L	-1.00	-0.91	-0.81	-0.75
T	-2.22	-2.23	-2.12	-2.13
7 L	1.01	0.93	0.81	0.75
T	2.23	2.25	2.17	2.15
8 L	2.81	2.27	2.03	1.96
T	4.67	3.67	3.32	3.15
9 L	6.61	5.67	5.32	5.14
T	0.90	0.71	0.62	0.62
10L	2.55	1.75	1.64	1.51
T	3.31	2.24	2.23	2.06

2E. Flange outside diameter: 420 mm, Flange thickness: 20 mm Flange
Gasket type:compressed asbesto

Gage no.	Pressure (kPa). 0	138	276	414
	Stresses (MPa)			
6 L	-1.10	-0.94	-0.82	-0.77
T	-2.80	-2.81	-2.74	-2.75
7 L	1.10	0.91	0.82	0.76
T	2.87	2.88	2.74	2.75
8 L	3.23	2.66	2.42	2.44
T	1.91	1.61	1.44	1.48
9 L	7.02	6.03	5.77	5.56
T	1.00	0.84	0.75	0.85
10L	2.91	2.12	2.03	1.94
T	3.92	2.87	2.82	2.83

3A. Flange outside diameter: 500 mm, Flange thickness: 30 mm Flange
Gasket type: synthetic rubber

..... Pressure (kPa).	0.....	138....	276....	414
Gage no.				
.....Stresses (MPa).....				
1 L.....	-0.63...	-0.59...	-0.41...	-0.38
T.....	-1.21...	-1.12...	-0.97...	-0.96
2 L.....	0.61...	0.60...	0.42...	0.37
T.....	1.22...	1.11...	0.93...	0.92
3 L.....	2.91...	2.40...	2.33...	2.26
T.....	0.83...	0.42...	0.04...	0.13
4 L.....	7.27...	6.31...	6.23...	6.17
T.....	0.94...	0.75...	0.63...	0.60
5 L.....	3.19...	2.07...	1.82...	1.67
T.....	3.21...	1.68...	1.56...	1.69

3B. Flange outside diameter: 480 mm, Flange thickness: 30 mm Flange
Gasket type: synthetic rubber

..... Pressure (kPa).	0.....	138....	276....	414
Gage no.				
.....Stresses (MPa).....				
1 L.....	-0.65...	-0.63...	-0.50...	-0.41
T.....	-1.72...	-1.61...	-1.43...	-1.42
2 L.....	0.64...	0.62...	0.51...	0.40
T.....	1.73...	1.62...	1.44...	1.41
3 L.....	3.15...	2.63...	2.52...	2.41
T.....	1.36...	0.91...	0.55...	0.64
4 L.....	7.41...	6.52...	6.43...	6.37
T.....	1.02...	0.83...	0.72...	0.69
5 L.....	3.30...	2.21...	2.13...	2.05
T.....	3.75...	2.19...	2.03...	2.19

3C. Flange outside diameter: 460 mm, Flange thickness: 30 mm Flange
Gasket type: synthetic rubber

Gage no.	Pressure (kPa). 0	138	276	414
	Stresses (MPa)			
1 L	-0.73	-0.65	-0.51	-0.44
T	-2.13	-2.06	-1.84	-1.83
2 L	0.75	0.67	0.53	0.46
T	2.16	2.06	1.87	1.86
3 L	3.32	2.80	2.75	2.64
T	1.76	1.36	0.96	1.07
4 L	7.66	6.73	6.64	6.53
T	1.15	0.96	0.85	0.82
5 L	3.56	2.45	2.32	2.21
T	4.12	2.60	2.45	2.56

3D. Flange outside diameter: 440 mm, Flange thickness: 30 mm Flange
Gasket type: synthetic rubber

Gage no.	Pressure (kPa). 0	138	276	414
	Stresses (MPa)			
1 L	-0.82	-0.76	-0.63	-0.46
T	-2.44	-2.31	-2.13	-2.15
2 L	0.81	0.73	0.64	0.47
T	2.45	2.35	2.19	2.18
3 L	3.55	3.07	2.92	2.88
T	2.05	1.61	1.25	1.35
4 L	7.80	6.93	6.84	6.73
T	1.26	1.05	0.96	0.93
5 L	3.57	2.68	2.54	2.47
T	4.47	2.90	2.76	2.81

3E. Flange outside diameter: 420 mm, Flange thickness: 30 mm Flange
Gasket type: synthetic rubber

Gage no.	Pressure (kPa). 0	138	276	414
	Stresses (MPa)			
1 L	-0.90	-0.81	-0.70	-0.51
T	-3.18	-3.67	-2.85	-2.84
2 L	0.92	0.84	0.76	0.53
T	3.11	3.04	2.83	2.82
3 L	4.17	3.63	3.56	3.43
T	2.73	2.33	1.96	2.02
4 L	7.44	7.52	7.56	7.33
T	1.45	1.24	1.16	1.15
5 L	4.38	3.27	3.12	3.06
T	5.13	3.69	3.43	3.55

4A. Flange outside diameter: 500 mm, Flange thickness: 20 mm Flange
Gasket type: synthetic rubber

Gage no.	Pressure (kPa). 0	138	276	414
	Stresses (MPa)			
6 L	-0.71	-0.60	-0.54	-0.40
T	-1.52	-1.40	-1.32	-1.31
7 L	0.73	0.66	0.54	0.44
T	1.55	1.41	1.34	1.33
8 L	3.40	2.98	2.74	2.61
T	1.53	1.04	0.74	0.88
9 L	8.12	7.20	6.93	6.89
T	1.25	1.05	0.97	0.94
10L	4.29	3.01	2.86	2.82
T	5.43	3.78	2.53	2.68

4B. Flange outside diameter: 480 mm, Flange thickness: 20 mm Flange
Gasket type: synthetic rubber

Gage no.	Pressure (kPa). 0	138	276	414
	Stresses (MPa)			
6 L	-0.76	-0.65	-0.59	-0.48
T	-2.02	-1.91	-1.83	-1.84
7 L	0.75	0.65	0.56	0.47
T	2.04	1.93	1.85	1.86
8 L	3.52	3.01	2.89	2.75
T	2.05	1.54	1.26	1.38
9 L	8.21	7.37	7.08	6.91
T	1.35	1.15	1.07	1.03
10L	4.33	3.15	2.92	2.90
T	5.99	4.23	3.02	3.17

4C. Flange outside diameter: 460 mm, Flange thickness: 20 mm Flange
Gasket type: synthetic rubber

Gage no.	Pressure (kPa). 0	138	276	414
	Stresses (MPa)			
6 L	-0.85	-0.72	-0.51	-0.49
T	-2.33	-2.24	-2.05	-2.04
7 L	0.88	0.76	0.57	0.43
T	2.31	2.24	2.01	2.06
8 L	3.85	3.36	3.13	3.04
T	2.35	1.84	1.57	1.66
9 L	8.56	7.61	7.30	7.28
T	1.43	1.23	1.15	1.11
10L	4.67	3.47	3.21	3.20
T	5.20	4.57	3.30	3.48

4D. Flange outside diameter: 440 mm, Flange thickness: 20 mm Flange Gasket type: synthetic rubber

Gage no.	Pressure (kPa). 0	138	276	414
	Stresses (MPa)			
6 L	-0.89	-0.77	-0.60	-0.54
T	-2.56	-2.47	-2.22	-2.21
7 L	0.90	0.80	0.61	0.50
T	2.57	2.44	2.23	2.24
8 L	4.06	3.57	3.35	3.23
T	2.70	2.23	1.98	2.00
9 L	8.80	7.81	7.56	7.43
T	1.60	1.40	1.32	1.28
10L	4.88	3.60	3.47	3.41
T	6.60	4.99	3.71	3.88

4E. Flange outside diameter: 420 mm, Flange thickness: 20 mm Flange Gasket type: synthetic rubber

Gage no.	Pressure (kPa). 0	138	276	414
	Stresses (MPa)			
6 L	-0.91	-0.79	-0.66	-0.59
T	-3.12	-3.07	-2.86	-2.49
7 L	0.92	0.79	0.67	0.61
T	3.15	3.09	2.89	2.03
8 L	4.69	4.18	3.90	3.15
T	3.34	2.88	2.57	2.50
9 L	9.30	8.41	8.19	8.07
T	1.83	1.60	1.54	1.51
10L	5.48	4.24	4.07	4.52
T	7.23	5.67	4.33	3.99